Let it bind, and light you may find

Investigation of 14F7's cellular journey and effects

Helene Sørum Kristiansen

Master Thesis in Biochemistry

60 credits

Department of Chemistry

Faculty of Mathematics and Natural Sciences

UNIVERSITY OF OSLO

05/2022

2022

Let it bind, and light you may find – Investigation of 14F7's cellular journey and effects

Helene Sørum Kristiansen

http://www.duo.uio.no/

Trykk: Reprosentralen, Universitetet i Oslo

“Science is the poetry of reality”

-Richard Dawkins

Acknowledgements

First, I would like to express my gratitude towards my main supervisor, Prof. Ute Krengel[1]. Thank you for the opportunity to work on this interesting project and for all the feedback, ideas and critical thinking along the way. I appreciated that your door was always open, and that you always made time for meeting me to answer all my questions and helping me sort out all the information. I also appreciated all the social events, from dinners, section beers and coffee breaks, to bowling and kräftskiva (even though I did not eat the crayfish). You create an including work environment, and I feel so lucky to been part of your research group for these past two years.

I would like to thank my co-supervisors Geir Åge Løset[2] and Cinzia Anita Maria Progida[3] for advice and great discussions throughout the project. Geir Åge, I admire all your knowledge and the fact that you always have new ideas and suggestions for solving problems. Cinzia, your door was always open to me and I am so grateful for all the advice and help with interpreting images and optimizing protocols. Also, thanks to the members of yours and Bakke's research group for including me in lunch gatherings and helping me in the lab. I would further like to give a huge thank you to Khalisah "Kelly" Liyana Binto Zulkefli[4]. I don't know how I would have made it without all your help. You've been the closest to a lab advisor I've had throughout my master project. You have always taken your time to answer my questions, helping me understand the basics of cell biology and imaging, helping me plan my experiments and to interpret the results. You have helped me become a better scientist, and I am greatly thankful for all the pep talks when I needed the emotional support. Also, thanks to Oslo NorMic Imaging Platform for letting me use the microscope for my project.

I want to thank Nina Frederikke Jeppesen Edin[5] for all the help with flow cytometry experiments and data processing. I've learned so much from you, and I am thankful for all the time you took to help me out. I am greatful for the help with cell cultivation from Joe Alexander Sandvik[6] help with the hypoxia experiment from Julia Marzioch[7]. Thanks to the

[1] Professor, Department of Chemistry, University of Oslo, Norway
[2] Co-founder, CEO/CSO at Nextera AS
[3] Professor, Department of Biosciences, University of Oslo, Norway
[4] Postdoc, Department of Biosciences, University of Oslo, Norway
[5] Associate professor, Department of Physics, University of Oslo, Norway
[6] Senior Engineer, Department of Physics, University of Oslo, Norway
[7] Senior Engineer, Department of Physics, University of Oslo, Norway

rest of the students at Biological and Medical Physics for taking me in and treating me like a member of your group.

Further, I want to thank Anders Aune Tveita[8] for kindly providing the h14F7' and HEK KI Oslo cells produced in his lab and Julia Heinzelbecker[9] for all the help answering my questions about the antibody and cells provided by Anders' research group. I am grateful for help with interpreting the proteomics data from Tuula Anneli Nyman[10]. I would have been completely lost without your help. Thank you, Yoshiki Narimatsu[11], for help with experiments performed at Copenhagen Center for Glycomics, Denmark and Henrik Clausen[12] for great discussions regarding our results. Thanks to BioCat for providing me with a travel grant making it possible for me to visit Copenhagen.

The work carried for my master's project would not have been possible without the help from Hedda Johannesen[13] familiarizing me with the project, previous results and answering my questions. Also, thank you to Giacomo Pesci[14] for all the help through your emails. I would also like to thank all the previous and current members of Krengel Structural Biology lab for help in the lab as well as all our social gatherings.

I then would like to thank my parents and brother for support and my dog, Dino, for always being overly happy when seeing me. Thanks to Jan-Vegard, Svein-Gisle, Thomas and Monica for always believing in me. I would not have been here today without your support. Thanks to my friends for listening to my complaints and encouraging me to keep pushing forward. A special thanks to Natalia and Varna for proofreading my thesis, and to Abelone for being such a great friend throughout our years at UiO, and I look forward to the following years of friendship.

Lastly, I want to give a pat on the back to myself. Life might always be hard and challenging, but look how far you have come.

Helene S. Kristiansen

Oslo, May 2022

[8] Researcher, Department of Immunology, Rikshospitalet, Norway
[9] Doctoral Research Fellow, Department of Immunology, Rikshospitalet, Norway
[10] Researcher, Department of Immunology, Rikshospitalet, Norway
[11] Associate Professor, Department of Cellular and Molecular Medicine, University of Copenhagen, Denmark
[12] Professor, Department of Cellular and Molecular Medicine, University of Copenhagen, Denmark
[13] PhD
[14] M. Sc

Populærvitenskapelig sammendrag

Kreft er en samling av sykdommer som er kjennetegnet ved at muterte celler vokser og deler seg ukontrollert, samt sprer seg til andre deler av kroppen, uavhengig av plassrestriksjon og tilgang på næring. Kreft rammer millioner av mennesker hvert år. Selv om det finnes ulike behandlinger, er kreft en av de ledende grunnene til at mennesker dør verden over. De tradisjonelle behandlingsmåtene for kreft er kirurgi, strålebehandling og cellegift. Disse behandlingene dreper kreftcellene, men også friske celler blir drept, i tillegg til at behandlingene medfører flere bivirkninger hos pasienten. Behovet for nye medisiner som mer effektivt dreper kreftceller uten å påvirke de friske cellene er stort. Kreftceller produserer molekyler av ulik sammensetning og konsentrasjon sammenlignet med friske celler. Dette utnyttes i immunterapi der kroppens eget immunforsvar stimuleres til å angripe kreftcellene. Et slikt molekyl som kun uttrykkes på overflaten av kreftceller, men ikke friske celler hos voksne mennesker, er Neu5Gc GM3. Dette skyldes at mennesker mistet genet *CMAH* gjennom evolusjon to til tre millioner år siden, men genet finnes fortsatt i andre dyr slik som aper. Antistoffet 14F7 kan gjenkjenne Neu5Gc og sette i gang mekanismer for å drepe cellen. Selve mekanismene som fører til celledød er ukjent per dags dato.

Vi hadde tilgang på ulike formater av antistoffet 14F7, og ønsket derfor å karakterisere de ulike formatenes binding og effekt. Vi observerte at det originale formatet av 14F7 ga sterkest binding. Vi benyttet også ulike konstruksjoner av celler med innsatt *CMAH*-gen fra sjimpanser, som gir celler som uttrykker Neu5Gc. Det ene konstruktet, laget i Anders Tveita sin lab i Oslo, viste seg å binde 14F7 sterkere. Basert på disse observasjonene valgte vi ut hvilket antistoff format og hvilket genmodifisert cellekonstrukt vi ønsket å benytte videre for cellebiologiske studier ved bruk av konfokal mikroskopi. Vi demonstrerte at 14F7 kunne binde til Neu5Gc inni cellen, som var lokalisert i vesikler. Vi utførte også proteomikkanalyser av ulike celler behandlet med 14F7 for å få innblikk i hvilke proteiner som reguleres når antistoffet binder. Det viste seg at cytoskjelettproteiner ble nedregulert ved behandling med 14F7, i tillegg til at vi observerte en endring i cellemorfologi og en økning i celledød. Denne masteroppgaven legger grunnlag for videre studier for å forstå 14F7s cellulære opptak og effekt for fremtidig klinisk bruk.

Abstract

Cancer is a collection of diseases characterized by mutated cells which grow and divide uncontrolled, as well as spread through metastasis. Cancer is the second leading cause of death globally and has become one of humanities biggest challenges. Traditional cancer treatments, like surgery, radiation therapy and chemotherapy, not only kill cancer cells, but also harm healthy cells. We are in need of more specific treatments causing less side effects. When a healthy cell is transformed to a cancerous cell, different genes are expressed, making it possible to distinguish them from normal healthy cells. This is exploited in immunotherapy where specific molecules are targeted. One such molecule is Neu5Gc GM3, a ganglioside only present on the cell surface of cancer cells in human adults. This is due to a deletion in the *CMAH* gene during evolution two to three million years ago, but the gene is expressed in e.g., apes. This tumor-specific ganglioside can be targeted by the antibody 14F7, which was first developed and produced in Cuba two decades ago. 14F7 has an unusually high binding affinity for Neu5Gc and has been reported to cause tumor cell death *in vitro* and *in vivo*.

The aim of this thesis was to characterize three different formats of 14F7: murine 14F7 (m14F7), humanized 14F7 (h14F7) and a humanized 14F7 variant produced in Oslo containing an alternative variable light chain (h14F7*). Our results using flow cytometry indicate that h14F7 gave the strongest binding. We also used two different constructs of knock-in cells. The *CMAH*-gene from chimpanzees was knocked in to unmodified HEK293 cells, inducing expression of Neu5Gc. One construct was made in the lab of Henrik Clausen at the University of Copenhagen and the other construct in the lab of Anders Tveita at Rikshospitalet, Oslo. The HEK KI-construct made at Rikshospitalet gave the strongest signal, illustrated by flow cytometry and imaging. The most promising combination of 14F7-format and HEK KI cells was further investigated in cell biological studies. Confocal microscopy was used to image the binding of 14F7 to its target on the cell surface as well as intracellular target. The signal for 14F7 was localized to the late endosome. Proteomic analysis revealed significant up- and downregulation of proteins in HEK WT, HEK KI Oslo and L1210 cells when incubated with h14F7. Changes in cell communication and/or signal transduction was upregulated, while cytoskeletal proteins were downregulated. Together, this provides new insight into understanding 14F7's cellular journey and effects for immunotherapy.

Abbreviations

14F7 Cuba	Humanized monoclonal 14F7 IgG_1 antibody produced in Cuba
14F7 Oslo	Humanized monoclonal 14F7 IgG_1 antibody produced in Oslo
ADC	Antibody-drug conjugate
ADCC	Antibody-dependent cell-mediated cytotoxicity
APC	Antibody-presenting cell
ARC	Antibody-radionuclide conjugate
AU	Absorption unit
BSA	Bovine serum albumin
C1	Construct 1, 14F7 scFv
CAR	Chimeric antigen receptor
CDC	Complement-dependent cytotoxicity
CDR	Complementarity-determining region
C_H	Constant heavy domain
CIM	Center of Molecular Immunology, Havana, Cuba
C_L	Constant light domain
CMAH	Cytidine monophospho-*N*-acetyl-neuraminic acid hydroxylase
Da	Dalton
DMEM	Dulbecco's Modified Eagle Medium
DNA	Deoxyribonucleic acid
EDTA	Ethylene diamine-tetra-acetic acid
EGFR	Epidermal growth factor receptor
F_c	Fragment crystallizable
F_v	Fragment variable
Fab	Fragment antigen binding
FACS	Fluorescence-activated cell sorting
FBS	Fetal bovine serum
FITC	Fluorescein isothiocyanate
FSC	Forward scattering
Gal	Galactose
GFP	Green fluorescent protein
Glc	Glucose
HAMA	Human anti-murine antibody
IgA	Immunoglobulin A
IgD	Immunoglobulin D

IgE	Immunoglobulin E
IgG	Immunoglobulin G
IgM	Immunoglobulin M
KI	Knock-in
KO	Knock-out
LC	Liquid chromatography
LC-MS	Liquid chromatography-mass spectrometry
mAb	Monoclonal antibody
MHC	Major histocompatibility complex
MS	Mass spectrometry
Neu5Ac	*N*-Acetyl neuraminic acid
Neu5Gc	*N*-Glycolyl neuraminic acid
NK cell	Natural killer cell
Nluc	NanoLuc luciferase
PBS	Phosphate buffered saline
Pen-Strep	Penicillin Streptomycin
PFA	Paraformaldehyde
PI	Propidium iodide
PNA	Peanut agglutinin
Rcf	Relative centrifugal force
RNase	Ribonuclease
RPMI	Roswell Park Memorial Institute
SSC	Side scattering
scFv	Single chain variable fragment
TCR	T-cell receptor
UiO	Universitetet i Oslo (University of Oslo)
UV	Ultraviolet
V_H	Variable heavy domain
V_L	Variable light domain
WHO	World Health Organization
WT	Wild type

Table of contents

1. Introduction

1.1 Cancer

Cancer is the world's second leading cause of death globally, with nearly 10 million deaths in 2020 (Figure 1, WHO). Cancer is a term for a collection of diseases characterized by uncontrolled abnormal cell growth forming tumors. The disease can start in almost any organ or tissue of the body as a primary tumor and invade neighboring organs or tissues. Tumors that have invaded neighboring tissue by the process of metastasis are termed malignant. Metastasis is a major reason for death from cancer. Most of the tumors that grow only locally without invading adjacent tissue are termed benign, some tumors can be malignant without spreading such as gliomas in brain cancer (Omuro and DeAngelis, 2013). Most of the primary tumors arising in humans are benign and harmless but become a problem when they expand and press on vital organs or tissues (Weinberg, 2018).

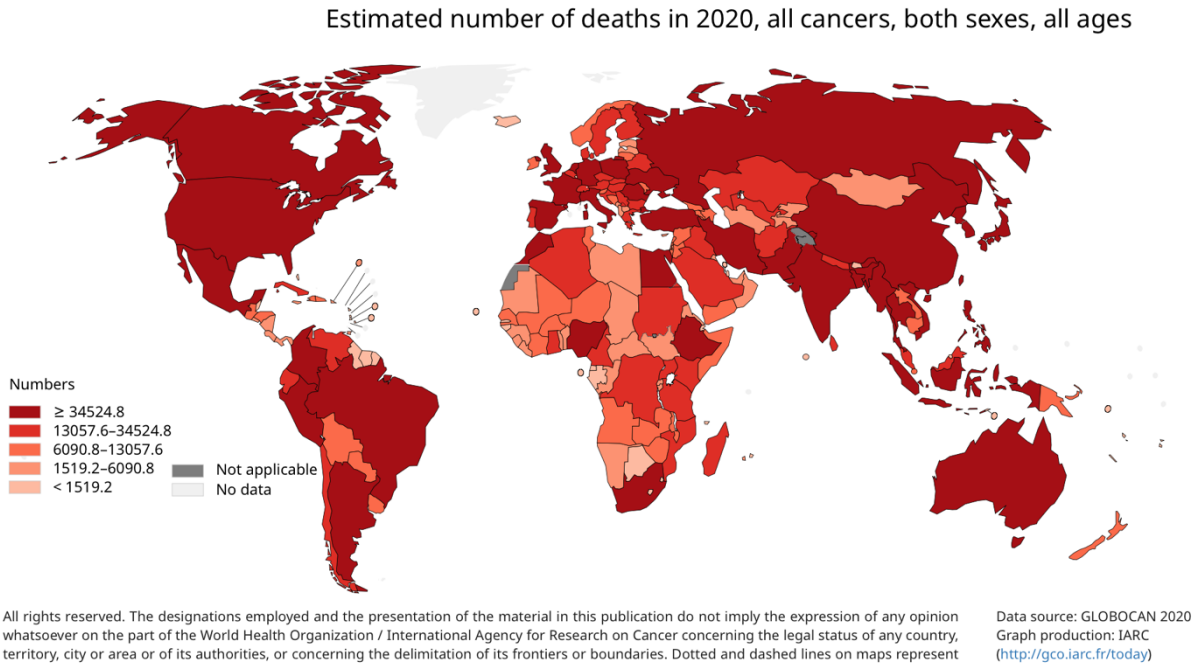

Figure 1. World map showing estimated number of deaths in 2020 including all cancers for both sexes and all ages. Figure from (WHO).

Cancer is triggered by DNA mutations arising from exposure to carcinogenic factors such as radiation, chemicals or viral infection. Tumor suppressor genes and oncogenes are specific genes highly involved in cancer development. In healthy tissue, tumor suppressor genes reduce the likelihood that a tumor will appear in the body and proto-oncogenes are usually not active. Proto-oncogenes are genes that have the potential to induce cell transformation and thus lead to cancer (Weinberg, 2018). What happens in the cell during cancer is that these genes are mutated, leading to defective tumor suppressor genes and highly active oncogenes.

1.1.1 Traditional cancer treatment

Since there are numerous different cancer types, that also means no cancer is the same. There is a large heterogeneity within each cancer type and from patient to patient. Nevertheless, most cancers are treated with the same methods. The traditional cancer treatments include surgery, chemotherapy, and radiation therapy(Pérez-Herrero and Fernández-Medarde, 2015; Wyld, Audisio and Poston, 2015; Allen, Her and Jaffray, 2017). Surgeons can remove solid tumors by surgery, and by this perform a local treatment for only the part of the body with the cancer. Drugs are used for chemotherapy and high doses of radiation for radiotherapy to kill cancer cells or shrink tumors within a patient. Patients often need a combination of these treatments to become cancer-free. In this process, not only are the cancer cells affected, but also healthy cells. This leads to various side effects that can be both toxic and severe for the body (Schirrmacher, 2019).

1.1.2 Targeted therapy and immunotherapy

As the understanding of how cancers initiate and progress improved, new cancer treatments were developed. Drugs that can interfere with molecular targets involved in tumor growth and progression have become an important part of cancer treatment. This form of treatment has been named targeted therapy as the drugs, usually small molecules or monoclonal antibodies, specifically target proteins involved in tumor progression. These targets can e.g. be signaling molecules, growth factor receptors, cell cycle proteins or modulators of apoptosis (Widakowich *et al.*, 2007).

When the target exerts its effect on the patient's immune system, the treatment is known as immunotherapy. The immune system is the body's natural defense system, and this system can be boosted by immunotherapy to fight the cancer. Immunotherapy is usually divided into passive and active treatments. The most common form today is passive immunotherapy where the patient receives a molecule that help the patient's immune system to kill the cancer. This form of treatment does not activate the patient's adaptive immune system. The other form, active immunotherapy, activates the adaptive immune system and thereby result in immunologic memory when a molecule is received to produce an anti-cancer response. Active immunotherapy is based on vaccination. Immunotherapy can result in less side effects compared to chemotherapy and radiotherapy, and lead to new patterns of antitumor responses. However, there are still many challenges with immunotherapy as the response time is longer and in some cases the immune system can get too aggressive and kill healthy cells (Hoos *et al.*, 2010; Bajwa *et al.*, 2019).

1.1.3 Cancer Moonshot initiative

In 2016, when Joe Biden served as US Vice President, he launched an initiative, named Cancer Moonshot, with the mission to accelerate the rate of progress against cancer (National Cancer Institute). The initiative focuses on: *"accelerating scientific discoveries, foster greater collaborations and improving the sharing of data".* The US Congress authorized to fund the Cancer Moonshot with 1.8 billion American dollars over a 7-year period starting in 2017. A report published in 2021 highlighted parts of the progress, i.e. a new collaboration between the Fusion Oncoproteins in Childhood Cancer and the Pediatric Immunotherapy Discovery and Development Network (Sharpless and Singer, 2021). The collaboration has led to development of new cancer models, identification of possible targets and testing of combination treatments in preclinical immunotherapy research for children and adolescents. On the 2nd of February 2022, Joe Biden announced an even more ambitious goal: "*To reduce the death rate from cancer by at least 50 percent over the next 25 years"* (National Cancer Institute). This initiative is only one out of many globally initiatives working towards the same goal: To put an end to cancer for good.

1.2 The immune system

The immune system is composed of cells and molecules responsible for a collective and coordinated immune response to foreign substances introduced into the body. Every individual's immune system can recognize, respond to and eliminate many foreign particles, called antigens, without responding to the body's own antigens and tissues (Abbas, Lichtman and Pillai, 2018). This is regulated by the body's ability to recognize "self" from "non-self". The immune system is divided into innate and adaptive immunity.

1.2.1 Innate immunity

The innate immunity is the body's early defense, present already at birth, that responds almost immediately to foreign substances. The innate immune system creates a physical and chemical barrier at the skin and lining of the gastrointestinal and respiratory tract to prevent, control and eliminate infection by many pathogens. The receptors recognize structures that are common to groups of related microbes, such as pathogen-associated molecular patterns (PAMPs) (Janeway and Medzhitov, 2002). The innate immunity can also recognize molecules produced and released by damaged or dying cells, known as damage-associated molecular patterns (DAMPs). There is a large group of cells that make up the innate immune system, i.e., phagocytes, dendritic cells, natural killer cells, mast cells and innate lymphoid cells. The innate immune system occurs through two types of protective reactions called inflammation and antiviral defense. Inflammation is a process where phagocytes and other leukocytes that destroy microbes are recruited. Antiviral defense in the innate immune system blocks viral replication or kill viral-infected cells without the need for an inflammatory reaction.

1.2.2 Adaptive immunity

The adaptive immune system takes longer time to develop and require activation of lymphocytes. Lymphocytes can recognize a large number of pathogens by the two major populations called B lymphocytes (B cells) and T lymphocytes (T cells) that mediate different adaptive immune responses (Bonilla and Oettgen, 2010). The fundamental properties of the adaptive immune system are specificity, diversity, memory and self-tolerance. The molecular recognition of antigens via MHC-presentation (major histocompatibility complex) in T cells or

directly on B cells makes the adaptive immune system highly specific by reacting to only a distinct subset of epitopes. The diversity of antigen receptors for B and T cells is a result of somatic rearrangements during cell maturation. The immunologic memory gives the body the ability to respond more rapidly and greater during a re-exposure to the same antigen, and self-tolerance ensures that the body do not respond against self-antigens (Swain, McKinstry and Strutt, 2012).

The adaptive immune system is composed of two types of responses. Cell-mediated response is where cytotoxic cells defend against infection. The microbes can either be intracellular by replicating within an infected cell or live within macrophages. The cytotoxic cells are generally divided into two types; the cytotoxic T cells and the helper T cells. Cytotoxic T cells will by their effector mechanism kill infected cells and eliminate reservoirs of infection, while helper T cells in their effector mechanism activate macrophages and neutrophils to kill the phagocytosed microbes. The other type of response is humoral response where antibodies secreted from B cells defend against infection in body fluids (Abbas, Lichtman and Pillai, 2018). Antibodies are produced in mature B cells and are the effector molecules of humoral immunity that can further mediate several effector functions.

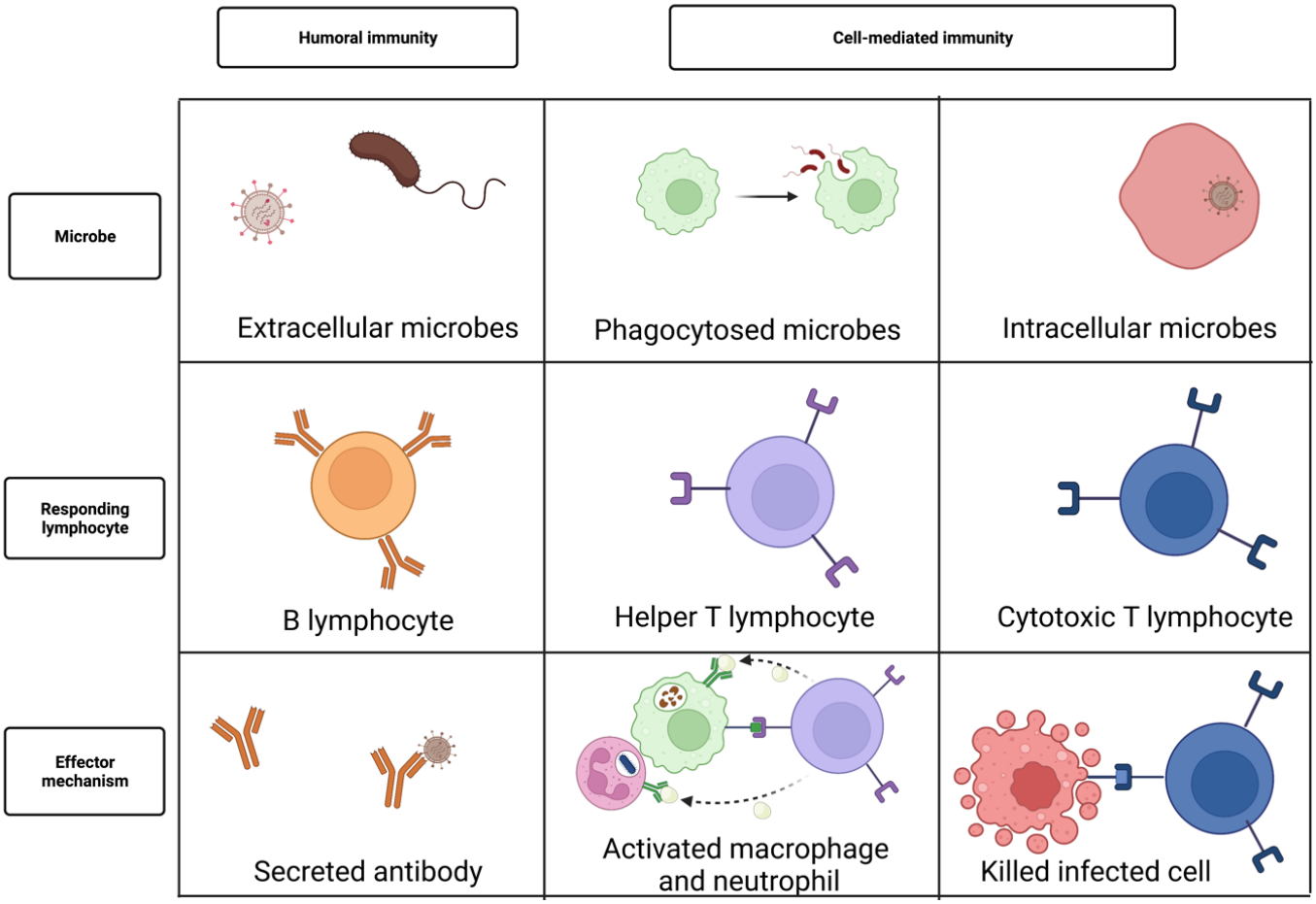

Figure 2. Adaptive immunity. In humoral immunity, B lymphocytes secrete antibodies to eliminate extracellular microbes. In cell-mediated immunity, helper T lymphocytes activate macrophages and neutrophils to kill phagocytosed microbes, or cytotoxic Y lymphocytes directly kill infected cells. This figure was created with BioRender and inspired by (Abbas, Lichtman and Pillai, 2018).

1.3 Tumor antigens

The surface of cells is covered by many different molecules that are important for i.e., cell survival and cell communication. However, specific surface molecules, called antigens, can be recognized by the immune system as foreign and trigger an immune response. Some antigens are only present on cancerous cells (tumor-specific), and some are over-expressed (tumor-associated). There is today a large number of tumor antigens that have been confirmed to play a role in antitumor immunity and immunosurveillance, and that show a potential to contribute to successful cancer therapy or prevention (Finn, 2017). Two types of antigens commonly expressed on cell surfaces are growth factor receptors and gangliosides. They are known to be involved in cancer and are therefore potential targets for detection of disease and development of therapy (Krengel and Bousquet, 2014).

1.3.1 Epidermal growth factor receptors

Epidermal growth factor receptors (EGFRs) are transmembrane tyrosine kinases located on the plasma membrane. When they are activated by a ligand, signals are transduced to intracellular pathways. Genes encoding growth factor receptors are often proto-oncogenes that can be altered by only a single mutation leading to cell transformation and proliferation (Normanno *et al.*, 2006). EGFRs have been shown to be overexpressed on cells in several cancers, including breast, lung, colon, prostate, brain, head and neck, renal and ovarian carcinomas (Wang *et al.*, 2001). A higher number of receptors tends to correlate with poorer clinical prognosis (Gullick, 1991; Salomon *et al.*, 1995; Modjtahedi *et al.*, 1998).

1.3.2 Gangliosides

The most common molecules located on the cell surface are glycoconjugates. Glycoconjugates are carbohydrates chemically bound to a protein (glycoprotein) or to a lipid (glycolipid). One group of such glycolipids covering all animal cells are gangliosides. Gangliosides are sialic-acid-containing glycosphingolipids consisting of a head group of carbohydrates exposed to the environment outside the cell and a hydrophobic tail anchoring the ganglioside to the membrane. Gangliosides are important molecules for several functions, such as cell-cell interactions, signal transduction, tumor progression and more (Hakomori, 2002).

The monosialodihexosylganglioside (GM3) is the most common and the simplest ganglioside in humans (Hakomori and Handa, 2015). The abbreviation indicates that it is a ganglioside (G), has only one sialic acid (M) and the number 3 is based on its relative mobility in electrophoresis compared to other monosialic gangliosides.

1.3.3 Neu5Gc GM3

The structure of gangliosides has large variations based on their carbohydrate chain composition, but there are mainly two different types. The two most common sialic acids in vertebrates are *N*-acetyl neuraminic acid (Neu5Ac) and *N*-glycolyl neuraminic acid (Neu5Gc). They differ only in one small substituent in the context of the trisaccharide: a methyl group present in Neu5Ac is replaced by a hydroxymethyl in Neu5Gc (Figure 3). The number 5 refers to the sidechain on carbon 5 in the ring structure. Neu5Gc is usually not expressed in human tissue, but it is overexpressed in several types of tumor cells. The enzyme responsible for the substitution is called cytidine monophospho-*N*-acetyl neuraminic acid hydroxylase (CMP-Neu5Ac hydroxylase, *CMAH*). Humans lost the gene encoding production through evolution two to three million years ago (Okerblom *et al.*, 2017). The different cancer types where Neu5Gc GM3 have been identified includes breast, kidney, bladder, ovary, uterus, testis, prostate and non-small cell lung carcinoma (Carr *et al.*, 2000; Oliva *et al.*, 2006; Blanco *et al.*, 2011, 2015; Hayashi *et al.*, 2013).

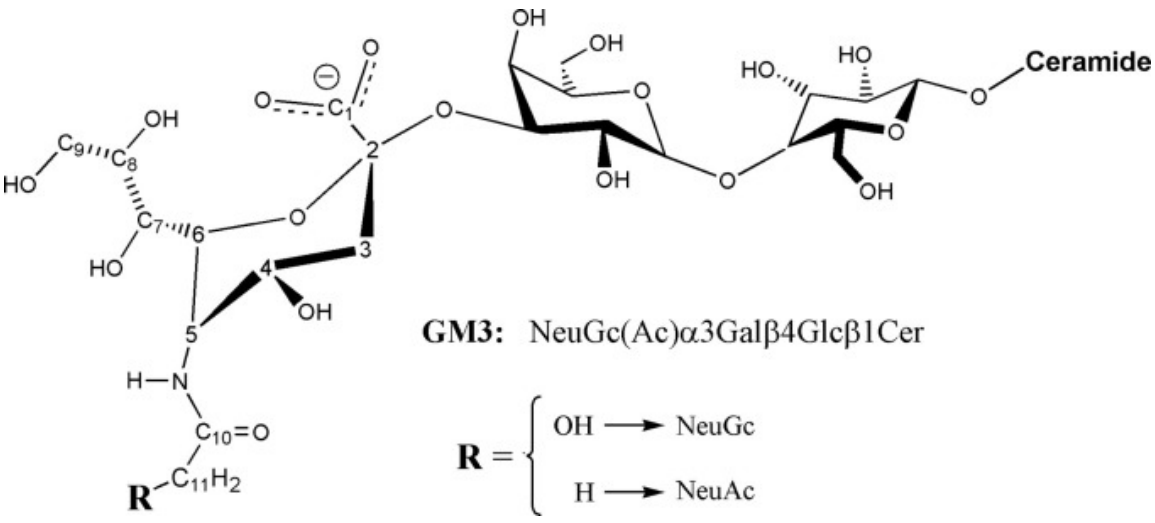

Figure 3. Structure of the gangliosides Neu5Gc and Neu5Ac. The R-group represents the difference between these two gangliosides, where Neu5Gc GM3 is only expressed on cancer cells, while Neu5Ac GM3 can be found expressed on all human cells. Figure published by (Krengel *et al.*, 2004) and used with permission for this thesis.

Studies have proposed that Neu5Gc GM3 can be incorporated or activated by different sources. One explanation of the expression is through dietary sources, where Neu5Gc is a normal component in red meat and fish (Malykh, Schauer and Shaw, 2001; Varki, 2001; Pam *et al.*, 2003; Banda *et al.*, 2012; Alisson-Silva, Kawanishi and Varki, 2016; Dhar, Sasmal and Varki, 2019). Sialidases in the human gut might release Neu5Gc from the diet, leading to uptake and metabolic incorporation in the body. However, little is known about the uptake and biological pathways involved. Another explanation for the expression is through hypoxia.

Normal cells with sufficient oxygen levels break down glucose into pyruvate in the cytosol through the process of glycolysis, and then pyruvate is transported to the mitochondria to further be broken down to carbon dioxide in the citric acid cycle. Hypoxia is a state in which there is a non-physiological level of oxygen. The cells are limited to only using glycolysis to generate pyruvate, which is further reduced to lactate and secreted from the cell. This phenomenon is common in a majority of malignant tumors stimulating a complex signaling network in cancer cells (Muz *et al.*, 2015). One response to lower oxygen levels is alterations in gene expression. Investigation of cells grown under hypoxic conditions may reveal proteins important for cancer formation and progression, such as Neu5Gc (Yin *et al.*, 2006; Bousquet *et al.*, 2015, 2018).

1.4 Anti-tumor antibodies

The use of monoclonal antibodies (mAb) in immunotherapy is today considered to be a main therapy method for cancer treatment, alongside the traditional cancer treatments. More than 20 different mAbs have been approved by the United States Food and Drug Administration (FDA) for clinical use as of 2020 (Zahavi and Weiner, 2020). Some of the antibodies currently used in cancer treatment are mentioned in section 1.4.3.

1.4.1 Structure of antibodies

All antibodies share the same basic structural characteristics, but display remarkable variability in the regions that bind antigens (Abbas, Lichtman and Pillai, 2018). The structure is symmetric composed of two identical light chains and two identical heavy chains, forming a shape similar to the letter “Y”. Both chains consist of repeating homologous units that fold independently in a globular motif called an Ig domain. The heavy and light chains form together an amino-terminal variable region that participate in the recognition and binding of antigens, called paratope, located at the tip of the arms of the “Y”-shape. The variable region contains six hypervariable regions, three on the light chain and three on the heavy chain. These regions are also known as complementarity-determining regions (CDRs) and form a binding site for an antigen, called epitope. The CDRs are therefore where the amino acid sequences differ the most (Abbas, Lichtman and Pillai, 2018). At the other end of the “Y” shape, the two heavy chains form a carboxy-terminal constant region that helps mediate in protective or effector functions. The constant region is highly conserved within the different isotypes (Wang *et al.*, 2018).

Antibodies are divided into five isotypes of immunoglobulins based on the heavy chain present: IgA, IgD, IgE, IgG and IgM. IgA (subtype 1 and 2) is secreted into mucus, tears and saliva, IgD is a B cell receptor, IgE is the antibody involved in allergic reactions, IgG (subtype 1-4) is the main antibody found in blood that can i.e., neutralize toxins and IgM is involved in primary response and complement activation. There are two types of light chains present in mammals, named kappa and lambda. The light chains consist of one constant domain and one variable domain.

The isotype IgG_1 (~155 kDa) is the most abundant isotype in the human serum but not common for anti-carbohydrate antibodies. The heavy chains consist of three constant and

one variable domain, while the light chain consists of one constant and one variable domain (Figure 4). The heavy and light chains are connected by disulfide bonds (Ma and O'Kennedy, 2015). The arms of the antibody are referred to as fragment antigen-binding (Fab, ~50 kDa) and the "stem" as fragment crystallizable (Fc, ~50 kDa). The tip of the Fab consists of two variable Ig domains that make up the fragment variable (Fv, ~25 kDa). These two Ig domains can be connected by a flexible linker to make a single-chain variable fragment (scFv, ~28 kDa), and the heavy chain of the scFv is alone called a nanobody (~15 kDa). Nanobodies and scFvs are not separate fragments of an antibody, but rather tools that can be used within research.

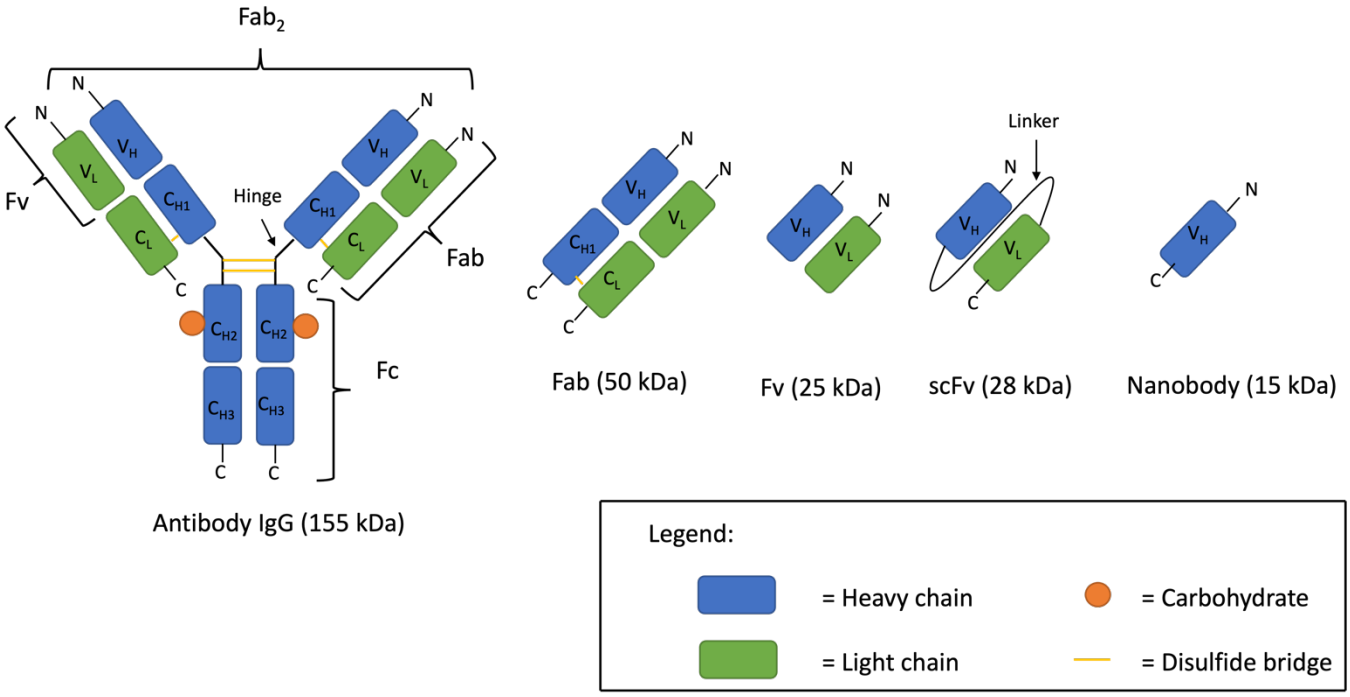

Figure 4. Sketch of the structure of IgG_1 and its fragments. Heavy chains are colored blue and light chains green. IgG carbohydrates are represented as orange circles and the disulfide bridges are represented as yellow sticks. This figure was created using Microsoft PowerPoint and adapted from Giacomo Pesci with permission (Pesci, 2020).

1.4.2 Antibody engineering

Antibodies can not only be produced within the human body, but also outside for use in research or as drugs or vaccines. The antibodies are often referred to as mAbs, which is a term describing that they are derived from a single cell. The hybridoma method for generating large amounts of antibodies of a single predefined specificity was first described by Köhler and Milstein in 1975 (Köhler and Milstein, 1975). They generated a hybridoma cell

line from fusion of a mouse myeloma cell line with B lymphocytes from a mouse spleen. The resulting hybridoma cell line can be cultured and produce antibodies with the same amino acid sequence (Posner *et al.*, 2019). Köhler and Milstein, together with Jerne, received the Nobel prize in medicine or physiology in 1984 for their work on production of mAbs (Nobel Prize Organisation, 2022a). After the hybridoma manufacturing was reported in 1975, the technique quickly spread to many areas of biological research, and development of mAbs for medical purposes soon followed (Kennett, 1981).

Since the hybridoma cell line is of murine origin, the mAbs produced lead to strong immunogenic reactions in the patients. When murine antibodies are injected into the human body, the immune system will recognize them as non-human, and an immune response will be activated. This immune response is termed human anti-mouse antibody (HAMA) where the injected antibodies are neutralized and removed from the circulation (Dillman *et al.*, 1994). To reduce the risk of a HAMA response, some of the regions of the murine mAb can be replaced by human sequences (Figure 5). Several technologies have been developed to produce antibodies with human sequences. The chimeric antibody consists of human constant regions and mouse variable region (Morrison *et al.*, 1984), the humanized antibody consists of human constant and variable regions, but with murine CDRs (Queen *et al.*, 1989), and the human antibody consists of only human sequences (Kempeni, 1999).

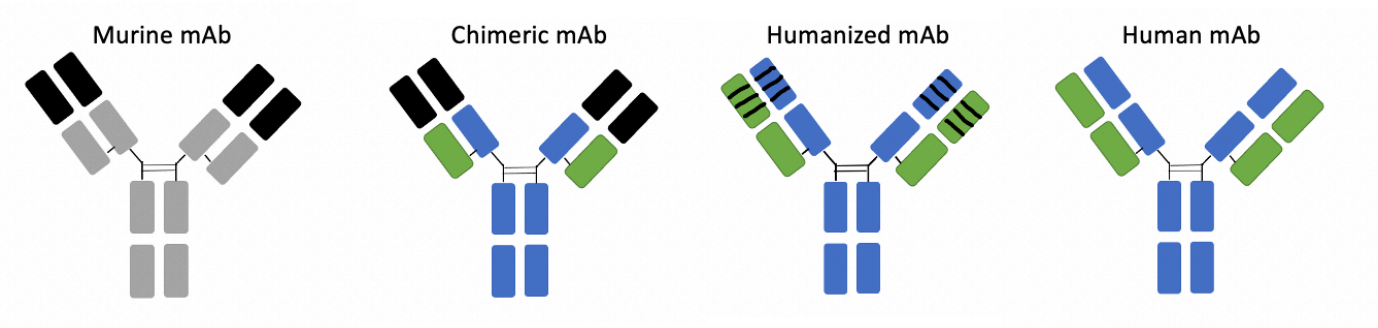

Figure 5. Sketch of different antibody formats. From left: murine monoclonal antibody, chimeric monoclonal antibody, humanized monoclonal antibody and human monoclonal antibody. This figure was created using Microsoft PowerPoint and adapted from Hedda Johannesen with permission (Johannesen, 2020).

1.4.3 Antibodies used in passive immunotherapy

One mechanism for killing cells with specific antigens on the cell surface using antibodies is through antibody-dependent cell-mediated cytotoxicity (ADCC). Antibodies can bind to Fc

gamma receptors (FcγRs) on innate immune cells. The interaction between the antibodies Fc fragment and FcγRs eliminate the tumor cells bound by antibody. NK cells are mainly responsible for the elimination (Su *et al.*, 2018). Another mechanism for killing is through complement-dependent cytotoxicity (CDC). Antigen-bound immunoglobulin M or G (IgM or IgG) binds to C1q, a multimeric pattern recognition molecule in the classical complement pathway. This leads to formation of a membrane attack complex (MAC) and resulting in cell lysis (Pawluczkowycz *et al.*, 2009; Diebolder *et al.*, 2014; Dahmani *et al.*, 2021). One antibody that can activate both ADCC and CDC is Rituximab (Rituxan, Genentec). It is used for blood cancer treatment, i.e. non-Hodgkin lymphoma (Maloney, Smith and Rose, 2002). Rituximab binds to CD20 on the cell surface of malignant B cells leading to cytotoxicity. Another method for toxicity in cancer cells is by having a toxic molecule, such as immunocytokines, or a radioactive atom attached to an antibody. These drugs are respectively referred to as antibody-drug conjugates (ADCs) and antibody-radionuclide conjugates (ARCs). Antibodies could also be used to detect tumor size and location by radioactive labeling, such as ^{99m}Tc-14F7 mAb used in breast cancer (Oliva *et al.*, 2006).

Antibodies can also be used for stimulating or inhibiting immune checkpoints. Immune checkpoints are receptors on the surface of T cells that initiate a cytotoxic response when binding to a matching antigen on a potentially dangerous cell. One mechanism used by cancer cells to avoid destruction is though inhibitory checkpoints by interacting with cytotoxic T-lymphocyte-associated protein 4 (CTLA4) and programmed cell death protein 1 (PD-1). Allison and Honja won the Nobel prize in physiology or medicine 2018 for their investigation of inhibition of negative immune regulation (Nobel Prize Organisation, 2022b). Another way of inhibiting cancer cell survival is by cell signal inhibitors. Cetuximab is an antibody that binds to EGFR and can inhibit cell growth (Fornasier, Francescon and Baldo, 2018). It is used to treat colorectal cancer, often in combination with chemotherapy or other drugs.

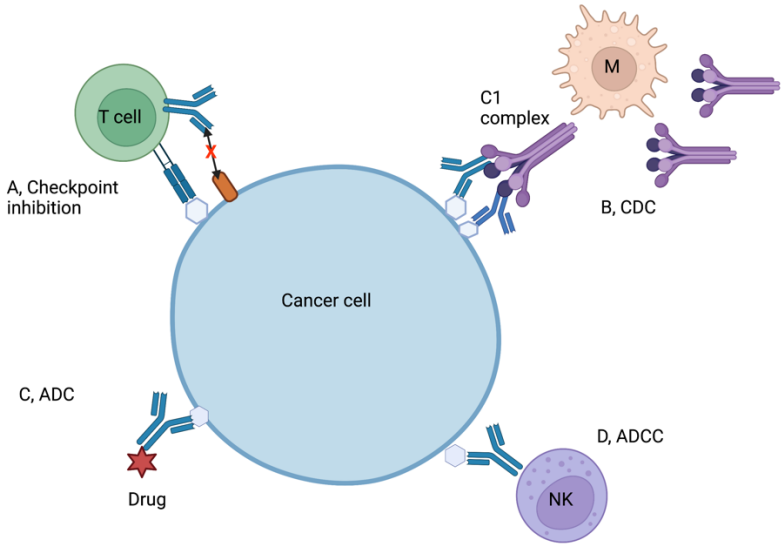

Figure 6. Illustration of some of the mechanisms used in passive immunotherapy. A, Checkpoint inhibition. **B**, Complement-dependent cytotoxicity. **C**, Antibody-drug conjugates. **D**, Antibody-dependent cell-mediated cytotoxicity. Abbreviations: Macrophage (M), Natural killer cell (NK). This figure was adapted by (Johannesen, 2020) with permission, and created using BioRender.

1.4.4 The monoclonal antibody 14F7

14F7 is a monoclonal IgG_1 antibody that binds specifically and with high affinity to *N*-glycolyl GM3 and discriminates it from *N*-acetyl GM3 (Carr *et al.*, 2000; Krengel *et al.*, 2004; Rojas *et al.*, 2004; Bjerregaard-Andersen *et al.*, 2018). *N*-glycolyl GM3 appears to be selectively expressed on malignant cells and not healthy cells, making the monoclonal antibody 14F7 a promising candidate for use in cancer treatment. The use of antibodies targeting antigens selectively expressed on malignant cells can minimize the interaction with healthy cells and reduce potential side effects.

This monoclonal antibody was developed in Havana, Cuba in 2000 by immunizing a BALB/c mouse with Neu5Gc GM3 coupled hydrophobically with very low-density human lipoproteins (Carr *et al.*, 2000), resulting in a m14F7 format. 14F7 was chimerized in 2008 (Roque-Navarro *et al.*, 2008) and later humanized in 2011 (Fernández-Marrero *et al.*, 2011). The structure of the 14F7 antigen-binding fragment (Fab) was solved in 2004 and suggested that the discrimination of the antigen is a result of a hydrophilic cavity (Krengel *et al.*, 2004). The structure of the scFv with an alternative light chain was later solved (Bjerregaard-Andersen *et al.*, 2018), followed by the crystal structure determination of 14F7 scFv in complex with the Neu5Gc GM3 trisaccharide (Bjerregaard-Andersen *et al.*, 2021).

The m14F7 was originally used for identification of Neu5Gc in melanoma and breast cancer tissue (Carr *et al.*, 2000), but showed the ability to kill murine tumor cells both *in vivo* and *in vitro* (Carr *et al.*, 2002). However, high concentrations of the antibody were needed to induce cytotoxic effects, therefore the antibody is an inefficient ADCC and CDC mediator. The cell-death mechanisms by 14F7 were further investigated in the murine cell line L1210 and P3X63, leading to observation of oncosis-like swelling, membrane lesion formation and cytoskeleton activation (Roque-Navarro *et al.*, 2008). The mechanisms for cell death observed in murine cell lines were retained for both the chimeric and humanized 14F7, but it was also reported that humanized 14F7 induced ADCC *in vivo* and *in vitro* (Roque-Navarro *et al.*, 2008; Dorvignit *et al.*, 2015).

1.4.5 14F7 formats

In addition to the murine and humanized 14F7 Fab formats produced in Cuba (Appendix F), a humanized 14F7 Fab format was constructed by our collaborator Anders Tveita at Institute for clinical medicine, Rikshospitalet, Oslo. He used the m14F7 V_H (Carr *et al.*, 2000) and the C1 V_L (Bjerregaard-Andersen *et al.*, 2018) and cloned the sequences into pFUSE expression vectors (Invivogen) containing the relevant constant region, following the manufacturer's instructions (personal communication).

Several scFv versions of 14F7 were produced and characterized by our group which retained the binding ability of the parental mAb (Bjerregaard-Andersen *et al.*, 2018, 2021). The construct with the highest stability and expression yields featured an alternative light chain variable region that was previously identified by phage display (Rojas *et al.*, 2004). The binding affinity of this construct and the humanized 14F7 produced in Cuba were compared by enzyme-linked immunosorbent assay (ELISA), estimating affinities of 4 nM and 2 nM respectively (Bjerregaard-Andersen *et al.*, 2018). Similar findings were previously reported for the m14F7 and 3Fm scFv (Rojas *et al.*, 2004). The antibody and scFv were in both publications reported to be Neu5Gc-specific and with no apparent cross-reactivity towards Neu5Ac GM3. The scFv was later coupled to the bioluminescent tag named NanoLuc (Nluc), prepared by our research group (Pesci, 2020). The enzymatic activity of the Nluc decrease in acidic conditions, making it a powerful tool for interaction studies *in vitro* (Hall *et al.*, 2012; Boute *et al.*, 2016). The preliminary experiments showed that the scFv-Nluc was functional and did internalize in different cell lines at different time points (Pesci, 2020).

1.5 Previous project-related work

1.5.1 Binding analysis and quantitative proteomics

The m14F7 developed in Cuba (section 1.4.4, sequence in Appendix F) was kindly provided by Center for Molecular Immunology, Havana (Carr *et al.*, 2000). This antibody was used by our research group for binding analysis using HeLa cells grown under normoxic (normal oxygen levels) and hypoxic conditions (Bousquet *et al.*, 2015, 2018). This study revealed that hypoxic conditions upregulated Neu5Gc GM3 expression in HeLa cells by three-fold. Changes in protein expression were also investigated by quantitative proteomics, revealing other proteins to also be significantly regulated. These proteins are involved in glycolysis, mitochondrial ribosomal proteins and translocases (Bousquet *et al.*, 2015).

For investigation of 14F7's recognition of its target Neu5Gc, a collection of HEK293 (human embryonic kidney) and CHO (Chinese hamster ovary) cells were utilized in the lab of our collaborator Prof. Henrik Clausen at University of Copenhagen. The collection consists of wild type (WT) cells, cells transfected with the *CMAH*-gene from chimpanzee to make knock-in cells expressing Neu5Gc GM3 (KI), and a B4GalT5/6 knock-out that prevent LacCer synthesis and therefore eliminate production of gangliosides (KO) (Yang *et al.*, 2015). We wanted to compare the binding of humanized 14F7 produced in Cuba bound to WT, KI and KO cells of both cell lines by flow cytometry. We were also interested in using neuraminidase to remove all sialic acids at the cell surface to use as an indication that Neu5Gc only binds to glycoconjugates. These experiments were performed by our group at Copenhagen Center for Glycomics in 2019, but due to time and sample restrictions, the measurements were only performed once (results unpublished).

1.5.2 Luminescence studies

The scFv coupled to a Nluc (Boute *et al.*, 2016; England, Ehlerding and Cai, 2016) was used in cell studies to evaluate the binding of the fusion protein to Neu5Gc GM3 and to investigate the internalization properties. Qualitative ELISA experiments confirmed the binding of the fusion protein to Neu5Gc GM3, and also revealed that the Nluc activity was retained while the protein is binding to the target (Pesci, 2020). These experiments were followed up by internalization experiments indicating that the scFv-Nluc was internalized, but through a kinetically slow internalization process. Of the cells used in this experiment, P3X63, HEK KI

and SKOV3 grown under both normoxic and hypoxic conditions, the murine P3X63 cells seemed to have the fastest uptake (Pesci, 2020). However, no additional controls were used to say if the putative internalization was specific or not.

1.6 Method-related theory

1.6.1 Flow cytometry

Flow cytometry is a laser-based technology to measure multiple physical and chemical characteristics of cells or particles. The technique can be used to measure cell size, granularity, and fluorescence intensity per cell. It is a widely used method for detection of whole cells and cellular components, such as organelles, DNA and protein content. This technique is based on light scattering and fluorescence emission. Flow cytometry is often referred to as fluorescence-activated cell sorting (FACS) because this technique provides a method for sorting cells based on specific characteristics from a heterogenous mixture.

The flow cytometer is composed of three main components: *the fluidic system*, *the optical system* and *the signal detection and processing system* (Figure 7). The fluidic system transports the cells from a solution and through the instrument. Sheath fluid is injected into the flow chamber to hydrodynamically focus the cells though a small nozzle. In this way, cells can pass the laser beam one cell at a time.

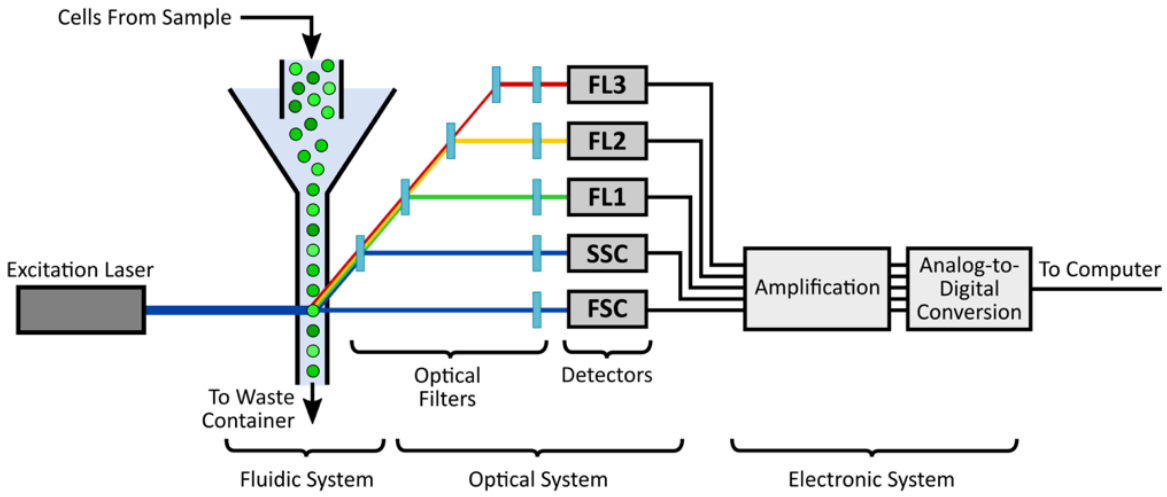

Figure 7. Schematic of a flow cytometer. The instrument consists of a fluidic system, optical system and electronic system. Cells from a sample are transported from solution and through the system. The cells are passed by the laser beam one cell at a time. Light from the laser is deflected at the edge of the cell and the scattered light (FSC and SSC) is detected. Filters are used to single out a specific wavelength for detection of fluorescence characteristics. Analog signals from the detectors are converted to a digital signal visible on a computer. Abbreviations: Forward scatter (FSC), side scatter (SSC), filter 1 (FL1), filter 2 (FL2), filter 3 (FL3). Figure from (Aatbio, 2019).

The optical system includes the laser, the lenses, and the collection optics. The laser and lenses shape and focus the laser beam (Adan *et al.*, 2017). When the light from the laser reaches the edges of the cell, the light will be deflected. This is known as light scattering (Figure 8). There are two types of light scattering; forward scatter (FSC) and side scatter (SSC), and these are affected by the cell or particle size and its internal complexity. FSC light is diffraction collected along the same axis as the laser beam and is proportional to cell size. SSC is collected 90 degrees to the laser beam and is mostly refracted and reflected light. The SSC is proportional to cell granularity.

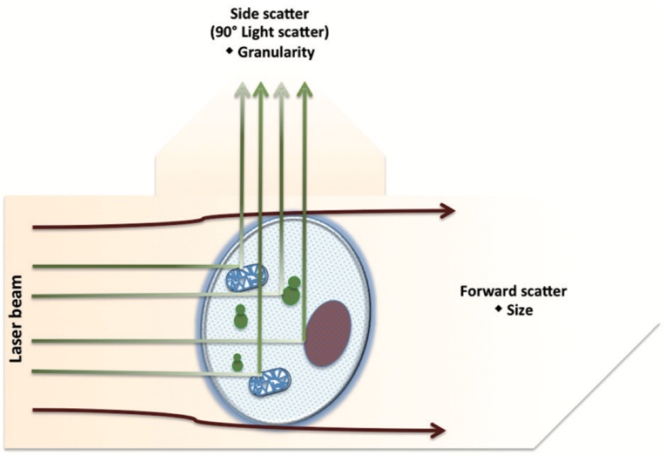

Figure 8. Light scattering. FSC is collected along the same axis as the laser beam and is proportional to cell size. SSC is collected 90 degrees to the laser beam and is proportional to cell granularity. Figure from (Adan *et al.*, 2017).

Flow cytometry can be used to detect a target protein by staining with a fluorochrome. The staining can either be directly with an antibody conjugated to a fluorochrome, or indirectly by using a primary antibody binding to the protein of interest and a fluorochrome-labeled secondary antibody binding to the primary. A fluorescent compound can absorb light energy at specific wavelengths, making electrons rise from the ground state to a higher energy level, known as an excited state. The electron falls quickly down to the ground state again, releasing energy as a photon of light (Adan *et al.*, 2017). The transition energy causing light is known as fluorescence and is reflected at the same angle as SSC (figure 8). Filters inside the flow cytometer are used to single out a specific fluorescence wavelength characteristic for a particular fluorochrome to be measured by a sensor (shown as FL1, FL2 and FL3 in figure 7).

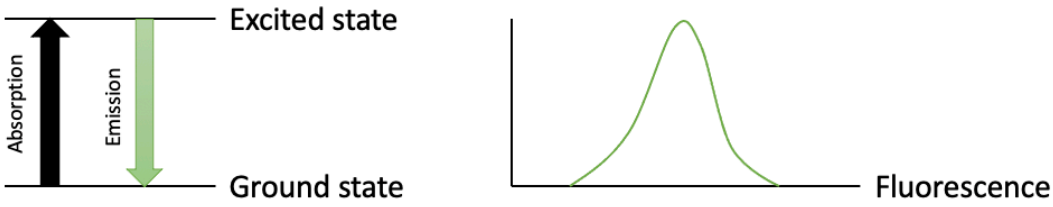

Figure 9. Schematic of energy absorption and emission leading to fluorescence. A fluorescent compound can absorb energy from light, making electrons rise to an excited state before it falls down again to the ground state and emits energy as fluorescence. This figure was created with Microsoft PowerPoint.

The signal from the cells flowing through the laser beam is detected and converted to voltage pulses, known as events, by sensors such as photodiodes (PDs) or photomultiplier tubes (PMTs) (Abcam). The flow cytometer measures the total pulse height and area, which correlates directly to the intensity of fluorescence for the event.

1.6.2 Confocal microscopy

Confocal microscopy is one type of light microscopy broadly used to image fixed or living tissue stained with one or more fluorescent probes. It is based on illuminating light and detection optics being focused on the same small spot in the sample, the focal point, that is imaged by the detector during a confocal scan (Figure 10A) (Elliott, 2020). The meaning of the word confocal refers to sharing the same focal point. This small spot is often referred to as the pinhole, and its purpose is to filter light so that only light from the focal plane is detected. By this, the out-of-focus light from the detector will not contribute to detection of blur in the image. This gives an image with high signal-to-noise ratio and greater contrast (Conchello and Lichtman, 2005). There are several types of confocal microscopes, such as the confocal laser scanning microscope (CLSM). A CLSM uses a laser beam the scans over the sample in x- and y-directions by the use of mirrors to produce an image of the optical section (Figure 10B).

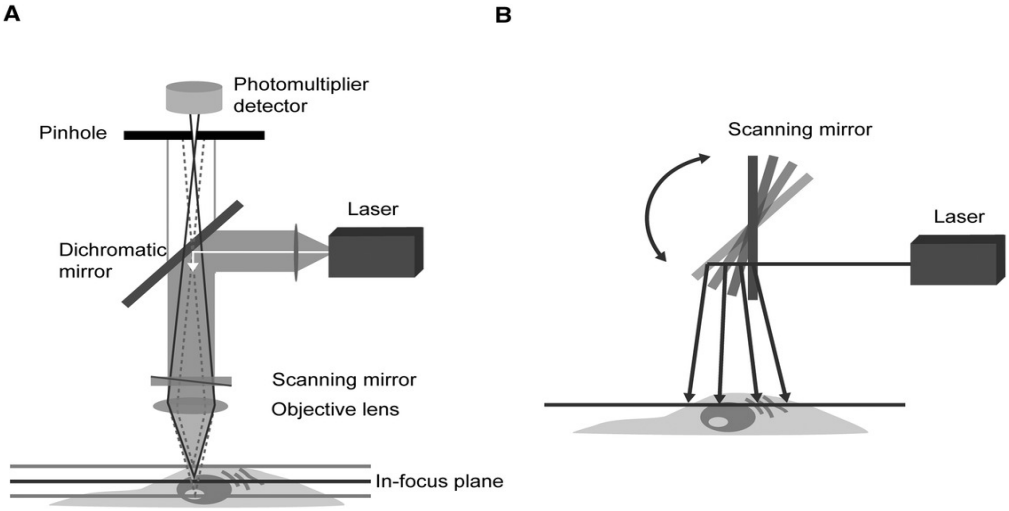

Figure 10. **Laser scanning confocal microscope.** A, Illustration of a confocal microscope. A laser beam is passed to a variable dichromatic mirror and reflected to the objective lens. The lens focuses the beam on a small point in the sample. B, Schematic of scanning mirrors sweeping over the sample point-by-point with the excitation beam to produce an image. Figure from (Elliott, 2020).

Imaging can be performed with live or fixed cells. There are several factors that must be considered when using live cells. First, the cells must be kept in an environment that does not induce stress that could alter cellular processes. Samples with mammalian cell lines should be kept at a stable 37 °C and with physiological pH level in the medium to hinder stress(Cole, 2014; Ettinger and Wittmann, 2014). The samples are therefore usually kept in a CO_2 chamber while performing live imaging. Another factor to consider is that illuminating light can cause artifacts in the living cells. Strong light used to excite fluorophores can lead to phototoxicity and photobleaching, resulting in a higher energy load on the cells causing impaired physiology or even death (Icha *et al.*, 2017). One strength of using live imaging is the specificity of labeling, imaging and analyzing proteins or cellular components that allow dynamic studies of biological processes (Ettinger and Wittmann, 2014).

1.6.3 Proteomics

The proteome is the entire set of proteins expressed by a genome, cell, organ or organism, and the study of the proteome under a defined set of conditions is known as proteomics (Aslam *et al.*, 2017). The proteome is highly complex and can be used to study i.e. the interaction of proteins and quantitative changes in a cell, tissue or organism (Graves and Haystead, 2002). As the proteome is dynamic and constantly submitted to environmental changes, the proteomic data will only give information about the protein environment at a certain time point. The environmental changes can be i.e., post-translational modifications,

translocations, up- or down-regulations or degradation. These data taken together can create a three-dimensional map of the cell's genome. Proteomics has a vital role in drug development, as well as diagnosis, prognosis and to monitor development of diseases(Aslam *et al.*, 2017). The term quantitative proteomics is used when quantitative differences are investigated in protein profiles of different samples (Pan *et al.*, 2009).

There are two main approaches for performing proteomic analysis of complex samples: top-down and bottom-up. In the top-down approach, intact proteins are injected into the MS before they are dissociated into fragments that together add up to the total mass of the protein (Figure 11). The main advantages for using this approach are the potential access to the complete protein sequence and the ability to characterize post-translational modifications (PTMs), while the limitations are that the approach works best for intact proteins under 50 kDa and that transferring intact proteins into gas-phase can be difficult due to high mass and their possibly different conditions for solubility (Wehr, 2006). In the bottom-up approach, proteins are cleaved into smaller peptides by proteolysis at specific positions in the amino acid sequence before peptide separation and detection (Figure 11) (Kelleher, 2004). The mass of the generated peptides is compared to theoretically generated peptides. Trypsin is commonly used for proteolysis as it cleaves by hydrolysis at the C-terminal end after the amino acids arginine (R) and lysine (L) if they are not followed by a proline (P). This proteomic approach is the most mature and widely used for identification and characterization of proteins, but is limited by i.e., that only a fraction of the protein is identified. When only a fraction of the protein sequence is obtained, the information about PTMs and alternative splicing products are lost (Wehr, 2006). The bottom-up approached was used in this thesis for protein determination using liquid chromatography (LC) coupled with mass spectrometry (MS) detection.

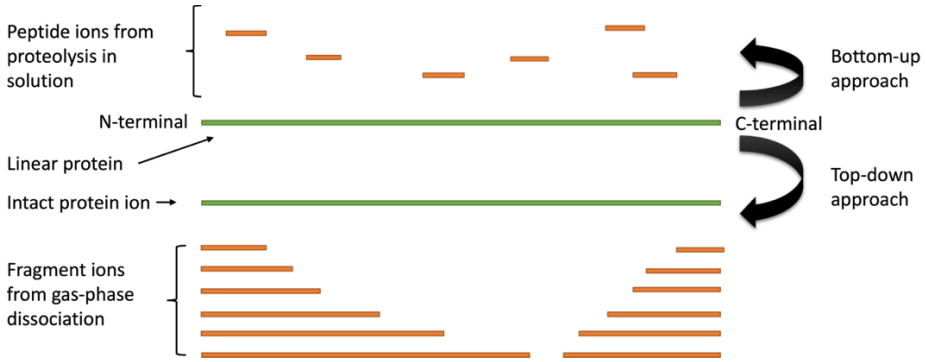

Figure 11. Illustration of the bottom-up and top-down approach for proteomics. In the bottom-up approach, proteins are cleaved into peptides that are analyzed. In the top-down approach, the intact protein ion together with fraction ions from gas-phase are analyzed. This figure was created using Microsoft PowerPoint and adapted from (Kelleher, 2004).

2. Aims of the thesis

The aim of this thesis was to investigate the antibody 14F7's target binding specificity, cellular localization and effects. To better understand 14F7's binding to Neu5Gc, we wanted to characterize different formats of 14F7 (section 1.4.5) to see which gave the strongest signal when bound to different cells. After finding the best suited format of 14F7, we wanted to investigate what happened to the cell when the antibody bound to its target. Work performed previously by our research group indicated by using bioluminescence that the antibody was internalized. The question was then where in the cell the antibody was internalized to and how are the uptake kinetics? Uncovering this information would be crucial for further work in developing 14F7 as a potential therapeutic agent for immunotherapy. Lastly, we wanted to gain insight to what happens inside the cell after antibody treatment by performing proteomic analysis. Understanding the processes and pathways involved leading up to cell death would also influence the further work on how 14F7 can be used clinically.

This thesis had three main objectives:

I. **Characterize the murine and two humanized versions of 14F7:** Using flow cytometry to compare the binding of different versions of 14F7 to different cell lines expressing its target and visualize the binding by confocal microscopy.
II. **Investigate the cellular localization of 14F7:** Using confocal microscopy to investigate internalization of 14F7 and its cellular localization.
III. **Investigate the effect of 14F7:** Using quantitative label-free proteomics to characterize the protein content in the cell upon antibody treatment and compare the regulated proteins for different cell lines.

3. Materials and methods

A complete list of chemicals and materials can be found in Appendix A and protocols for solutions and buffers in Appendix B.

3.1 Cells

3.1.1 Cell lines

Four different cell lines were used in the experiments of this thesis (Table 1). HEK293 is a human embryonic kidney cell line and is one of the most widely used cell lines in research. It was originally isolated by Alex Van der Eb in the 1970s, and the cell line was transformed by exposing cells to sheared fragments of human adenovirus type 5 DNA by Frank Graham (Graham *et al.*, 1977). The number 293 refers to Grahams 293rd experiment. The origin of the cell line is from a single healthy, electively terminated female fetus of unknown parentage. This cell line is throughout this thesis referred to as HEK wild type (WT). Two different knock-in strains of HEK293 cells have also been used. For both strains, the *CMAH*-gene from chimpanzee have been transfected to the WT cells, making the knock-in cells express Neu5Gc GM3. One construct, referred to as HEK KI Cph, has been made in the lab of our collaborator Prof. Henrik Clausen (Copenhagen Center for Glycomics, Denmark). They used zinc finger nucleases (ZFNs, Sigma-Aldrich) directed to *CMAH* to transfer the gene to unmodified WT HEK293 cells (Steentoft, Bennett and Clausen, 2013; Yang *et al.*, 2015). The other knock-in cell, referred to as HEK KI Oslo, was made in the lab of Anders Tveita (Rikshospitalet, Oslo, Norway). The HEK KI Oslo cells were made by retroviral transduction by bicistronic expression of *CMAH* and green fluorescent protein (GFP) separated by an internal ribosome entry site (IRES) element (personal communication). The vector used was MSCV-IRES-GFP (Addgene, cat. 20672), and cells that overexpressed GFP were selected for. One knock-out strain of HEK293 has also been used where the B4Gal5/6 gene, causing galactosylation, has been removed, referred to in this thesis as HEK KO Cph. The HEK WT, HEK KI Cph and HEK KO Cph cells were kindly provided by Henrik Clausen and HEK KI Oslo cells were kindly provided by Anders Tveita. The HEK KO Cph cells were only used when visiting the lab of Henrik Clausen at Copenhagen Center for Glycomics.

The murine cell lines used are L1210 and P3X63 Ag.8. The L1210 is a mouse lymphocytic leukemia cell line and the P3X63 is a mouse myeloma cell line (Table 1). CHO (Chinese hamster ovary) cells were also used, which is an epithelial cell line. The L1210 and P3X63 cells were kindly provided by Anders Tveita, while the CHO cells were only used for experiments performed when visiting the lab of Henrik Clausen at Copenhagen Center for Glycomics.

Table 1. **Name, origin of cell lines, medium for cultivation and supplier.**

Name of cell line	Origin	Medium	Supplier
CHO WT CHO KI CHO KO	Hamster	50/50 mixture of Ex-cell CD CHO Serum and BalanCD CHO Growth A	CHO WT, KI and KO were kindly provided by Copenhagen Center for Glycomics, Denmark
HEK293 WT HEK293 KI Cph HEK293 KI Oslo HEK293 KO Cph	Human	DMEM supplemented with 10% FBS and 1% Pen-Strep	HEK293 WT, KI Cph and KO Cph were kindly provided by Copenhagen Center for Glycomics, Denmark. HEK293 KI Oslo was kindly provided by Anders Tveita at Rikshospitalet, Oslo, Norway
L1210 WT	Mouse	RPMI 1640 supplemented with 10% FBS, 5 ml NEAA, 5 ml sodium pyruvate and 5 ml Pen–Strep	L1210 was kindly provided by Anders Tveita at Rikshospitalet, Oslo, Norway
P3X63 Ag.8 WT	Mouse	RPMI 1640 supplemented with 10% FBS, 5 ml NEAA, 5 ml sodium pyruvate and 5 ml Pen-Strep	L1210 was kindly provided by Anders Tveita at Rikshospitalet, Oslo, Norway

3.1.2 Cell cultivation and seeding

The HEK cells are adherent cells, meaning they attach to the bottom of the cell flask when cultivated. To loosen the cells from a T25 cell flask, the old medium was aspirated, the cells were washed once with 5 ml preheated PBS by tilting the cell flask carefully from side to side before the PBS was aspirated, and 1 ml of preheated trypsin with ethylene diamine-tetra-acetic acid (EDTA, Lonza) was added and incubated at 37 °C for 3 minutes. Trypsin is a protease that cleaves C-terminally lysine or arginine. EDTA is often included in the trypsin mixture as it chelates the divalent cations (i.e., Ca^{2+}, Mg^{2+}) and weakens the interaction between cells. The cell flask was taken out from the incubator after 3 minutes and the cells were observed under a light microscope to ensure that the cells had loosened from the flask.

4 ml of preheated medium was added, and the cells resuspended thoroughly to remove cell clusters. After obtaining a cell suspension, the cells were seeded in various dilutions depending on the confluency in the cell flask and the number of days from seeding until analysis was to be performed. The confluency in the cell flask was determined by observation of the cells under a light microscope. The HEK cell line was cultivated in Dulbecco's Modified Eagle Medium (DMEM, Gibco) supplied with 10% Fetal Bovine Serum (FBS, Biochrom) and 1% Penicillin-Streptomycin (Pen-Strep, Lonza). The cell line was cultivated in T25 flasks (25 cm^2, VWR) and incubated at 37 °C with 80% humidity and 5 % CO_2 in a 371 Steri-Cycle CO_2 incubator. The work with HEK cells was performed in three different labs. The cell work for flow cytometry experiments and sample preparation for proteomics was performed in the lab of Ass. Prof. Nina F. J. Edin at the Department of Biological and Medical Physics, imaging experiments were performed in the lab of Prof. Cinzia Progida at the Department of Biosciences and the experiments comparing HEK and CHO cells in the lab of Prof. Henrik Clausen at Copenhagen Center for Glycomics.

The L1210, P3X63 and CHO cell lines are suspension cells, meaning the cells float in suspension when cultivated. The murine cell lines were cultivated in Roswell Park Memorial Institute (RPMI, Lonza) 1640 supplied with 10% FBS, 5 ml MEM Non-Essential Amino Acid solution (NEAA, Thermo Scientific), 5ml sodium pyruvate and 5 ml Pen-Strep. The cell counter Iprasense with the software Norma XS was used for cell counting. The amount of wanted cells were transferred from the old flask and into a new, and fresh, pre-heated medium was added to a total volume of 5 ml. Both murine cell lines were cultivated in T25 flasks and incubated at 37 °C with 80% humidity and 5 % CO_2 in a 371 Steri-Cycle CO_2 incubator. The CHO cells were cultivated in Nunc cell culture 6 well plates with a 50/50 mixture of Ex-cell CD CHO Serum (SAFC) and BalanCD CHO Growth A (Fujifilm). These cells were counted manually using a cell counter chamber and trypan blue (Gibco) to distinguish between alive and dead cells. The amount of wanted cells were transferred to a new well and fresh medium was added to a total volume of 2 ml. The 6 well plate was incubated at 37 °C with 80% humidity and 5 % CO_2. The work with L1210 and P3X63 Ag.8 cells was performed in the lab of Ass. Prof. Nina F. J. Edin at the Department of Biological and Medical Physics and the work with CHO cells was performed in the lab of Prof. Henrik Clausen at Copenhagen Center for Glycomics.

All cell treatment during seeding and cultivation was performed under stile conditions in a Laminar Air Flow (LAF) bench in the lab where the cell work was performed. The surfaces inside the LAF bench were washed with 70% ethanol before and after use, and all equipment and flasks containing solutions were wiped down with 70% ethanol before placed inside the LAF bench.

3.1.3 Hypoxia

HEK WT cells were grown under hypoxic conditions (4 % O_2, 5 % CO_2, 37 °C) in a hypoxia chamber (INVIVO$_2$ 1000). 4% oxygen in gas phase gives a much lower concentration of oxygen within the cells. A 100% confluent cell flask will have an oxygen level under 0.1 %. The cells were grown in hypoxia for two different purposes. Firstly, we wanted to observe how HEK WT cells grow under hypoxic conditions. To do so, newly seeded cells in T25 flasks were placed inside the hypoxia chamber and one flask was taken out every 24 hours for seven days and the cells counted using Iprasense. This was performed in parallel with cells grown in T25 flasks under normoxic conditions. For the second purpose, we wanted to investigate if HEK WT cells express Neu5Gc GM3 under these conditions. Cells grown in T25 flasks to a confluency of 70-80% were put into the hypoxia chamber and incubated for 24 or 72 hours before they were analyzed by flow cytometry. All equipment and solutions were placed inside the chamber 24 hours prior to the cells.

3.2 The antibody 14F7

3.2.1 Constructs of 14F7

Three different constructs of 14F7 were used in this thesis, two humanized 14F7 and one murine (Table 2). One of the humanized constructs was developed and kindly provided by Center for Molecular Immunology in Cuba, referred to as h14F7 throughout this thesis. The amount of this antibody available to us is limited. A second humanized 14F7 format was developed and kindly provided by Anders Tveita at Rikshospitalet in Oslo. This format has throughout this thesis been referred to as h14F7* Oslo. Amino acid sequences for these three formats can be found in Appendix F.

Table 2. The different construct of the primary antibody 14F7 used in this thesis.

Name	Concentration of stock	Supplier
Humanized 14F7 (h14F7)	5 mg/ml	Kindly provided by Center for Molecular Immunology, Cuba (Fernández-Marrero *et al.*, 2011)
Humanized 14F7 (h14F7*)	1 mg/ml	Kindly provided by Anders Tveita at Rikshospitalet, Oslo
Murine 14F7 (m14F7)	1 mg/ml	Creative Biolabs Ref: PABC-051 First developed by (Carr *et al.*, 2000)

3.2.2 Conjugation of 14F7

Conjugation of m14F7 and h14F7* was performed using Alexa Fluor 647 Antibody Labeling Kit (Thermo Scientific, Cat. A20186), making the labeled antibody absorb light at 650 nm. The conjugation was performed following the manufacturer's protocol. The 1M sodium bicarbonate solution that followed in the kit was not used, but a fresh solution was prepared the day before the labeling and stored at 4 °C. The antibody to be labeled was diluted to 1 mg/ml and added 1/10th volume of 1M sodium bicarbonate buffer. 100 µl of the prepared antibody solution was transferred to a vial of reactive dye. The vial was closed properly and inverted gently a few times, before one hour of incubation at room temperature. The vial was gently inverted every 10 minutes during the incubation. A spin column was placed in a 13x100 mm class tube. The two frits in the bottom of the column were wetted with Milli-Q

H_2O before the resin was added to the column. The purification resin was stirred before 1.0 mL of the suspension was added to the column and let set by gravity. The suspension was added until a resin bed volume of 1.5 ml. The column buffer was drained into a collection tube by 3 minutes of centrifugation at 1100 rcf. 100 μl of the labeled antibody was added dropwise to the center of the spin column. After the solution had absorbed into the resin bed, the column was placed into an empty collection tube and centrifuged for 5 minutes at 1100 rcf. After centrifugation, the collection tube contained labeled protein in approximately 100 μl of PBS with a pH of 7.2 with 2 mM sodium azide. 100 μg of 14F7 was used, resulting in about 100 μl of 0.33 mg/ml conjugated m14F7 and 100 μl of 0.58 mg/ml conjugated h14F7*.

3.3 Flow cytometry

The experiments described in section 3.3. have been performed using flow cytometry to measure the fluorescence emission. The detection of bound antibody described in section 3.3.1-3.3.2 and 3.3.4-3.3.6 was performed using the BD Accuri C6 Flow Cytometer (BD Biosciences, USA) located at the Department of Biological and Medical Physics, University of Oslo. The acquired data from these experiments was processed using the software CFlow Plus (Accuri). The detection for bound antibody and controls described in section 3.3.3 was performed using the Spectral Cell Analyzer SA3800 (Sony Biotechnology, USA) located at Copenhagen Center for Glycomics, University of Copenhagen. The acquired data from this experiment was processed using FlowJo X (BD Biosciences).

3.3.1 Protocol for comparison of the binding of 14F7 to different murine and mammalian cell lines

Every replicate of each cell line was grown in individual T25 cell flasks for 3-4 days until the cells reached 80-90 % confluency (see section 4.1.2 for cell cultivation and seeding). The old medium was aspirated, and 1 ml of pre-heated Trypsin EDTA (200 mg/L, Lonza) was added to the cell flask and incubated for 3 minutes at 37 °C. Then 4 ml of fresh, pre-heated medium was added, and the cells resuspended thoroughly. The cell suspension was transferred to a 15 ml Falcon tube and spun down at 200 rcf for 5 minutes. The supernatant was discarded, and the cells were washed by adding 1 ml of wash buffer (49 ml PBS, 1 ml FBS and 200 μl of 0.5 M EDTA (Sigma-Aldrich)) and spun down at 200 rcf for 5 minutes. The supernatant was discarded, and the cells were washed once more. The cells were fixed in 4 % PFA (see Appendix B) for 15 minutes on ice and in the dark. The cells were washed two times before they were split into two 1.5 ml Eppendorf tubes, where half of the cells were incubated in 50 μl of the primary antibody 14F7 (murine or humanized Cuba/Oslo, Table 3) and the other half with 50 μl wash buffer for 1 hour on ice and in the dark. The samples were then washed twice before both samples were incubated with 50 μl secondary antibody for 30 minutes on ice and in the dark. Anti-human secondary antibody was used for humanized 14F7 as primary antibody and anti-mouse for m14F7. The sample not incubated with a primary antibody was given the same secondary antibody as the parallel sample. After another washing step, the cells were incubated for 15 minutes with the FACS buffer (36.8 ml PBS, 12.5 ml of 0.4 mg/ml RNase (Sigma-Aldrich), 0.7 ml of 1 mg/ml Propidium iodide (PI, Thermo Scientific)) on ice and in the dark before they were filtered and analyzed by flow cytometry.

Table 3. Cell lines, primary and secondary antibodies used for comparison of the binding of 14F7 to different murine and mammalian cell lines.

Cell line	Primary antibody	Secondary antibody
L1210	m14F7	Goat anti-mouse FITC (Abcam, Ref: ab6785, LOT: GR3274516-6)
P3X63 Ag.8	m14F7	Goat anti-mouse FITC (Abcam, Ref: ab6785, LOT: GR3274516-6)
HEK WT	m14F7	Goat anti-mouse Alexa Fluor 647 IgG (Invitrogen, Ref: A32728)
HEK KI Copen	m14F7	Goat anti-mouse Alexa Fluor 647 IgG (Invitrogen, Ref: A32728)
HEK KI Oslo	m14F7	Goat anti-mouse Alexa Fluor 647 IgG (Invitrogen, Ref: A32728)
HEK WT	h14F7*	Goat anti-human Alexa Fluor 647 IgG (Invitrogen, Ref: A21445)
HEK KI Copen	h14F7*	Goat anti-human Alexa Fluor 647 IgG (Invitrogen, Ref: A21445)
HEK KI Oslo	h14F7*	Goat anti-human Alexa Fluor 647 IgG (Invitrogen, Ref: A21445)

4.3.2 Protocol for HEK WT cells grown under hypoxia

Approximately 0.2 * 10^5 HEK WT cells were seeded in 14 individual T25 cell flasks. Seven of the cell flasks were placed under normoxic conditions and the other seven under hypoxic conditions (see section 3.1.3). One cell flask grown under each of the two conditions were taken out every 24 hours for seven days and counted using Iprasense. To obtain a cell suspension, the cells grown under normoxic conditions were trypsinized and resuspended in fresh, warm medium in a LAF bench (section 3.1.2) and cells grown under hypoxic conditions were handled corresponding inside the hypoxia chamber. The amounts of cells were plotted in a scatter graph in Microsoft Excel and an exponential trendline was added for each growth condition.

HEK WT cells were seeded in new T25 flasks and incubated under normoxic conditions until reaching a confluency of 80-90 %. The cell flasks were then placed inside the hypoxia chamber for 24 or 72 hours. When taking the flasks out, the cells were trypsinized with 1 ml

inside the hypoxic chamber and then 4 ml medium was added. The cell suspension was resuspended thoroughly before spun down at 200 rcf for 5 minutes. The cells were then washed two times with wash buffer and then fixed with 4% PFA inside the hypoxic chamber. The further steps for flow cytometry preparation of the cells were as stated in section 3.3.1 (experiment A). The primary antibody used was m14F7 and goat anti-mouse conjugated to FITC as the secondary antibody.

3.3.3 Protocol for binding of 14F7 to HEK and CHO cells

Cells were grown in Nunc cell culture 6 well plates (Thermo Scientific) until they reached 80 % confluency. The old medium was aspirated from the wells containing HEK cells, and the wells were added 300 μl trypsin each. After 3 minutes, the cells had detached from the bottom of the well and 1 ml of medium was added. The cell suspension was thoroughly resuspended before it was transferred to a 15 ml falcon tube and spun down at 300 rcf for 2 minutes. The cell suspension in the wells containing CHO cells was directly transferred to 15 ml falcon tubes and spun down. The supernatant was discarded, and the cells were washed twice with1 ml PBS and spun down at 300 rcf for 2 minutes. After the supernatant was discarded, the pellet was redissolved in 1 ml PBS before the cell suspension was split into two 15 ml falcon tubes, where one of the two falcon tubes was added 10 μl neuraminidase (10 U/ml, Sigma-Aldrich). The two falcon tubes with cell suspension were incubated for 1 hour at 37 °C. The cells were then washed two times and the pellet was resuspended in PBS. 100 μl of the cell suspension was transferred to the wanted wells on a 96 well cell culture plate (Sigma-Aldrich. The 96 well plate was spun down at 300 rcf for 2 minutes and the supernatant discarded by turning the plate quickly upside down over then sink and then tapping the plate lightly on a stack of paper. The wells were then added 50 μl of either the antibody 14F7, PNA (Vector Laboratories), anti-Neu5Gc (Biolegend) or FACS buffer (PBS with 1% BSA, Sigma-Aldrich) and incubated 1 hour on ice and in the dark (Table 4). The cells were then washed twice with 100 μl FACS buffer, before added 50 μl of either secondary antibody or PanLectenz complex (Lectenz Bio) and incubated for 1 hour on ice and in the dark. The cells were then washed twice and resuspended in 100 μl FACS buffer before analyzed by flow cytometry.

Table 4. Primary and secondary antibodies used for binding of 14F7 to CHO and HEK cells, and the dilution series used for HEK and CHO cell lines.

Primary antibody	Secondary antibody	Dilution series for HEK cells	Dilution series for CHO cells
h14F7	Goat anti-human Alexa Fluor 647	5 – 2.5 - 1.25 - 0.675 μg/ml	5 – 2.5 - 1.25 - 0.675 μg/ml
h14F7*	Goat anti-human Alexa Fluor 647 IgG	5 – 2.5 - 1.25 - 0.675 μg/ml	-
PNA	Streptavidin Alexa Fluor 647 conjugate	0.1 – 0.05 – 0.025 μg/ml	0.05 – 0.025 μg/ml
Neu5Gc	Goat anti-chicken Alexa Fluor 488	1:1000	1:1000
-	PanLectenz pre-complex mixed with Streptavidin Alexa Fluor 647 conjugate	1 – 0.5 – 0.25 μg/ml	0.5 μg/ml
-	Mixture of secondary antibodies	-	-

3.3.4 Protocol for comparison of EGFR on HEK WT, KI Cph and KI Oslo cells

Cells were seeded and treated as described in section 4.3.1. Cetuximab, a chimeric antibody binding to EGFR on the cell surface (Berger *et al.*, 2011), was used as primary antibody and goat anti-human Alexa Fluor 647 as secondary antibody.

3.3.5 Protocol for incubation of 14F7 to visualize possible cell death

Cells were seeded in 24 well plates (Thermo Scientific) and grown at 37 °C until reaching a confluency of about 80%. The old medium was aspirated, and half of the wells were added 14F7 diluted in DMEM supplemented with 10% FBS and 1% Pen-Strep to a final concentration of 60 μg/ml, while the other wells were added medium without antibody. M14F7 was used for the murine cell lines P3X63 and L1210 and h14F7 for HEK WT and KI Cph. Samples were incubated for 24, 26 or 50 hours at 37 °C, before they were trypsinized with a few drops of trypsin and incubated for 3 minutes at 37 °C. Preheated medium was added to the wells and the cells were resuspended and transferred to 15 ml falcon tubes. The cells were spun down at 200 rcf for 5 minutes at 4 °C and the supernatant was removed.

The cells were washed twice by adding 1 ml PBS and spun down at 200 rcf for 5 min at 4 °C, and the supernatant aspirated. Lastly, the cell pellet was solved in 250 μl PBS before 1 μl PI (1 mg/ml) was added. The samples were filtrated and analyzed by flow cytometry.

3.3.6 Protocol for binding of conjugated murine and humanized 14F7

Every replicate of each cell line was grown in individual T25 cell flasks for 3-4 days until the cells reached 80-90 % confluency. The old medium was aspirated, and 1 ml of pre-heated trypsin was added to the cell flask and incubated for 3 minutes at 37 °C. Then 4 ml of fresh, pre-heated medium was added, and the cells resuspended thoroughly. The cell suspension was transferred to a 15 ml Falcon tube and spun down at 200 rcf for 5 minutes. The supernatant was discarded, and the cells were washed by adding 1 ml of wash buffer (49 ml PBS, 1 ml FBS and 200 μl EDTA) and spun down at 200 rcf for 5 minutes. The supernatant was discarded, and the cells were washed once more. The cells were fixed in 4 % PFA for 15 minutes on ice and in the dark. The cells were washed two times before they were split into four 1.5 ml Eppendorf tubes (table). One sample was not added any antibody, the second was added 50 μl of the primary antibody (m14F7 or h14F7*), the third was added 50 μl wash buffer and the fourth added 50 μl conjugated antibody (murine or humanized, section 4.2.2). All samples were incubated for 1 hour on ice and in the dark. All samples were then washed twice. The first and fourth sample were left on ice and in the dark while the last steps were carried out for the two other samples. The second and third sample were incubated with 50 μl secondary antibody (goat anti-mouse Alexa Fluor 647 for m14F7 and goat anti-human Alexa Fluor 647 for h14F7*) for 30 minutes on ice and in the dark. Anti-human secondary antibody was used for the h14F7* as primary antibody and anti-mouse for m14F7. After washing the second and third sample, all four samples were incubated for 15 minutes with FACS buffer (36.8 ml PBS, 12.5 ml RNase, 0.7 ml PI) on ice and in the dark before they were filtered and analyzed by flow cytometry.

3.3.7 Analysis

FSC and SSC were used to gate the single cells of the wanted population, as illustrated in Figure 12. Figure 11A shows gating of the wanted population using FSC at the x-axis and SSC at the y-axis. Figure 11B shows gating of single cells using FSC area at the x-axis and FSC height at the y-axis. Gating of all replicates for all experiments were performed similarly.

Propidium iodide (PI) was used in the FACS buffer for experiments described in section 3.3.1-2, 3.3.4 and 3.3.6 to further select the cells in the G1 phase in the cell cycle to have a more homogenous population of cells for the detection of fluorescent signals. PI was also added to the cells in section 3.3.5 before analysis by flow cytometry. Cells in this experiment were not fixed and therefore alive when measured with the flow cytometer. Cells in the process of dying or with ruptured membrane will take up PI, and this allows to detect viable cells from the rest of the cells, which was the purpose of the experiment in section 3.3.5.

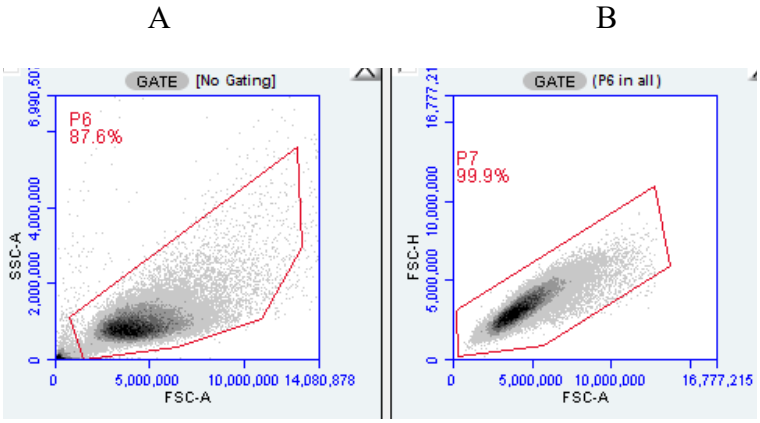

Figure 12. Illustration of gating for FSC and SSC. A, Gating of wanted population for SSC plotted against FSC. **B,** Gating of single cells for FSC height plotted against FSC area.

3.4 Imaging

Imaging has been used for the purpose of experiments described in section 3.3.1, 3.3.6, 3.4.3 and 3.4.4. The fixed cells left over from flow cytometry analysis described in section 3.3.1 and 3.3.6 were mounted on microscope slides and imaged (section 3.4.2). Cells imaged from the protocols described in section 3.4.3 and 3.4.4 were stained differently.

3.4.1 Confocal microscopy

Confocal imaging was conducted using PlanApo 60x/1.35 oil immersion objective on an Olympus FV1000 confocal laser scanning microscope. Acquired images were processed using the software Fiji (ImageJ).

3.4.2 Protocol for mounting fixed cells on microscope slides

Cells left over from flow cytometry experiment B were used for imaging. The cells were stored in 1.5 ml Eppendorf tubes at 4 °C after the FACS analysis. To mount the cells on microscope slides (Thermo Scientific), the Eppendorf tubes were spun down at 200 rcf for 5 minutes and the supernatant was removed. The cell pellet was dissolved by adding 10 μl Mowiol (Sigma-Aldrich) and vortexed for 20 seconds. The 10 μl of cell suspension was transferred to a microscope slide and covered with a coverslip (Hecht Assistant). The microscope slide was kept in a covered chamber at room temperature overnight, and then stored in the dark at 4 °C until images were acquired.

3.4.3 Protocol for imaging binding of 14F7 on the cell surface and inside the cell

One coverslip (Hecht Assistant) was placed per well in a 24 well plate (Thermo Scientific). The coverslips were each coated with 200 μl of 20 μg/ml Fibronectin (Sigma-Aldrich) and left inside the LAF bench at room temperature for 2 hours. The coverslips were then washed four times by adding 400 μl PBS (Sigma-Aldrich) and tilting the plate slightly, before removing the PBS. Each coverslip was seeded with $0.75*10^5$ HEK KI Oslo cells and placed in the incubator at 37 °C for about 48 hours to reach a confluency 80-90%. The 24 well plate with

the coverslips inside the wells was taken out from the incubator and the cells were washed one time with PBS prior to fixation with 200 μl of 4% PFA (Merck) for 15 minutes at room temperature inside a fume hood. Afterwards, the cells were washed three times with PBS. For comparison of 14F7 binding to receptors on the cell surface and to receptors inside the cells, half of the samples were permeabilized with 0.1% Triton X–100 (Sigma-Aldrich) for 4 minutes at room temperature and in the dark. The permeabilized samples were washed three times with PBS before all samples were blocked with 5% FCS (Sigma-Aldrich) solved in PBS + 0.02% sodium azide (Sigma-Aldrich) for 30 minutes at room temperature and in the dark and finally washed one time with PBS. For staining, the cells were incubated with either 20 μl h14F7* (Appendix A Table S1) or 20 μl PBS for one hour in a wet and covered chamber at room temperature. All samples were washed three times with PBS before they were all stained with 20 μl goat anti-human Alexa Fluor 647 (Appendix A Table S2) for 30 minutes in a wet and covered chamber at room temperature. All samples were again washed three times with PBS and stained with 200 μl DAPI (1:5000 dilution) for 5 minutes in the 24 well plate at room temperature. DAPI is a fluorescent dye for nucleic acid staining. After staining, the coverslips were washed one time with PBS and rinsed one time with distilled water, before the coverslips were mounted with 10 μl Mowiol, a hydrophilic mounting medium, on microscope slides and left to set overnight in a covered chamber at room temperature.

3.4.4 Protocol for immunofluorescent staining

Coverslips were coated with fibronectin and seeded with HEK KI Oslo cells as described in section 4.4.2. The 24 well plate with the coverslips inside the wells was taken out from the incubator and the cells were washed one time with PBS prior to fixation with 200 μl of 4% PFA for 15 minutes at room temperature inside a fume hood. Afterwards, the cells were washed three times with PBS. All samples were permeabilized with 0.25% Saponin for 10 minutes at room temperature and in the dark. Analysis of 14F7 intracellular localization relative to the endocytic pathway was performed by labeling the early and late endosome using antibodies specific for EEA1 (early endosome) and Lamp (late endosome). The samples were first stained with 20 μl h14F7* (1:100 dilution) for one hour in a wet and covered chamber. The samples were washed three times in 0.25% saponin for 5 minutes, before they were incubated with 20 μl goat anti-human Alexa Fluor Alexa Fluor 647 (1:400 dilution) for 30 minutes in a wet and covered chamber. The samples were again washed three times with 0.25% saponin for 5 minutes before they were incubated with either 20 μl

mouse anti-EEA1 (1:200 dilution) or 20 μl mouse anti-Lamp1 (1:1000 dilution) for one hour in a wet and covered chamber. The samples were washed three times and then incubated with 20 μl goat anti-mouse Alexa Fluor 555 (1:500 dilution) for 30 minutes in a wet and covered chamber. All samples were again washed three times with 0.25% Saponin and stained with 200 μl DAPI (1:5000 dilution) for 5 minutes in the 24 well plate at room temperature. After staining, the coverslips were washed one time with PBS and rinsed one time with distilled water, before the coverslips were mounted with 10 μl Mowiol on microscope slides and left to set overnight in a covered chamber at room temperature. Controls were included to make sure there was no cross-binding between antibodies from different species (See Appendix D). The controls were prepared in parallel to the samples but were only incubated with one primary antibody and one secondary antibody. One control was incubated with humanized 14F7 and goat anti-mouse Alexa Fluor 555, a second with mouse EEA1 and goat anti-human Alexa Fluor 647, and a third with mouse Lamp1 and goat anti-human Alexa Fluor 647.

3.5 Proteomic analysis

Proteomic analysis was used for the purpose of experiment F. Preparation of the samples until freezing was performed at Department of Biological and Medical Physics, University of Oslo. Following label-free quantitative proteome analysis was done at the Proteomics Core Facility at Rikshospitalet, Oslo.

3.5.1 Protocol for proteomic analysis of untreated and 14F7-treated cells

Preparation of samples:
Cells were grown in individual cell flasks until a confluency of 80-90 %. About 10 x 10^5 cells were transferred to one well on a Nunc cell culture 6-well plate and another 10 x 10^5 cells to another well. The plate was incubated until the next day to let the cells adhere to the bottom of the well. The next day, the medium was aspirated and replaced with fresh, warm serum-free medium. One of the wells was added 0.125 μg 14F7 and the plate was incubated for 3 hours at 37 °C. The cells from each well were then transferred to 15 ml falcon tubes and spun down at 200 rcf for 5 minutes. The supernatant was discarded, and the pellet was solved in PBS and transferred to a 1.5 ml Eppendorf tube before another round of centrifugation at 200 rcf for 5 minutes. The supernatant was discarded, and the pellet was resolved in 300 μl PBS and immediately flash frozen in liquid nitrogen and stored in a freezer at –80 °C until analysis. The experiment was performed in triplicates and the cell lines HEK WT and HEK KI Oslo were added h14F7, while the cell line L1210 was added m14F7.

Cell lysis:
All samples were thawed on ice and centrifuged at 3000 rcf to pellet the cells. Pellets were not observed for the samples containing L1210 cells. These samples were added 25 μl of 10% SDS to 500 μl sample. For the other samples containing HEK cells, the supernatant was removed, and the pellet was dissolved in 50 μl of RIPA buffer containing protease inhibitors. All samples were vortexed and sonicated for 10 seconds (25%) with the probe sonicator. Protein concentration was measured with BCA.

Protein aggregation capture and digestion:
A volume corresponding to 15 μg was used for each sample, and buffer was added up to 50 μl. 120 μl ACN and 10 μl MAgReSyn Amine beads (20 mg/ml, ReSyn Biosciences) was added. The samples were vortexed, then let stand for 10 minutes before vortexed again and

kept at room temperature for 10 minutes. The tubes were transferred to a magnetic stand and the supernatant was discarded. The beads were washed first with 100 µl of ACN, then 100 µl of 70% ethanol and then dried for 5 minutes at room temperature. The beads were dissolved in 100 µl of 50 mM NH_4HCO_3, before 1 µl of 0.5 M DTT was added and incubated for 30 minutes at 56 °C. 2.7 µl of 550 mM IAA was added and incubated for 20 minutes in the dark at room temperature. 1 µg of Trypsin was added, and protein was digested overnight at 37 °C.

Purification and LC-MS analysis:
The samples were purified by liquid chromatography (LC) and analyzed by mass spectrometry (MS) using NanoElute TimsTOF with a C18 Aurora 25 cm column. The injection volume was 1 µl and the gradient 60 minutes.

3.5.2 Protein identification and label-free quantification

The resulting tryptic peptides were purified using home-made C18 Stage tips-columns followed by nanoLC-MS/MS analysis using nanoElute coupled to timsFOF flex (Bruker). For protein identification and label-free quantification the data from LC-MS/MS was analyzed by MaxQuant ver. 2.0.1.0 and Perseus ver. 1.6.1.5. For quantitative comparison the LFQ-values were log10 transformed, filtered with a minimum of 2 out of 3 valid values in at least one group, missing values were imputed from normal distribution and t-test with $p<0.05$ as the criteria was done.

3.5.3 Data illustration

The analyzed data was further categorized by the bioinformatic tools Funrich (http://funrich.org) and Panther (http://www.pantherdb.org) into biological process and protein class of the up-and downregulated proteins. The figures for illustrating the proteomics data were created using Origin.

4. Results

In preparation for clinical studies, we compared the effect of different formats of the anti-tumor antibody 14F7 on different cells. To simulate the expression of Neu5Gc GM3 in cancer cells, we used two constructs of knock-in cells. Flow cytometry was used to determine the antibody format and the KI cells with strongest binding (Section 4.1). We further used confocal microscopy (Section 4.2) and quantitative proteomics (Section 4.3) to investigate 14F7's intracellular localization and effects.

Raw data from flow cytometry experiments can be found in Appendix C, and controls for experiments where confocal microscopy was used in Appendix D. The mass spectrometry proteomics data will be deposited to the ProteomeXchange Consortium (http://proteomecentral.proteomexchange.org/cgi/GetDataset) via the PRIDE partner repository.

4.1 Characterization of different 14F7 formats

4.1.1 Comparison of the binding of 14F7 to different murine and mammalian cell lines by flow cytometry and microscopy

A protocol established by Bousquet *et al.* (2015) for measuring the binding of 14F7 to HeLa cells using flow cytometry was optimized to use for HEK cells. Binding analysis using flow cytometry with four different conditions on HEK WT, KI Cph and KI Oslo were performed. The cells were treated with either m14F7 or h14F7* as primary antibody, and secondary antibody conjugated to FITC or Alexa Fluor 647 (AF647). The averages of the median fluorescent signals are showed in a bar plot (Figure 13 panel A). The bars represent one experiment each with three independent biological replicates for each condition, except for the condition using m14F7 as primary antibody and goat anti-mouse FITC as secondary antibody where only two independent biological replicates were carried out. Figure 13 panel A illustrate cells incubated with primary and secondary antibody, with cells incubated in parallel with only secondary antibody. This was used to detect if the secondary antibody bound to something in the sample and gave a fluorescent signal. The red bars indicate cells incubated with m14F7 as primary antibody and anti-mouse Alexa Fluor 647 (AF647) as secondary antibody. The cyan bars indicate cells incubated with h14F7* as primary antibody

and anti-human AF647 as secondary antibody. The same trend in increasing fluorescent signal for HEK WT to KI Cph to KI Oslo is observed for both the black and cyan bars. The parallel samples only incubated with the secondary antibody (orange and blue) have relatively low signal compared to the red- and cyan-colored bars. The yellow bar indicates cell incubated with m14F7 as primary antibody and anti-mouse FITC as secondary antibody, and the purple bars indicate cells incubated h14F7 as primary antibody and anti-human FITC as secondary antibody. The yellow and purple bars have a slightly higher fluorescent signal for HEK KI Cph than for HEK WT. The samples incubated in parallel with only FITC-conjugated secondary antibody (green and pink bars) have a fluorescent signal almost as high as the samples incubated with primary and secondary antibody (yellow and purple bars).

FITC was not used as fluorochrome for HEK KI Oslo cells as these cells contain green fluorescent protein (GFP) in their genome. FITC absorbs light at 488 nm and would therefore not be possible to use as a fluorochrome combined with expressed GFP as the signals would overlap. HEK WT does not express Neu5Gc, and the fluorescence signal would therefore be expected to be lower for WT then for the two different KI cells. As shown in Figure 13 panel A, there was a difference in the signal detected for WT and KI cells when comparing with the same primary and secondary antibodies, and out of the two KI cells KI Oslo gave the strongest fluorescent signal. As these cells were knock-in with the same gene, we wondered what the reason could be for the difference in measured fluorescent signal.

Two murine cell lines, L1210 and P3X63, were compared by measuring the median fluorescence signal from one experiment with three independent biological replicates. m14F7 was used as the primary antibody and goat anti-mouse FITC as the secondary antibody. Figure 13 panel B shows that the fluorescent signal for the two cell lines were about the same, indicating similar content of Neu5Gc GM3.

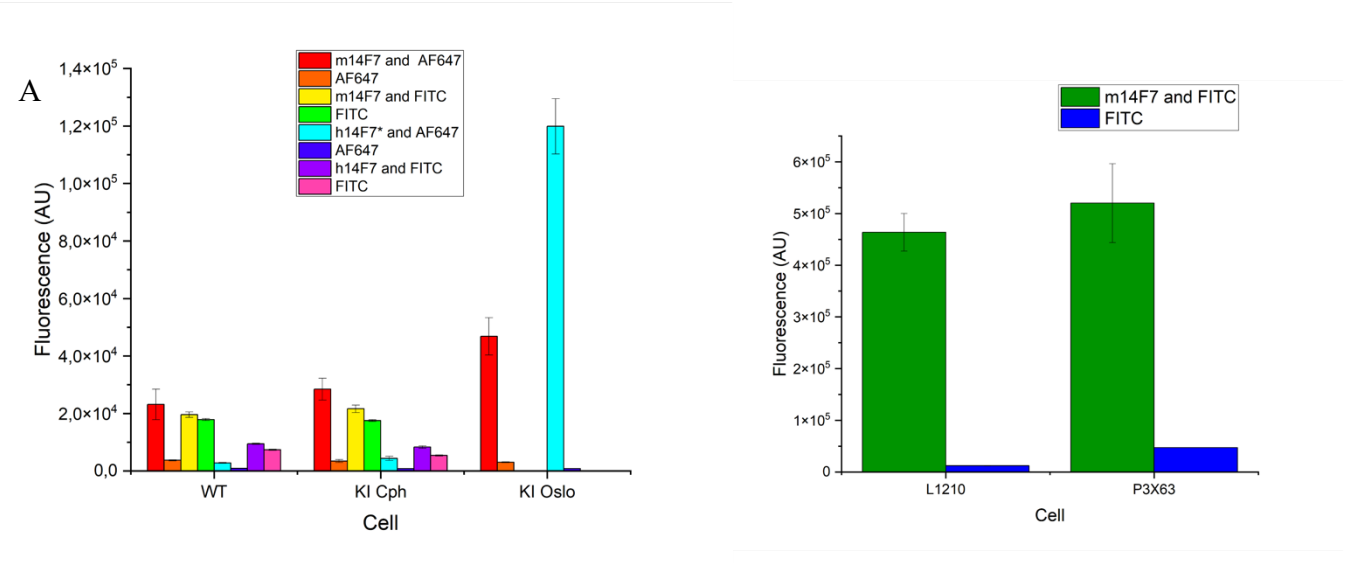

Figure 13. Binding of 14F7 to human and murine cells by measured by flow cytometry. **A,** Binding of humanized 14F7 to HEK WT, KI Cph and KI Oslo cells. This figure shows the measured signal from one experiment with three independent replicates for each condition, except for the condition using m14F7 and FITC where only two independent replicates were used. The error bars represent the standard deviation of the measured median fluorescence signal for the replicates. **B,** Binding of m14F7 to L1210 and P3X63. The figure shows the measured signal from one experiment with three independent replicates for each condition. The error bars represent the standard deviation of the measured median fluorescence signal for the replicates. Figure A and B was created using Origin.

Since the HEK KI Oslo cells incubated with h14F7* as primary antibody and AF647 conjugated to the anti-human secondary antibody gave such a high signal (cyan bars, Figure 13 panel A), we wanted to look at the binding under a microscope and compare the binding to the HEK KI Cph cells treated correspondingly. The cells left over from flow cytometry were mounted on microscope slides and imaged using a 478 nm, 559 nm, and 635 nm laser. Figure 14 shows the images of HEK KI Cph cells and HEK KI Oslo stained with PI (blue) and h14F7* (red). The green fluorescence signal is emitted in the HEK KI Oslo cells by GFP protein (section 3.1.1). The merged images are in the rightmost column. Images of the negative controls for this experiment can be found in Appendix D.

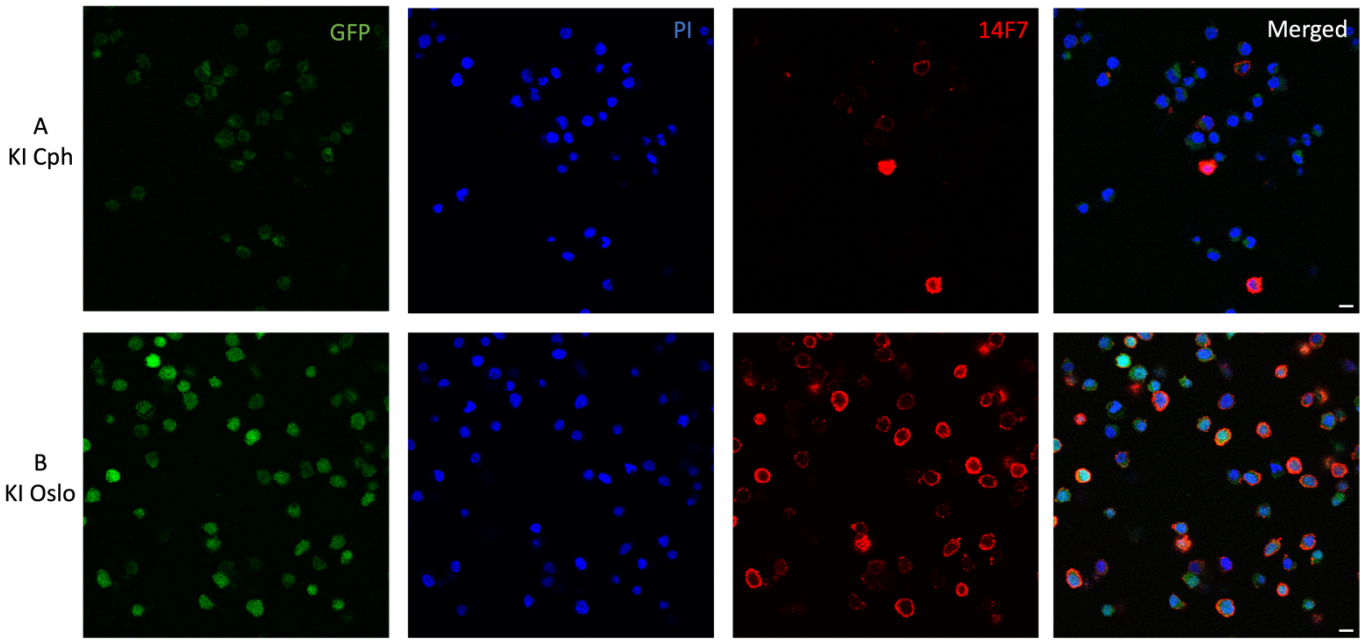

Figure 14. Binding of h14F7* to KI Cph and KI Oslo. The cells were fixed, before they were stained with antibodies and dyes. **A**, HEK KI Cph stained with h14F7* (red) as primary antibody and goat anti-human Alexa Fluor 647 as secondary antibody, as well as PI (blue). **B**. HEK KI Oslo stained with h14F7* (red) as primary antibody and goat anti-human Alexa Fluor 647 as secondary antibody, as well as PI (blue). GFP protein is expressed in the HEK KI Oslo cells therefore they emit signal. The merged images are in the rightmost column. This figure shows that there is a detectable signal for the antibody staining for both KI cells, but more cells have the antibody bound for KI Oslo. The cells were imaged by Olympus FV1000 confocal laser scanning microscope with a PlanApo 60x/1.35 oil immersion objective. Scale bar: 10μm

By comparing the merged images in Figure 14, it was possible to see that several of the HEK KI Oslo cells have the antibody bound, visualized as a red ring around the cell, than the HEK KI Cph cells. This observation corresponded well with the higher fluorescent signal for HEK KI Oslo cells measured by flow cytometry (Figure 13 panel A). Nevertheless, not all the cells in the samples seemed to bind the antibody, even when adjustments like brightness and contrast was changed to inspect the image closely.

4.1.2 Observations of HEK WT cells grown under hypoxia

It has previously been reported that HeLa cells grown under hypoxic conditions express Neu5Gc 3-fold higher compared to normoxic growth (Yin *et al.*, 2006; Bousquet *et al.*, 2015; Dorvignit *et al.*, 2015). We therefore wanted to investigate if this also was the case for HEK WT cells. Firstly, we wanted to observe the rate of cell growth for HEK WT cells under hypoxic conditions compared to normoxic conditions. Figure 15 panel A shows the difference in cell growth under these two conditions. Based on these results, it was concluded that the HEK WT cells placed under hypoxia do not follow a normal growth curve. The cells were viewed under a light microscope but did not differ in morphology. Other measurements of the cells were not performed. It was decided for the following part of the experiment to first grow cells under normoxia until a confluency of 80-90% before the cells were placed under hypoxia. The cells were treated with m14F7 as primary antibody and goat anti-mouse FITC as secondary antibody. Figure 15 panel B shows that the median fluorescence signal is about the same for cells grown 24 and 72 hours under hypoxic conditions. The measured fluorescent signal for HEK WT grown under normoxia (from Figure 13 panel A) is compared to the signal from WT grown under hypoxic conditions in Figure 15 panel C. The cells were in both cases incubated with m14F7 as primary antibody and anti-mouse FITC as secondary antibody.

The hypoxia experiment was performed once with three independent biological replicates. At the time this experiment was performed, we did not have access to h14F7*, and due to limited amounts of h14F7, we chose to use m14F7. We also only had access to goat anti-murine FITC as secondary antibody at the time the experiment was carried out.

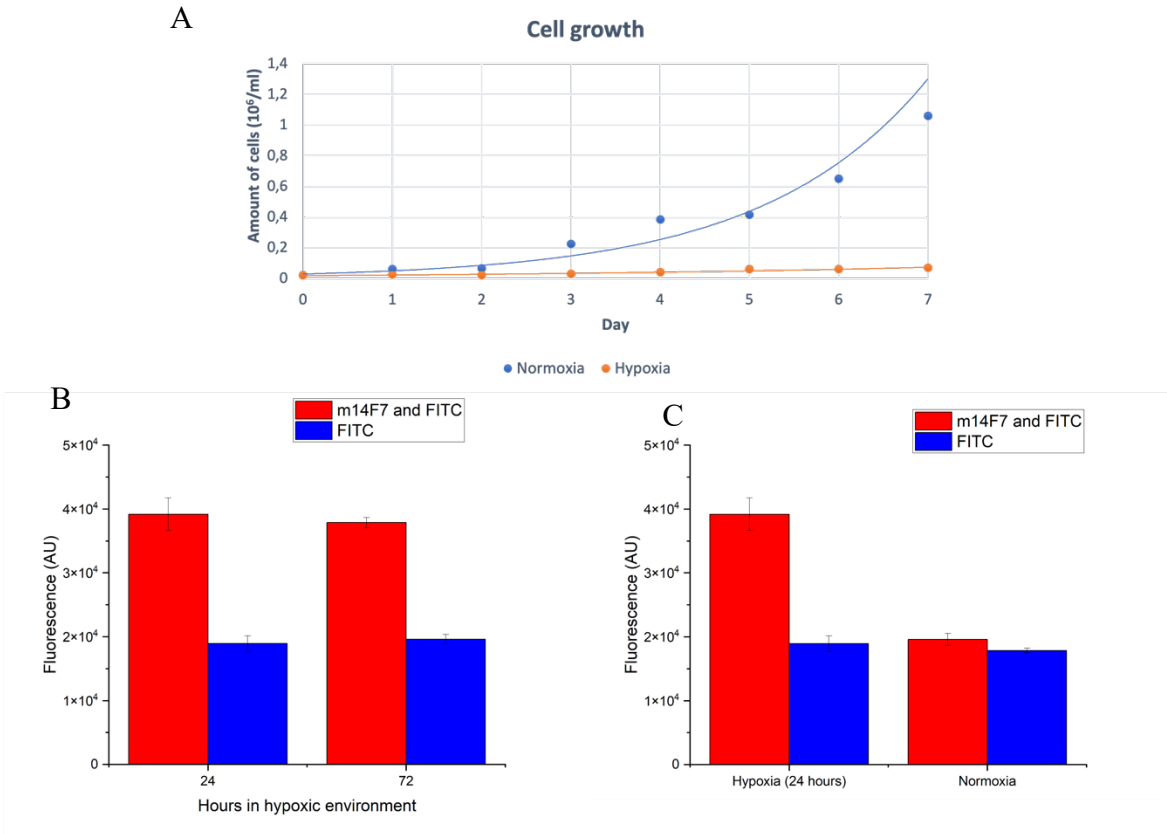

Figure 15. A, Comparison of cell growth of HEK WT under normoxic and hypoxic conditions. Exponential curves have been fitted to the points in the plot. The number of cells were counted once for each cell flask. **B, Comparison of median fluorescent signal of HEK WT cells grown under hypoxic conditions for 24 and 72 hours analyzed by flow cytometry.** The red bars indicate cells incubated with m14F7 as primary antibody and anti-mouse FITC (FITC) as secondary antibody. The blue bars indicate cells incubated with only secondary antibody. The experiment was performed once with three independent biological replicates for each condition. **C**, **Comparison of median fluorescent signal of HEK WT grown 24 under hypoxic conditins and HEk WT grown under normoxic conditions.** The error bars represent the standard deviation of the measured median fluorescence signal for the replicates. Panel A was created using Microsoft Excel and panel B and C using Origin.

4.1.3 Comparison of the binding of 14F7 to HEK and CHO cells

The binding analysis performed (Figure 13 panel A) were performed in Oslo using fixed (dead) cells. We did not have access to appropriate controls, and therefore wanted to reproduce our preliminary results using positive and negative controls. We also wanted to perform the experiments using live cells, as this would be a more realistic experiment to measure the binding of 14F7 for the future use of this antibody in the clinic. Our collaborator, Prof. Henrik Clausen at University of Copenhagen, had appropriate controls available in his

lab, therefore we followed up our initial flow cytometry experiments in his lab at Copenhagen Center for Glycomics.
The binding of humanized 14F7 was investigated using a collection of WT, KI of the *CMAH* gene and KO of the B4GalT5/6 gene for the HEK and CHO cell lines (Section 4.1.1). The cells were incubated with humanized 14F7 and analyzed by flow cytometry. Figure 16 panel A shows the median fluorescence signal for HEK cells incubated with h14F7 as primary antibody in a dilution series from 5-0.625 μg/ml and goat anti-human Alexa Fluor 647 as secondary antibody. A concentration-dependent binding to HEK KI Cph was observed, and very low binding to HEK WT and KO Cph. The same trend was observed when incubating HEK WT, KI Cph and KO Cph with h14F7* as primary antibody with the same dilution series and goat anti-human Alexa Fluor 647 as secondary antibody (Figure 17 panel B), but with about one third of the measured fluorescence signal for HEK KI Cph compared to incubation with h14F7 (Figure 17 panel A).

Half of the cells were preincubated with neuraminidase to remove all sialic acids at the cell surface as a negative control, but the humanized 14F7 had about identical binding for both the cells incubated and not incubated with neuraminidase (Figure 17 panel A and B), raising the question whether the neuraminidase was active. We used peanut agglutinin (PNA) and PanLectenz as controls for the neuraminidase activity. PNA binds to *N*-acetylgalactosamine structures present in glycoconjugates, such as gangliosides (Howard and Batsakis, 1982). PNA was incubated with the cells in dilution series 0.1-0.025 μg/ml and Streptavidin Alexa Fluor 647 as secondary antibody. Figure 16 panel C shows that the PNA had a concentration-dependent binding to the HEK cells treated with neuraminidase, and very low binding to cells not treated with neuraminidase. PanLectenz is a sialic acid affinity reagent engineered for detection of sialoglycans that can be found in glycoconjugates (Lehmann, Tiralongo and Tiralongo, 2006). PanLectenz was incubated in dilution series 1-0.25 μg/ml, and Figure 17 panel D shows binding of PanLectenz to the cells not incubated with neuraminidase while the neuraminidase-treated cells had almost no binding. The median fluorescent signal for cells not treated with neuraminidase was about one forth for HEK KI Cph cells compared to HEK WT and KO Cph. A polyclonal IgM anti-Neu5Gc GM3 primary antibody was used as positive control with the secondary antibody goat anti-chicken Alexa Fluor 488. The positive control gave approximately the same measured fluorescent signal for all HEK cells with and without neuraminidase treatment (Figure 17 panel E). A mixture of all the secondary antibodies was used as a last control to determine that they did not bind to the cells giving a significant fluorescent signal that would interfere with the measured fluorescent signal when using primary antibodies (Figure 17 panel F)

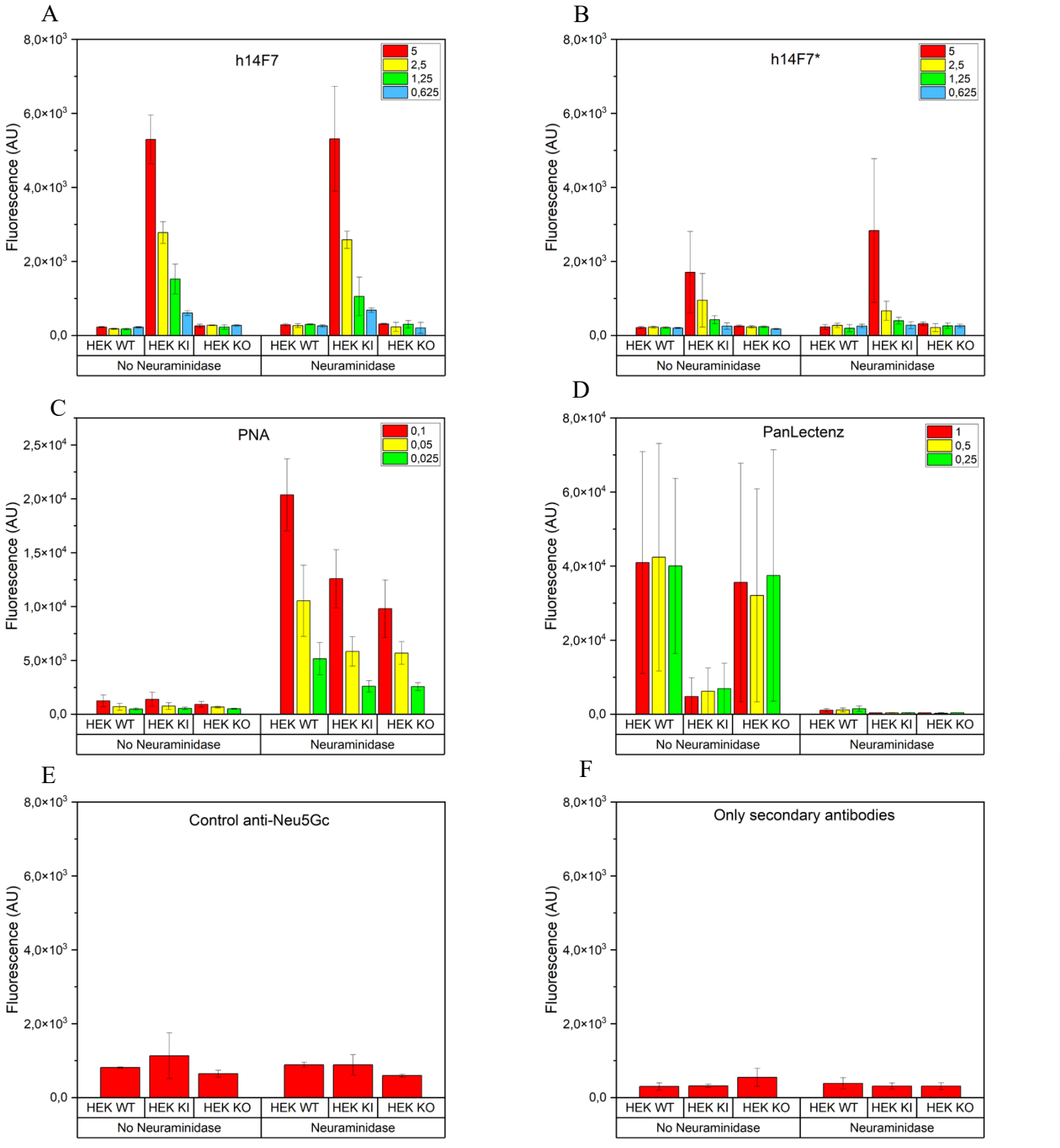

Figure 16. Median fluorescence signal measured by flow cytometry of HEK WT, KI Cph and KO Cph. A, Cells incubated with h14F7 (dilution series 5-0.625 μg/ml indicated in the colored legend) as primary antibody and goat anti-human Alexa Fluor 647 as secondary antibody. **B**, Cells incubated with h14F7* (dilution series 5-0.625 μg/ml indicated in the colored legend) as primary antibody and goat anti-human Alexa Fluor 647 as secondary antibody. **C**, Cells incubated with PNA (concentration series 0.1-0.025 μg/ml indicated in the colored legend) and Streptavidin Alexa Fluor 647. **D**, Cells incubated with PanLectenz (dilution series 1-0.25 μg/ml indicated in the colored legend) mixed with Streptavidin Alexa Fluor 647. **E**, Cells incubated with anti-Neu5Gc GM3 as primary antibody and goat anti-chicken

Alexa Fluor 488 as secondary antibody. **F**, Cells incubated with a mixture of the secondary antibodies goat anti-human Alexa Fluor 647, Streptavidin Alexa Fluor 647 and goat anti-chicken Alexa Fluor 488. The experiment was performed twice with two replicates. The error bars represent the standard deviation of the measured median fluorescence signal for the replicates. This figure was created with Origin.

The same analysis was performed with CHO WT, KI and KO cells to confirm the observations of binding for HEK, but with some changes in dilution series and also without using the h14F7* antibody. Figure 18 panel A shows the binding of h14F7 to CHO cells in a dilution series 5-0.625 μg/ml. As for HEK cells in Figure 17 panel A, the 14F7 binds to both the neuraminidase-treated and untreated CHO cells (Figure 18 panel A). PNA was incubated with CHO cells at two different concentrations, 0.05 μg/ml and 0.025 μg/ml. Figure 18 panel B shows the same trend in concentration-dependent binding for neuraminidase-treated CHO cells as for the HEK cells. PanLectenz was incubated with the CHO cells with a concentration of 0.5 μg/ml and showed the same trend as HEK cells in binding for the cells not treated with neuraminidase (Figure 18 panel C). Both the positive control of anti-Neu5Gc (Figure 18 panel D) and the control with only secondary antibodies (Figure 18 panel E) show very low fluorescent signals measured.

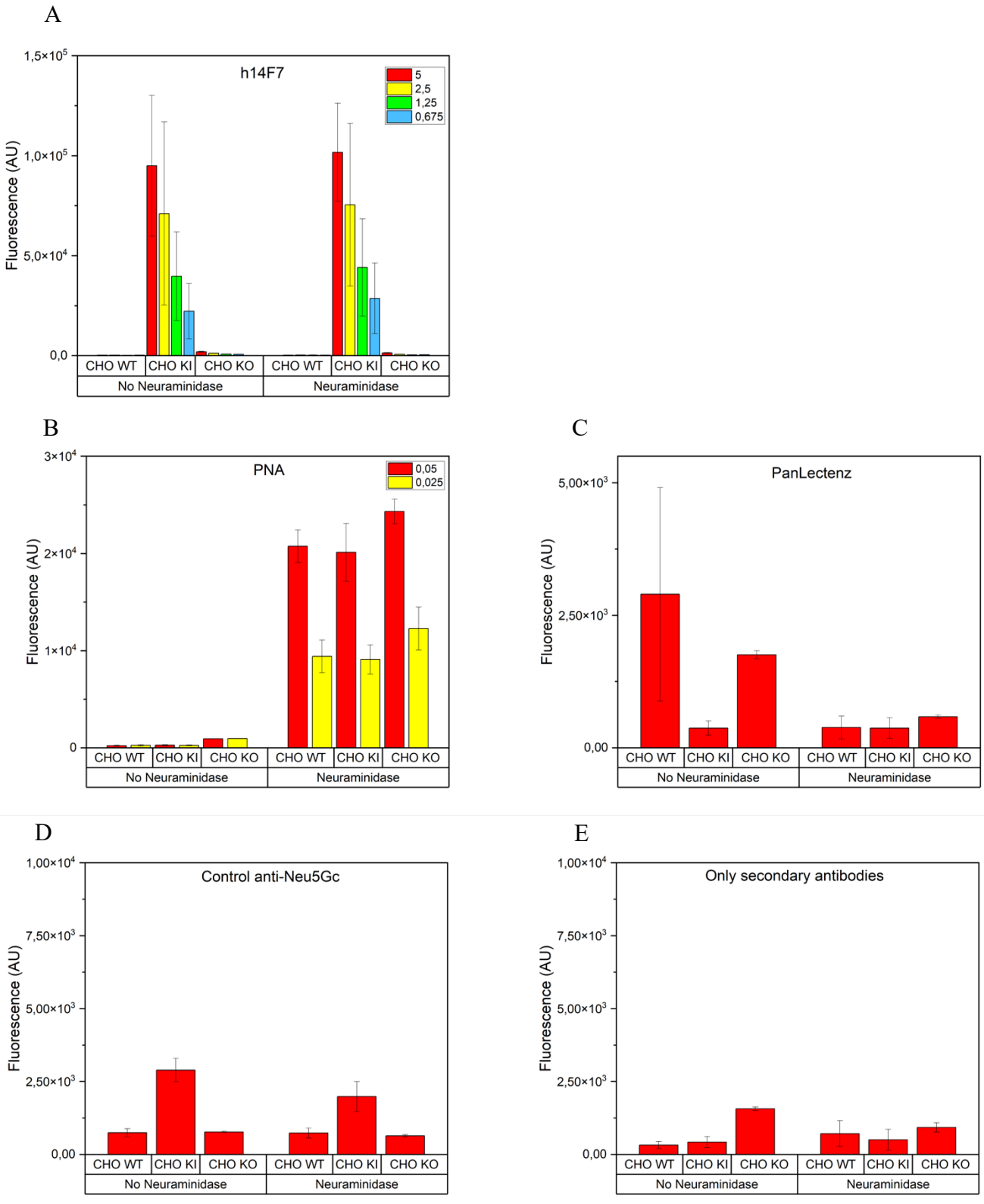

Figure 17. Median fluorescence signal measured by flow cytometry of CHO WT, KI and KO. **A**, Cells incubated with h14F7 (dilution series 5-0.625 μg/ml indicated in the colored legend) as primary antibody and goat anti-human Alexa Fluor 647 as secondary antibody. **B**, Cells incubated with PNA (concentration series 0.05-0.025 μg/ml indicated in the colored legend) and Streptavidin Alexa

Fluor 647. **C**, Cells incubated with PanLectenz (dilution series 0.5-0.25 μg/ml indicated in the colored legend) mixed with Streptavidin Alexa Fluor 647. **D**, Cells incubated with anti-Neu5Gc GM3 as primary antibody and goat anti-chicken Alexa Fluor 488 as secondary antibody. **E**, Cells incubated with a mixture of the secondary antibodies goat anti-human Alexa Fluor 647, Streptavidin Alexa Fluor 647 and goat anti-chicken Alexa Fluor 488. The experiment was performed twice with two replicates. The error bars represent the standard deviation of the measured median fluorescence signal for the replicates. This figure was created with Origin.

The same experiment with the same dilution series illustrated in Figure 16 was repeated using HEK WT, KI Cph and KI Oslo to investigate if the two KI constructs gave about the same fluorescent signal when treated in the same manner. Figure 18 panel A shows h14F7 bound to the three different cell types. HEK KI Oslo had a stronger binding compared to KI Cph. This was also the same trend observed in Figure 18 panel B where h14F7* was used. However, the measured fluorescence signal in Figure 18 panel B was about half to one third of what was measured with h14F7 in Figure 18 panel A. We were then questioning if one of the humanized 14F7 formats were better than the other and hence preferable to use for further experiments. The incubation with neuraminidase did again not lead to a difference of signal compared to untreated cells. Figure 18 panel C shows the same trend as illustrated in Figure 16 panel C and 17 panel B in concentration-dependent binding of PNA for all three cell types. The measured binding of PanLectenz in panel D is very low, indicating almost no binding. This is most likely due to human error sample preparation. The measured fluorescence signal for the positive control for Neu5Gc (Figure 18 panel E) was similarly as in Figure 16 panel E and Figure 17 panel D, and the control with only secondary antibodies (Figure 18 panel F) shows almost no binding. The slightly higher signal for HEK KI Oslo cells in Figure 18 panel E could be due to the signal of the secondary antibody used, goat anti-chicken Alexa Fluor 488, being measured together with GFP expressed in the cells, which absorbs light at approximately the same wavelength.

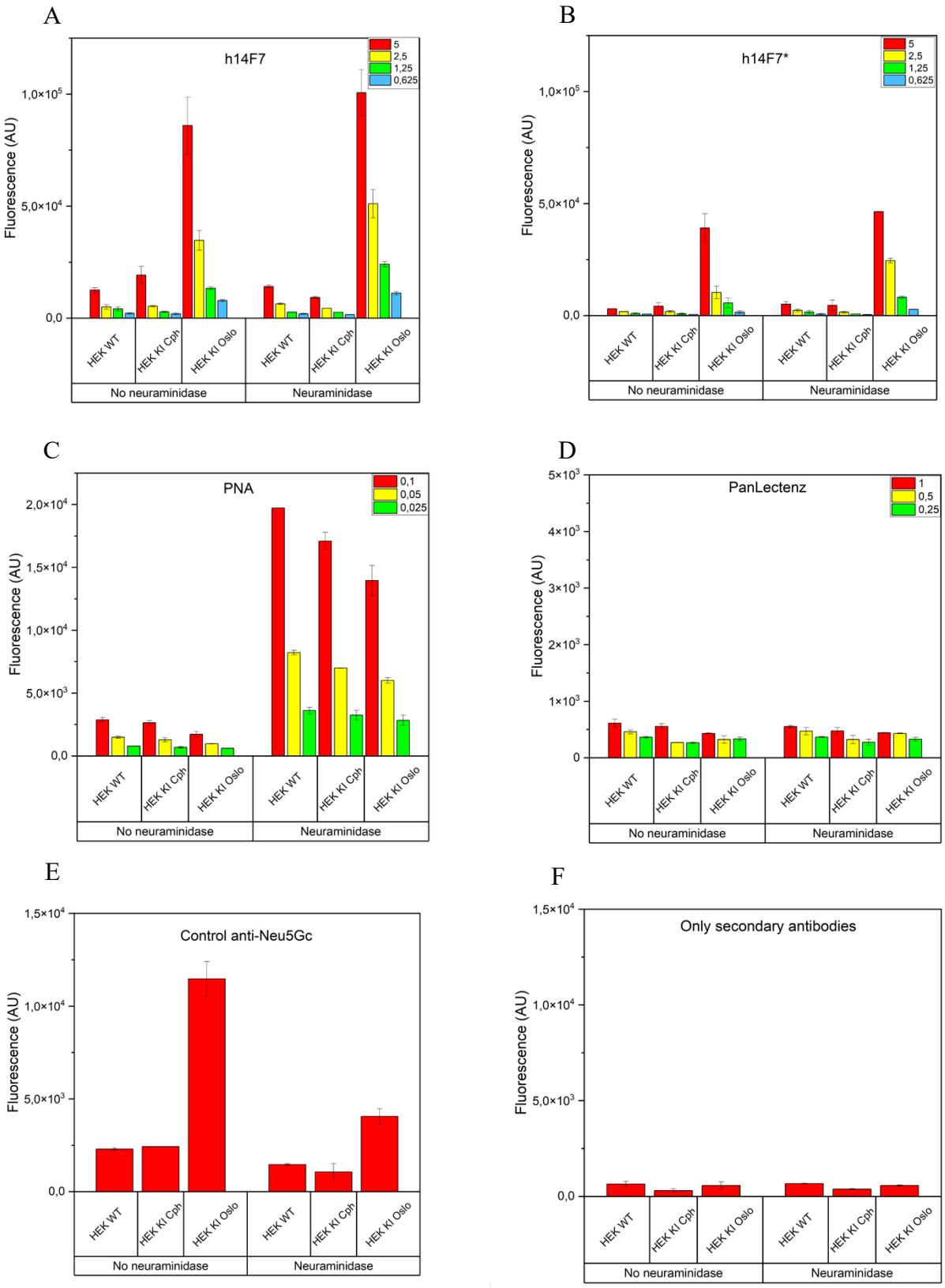

Figure 18. Median fluorescence signal measured by flow cytometry of HEK WT, KI Cph and KI Oslo. A, Cells incubated with h14F7 (dilution series 5-0.625 μg/ml indicated in the colored legend) as primary antibody and goat anti-human Alexa Fluor 647 as secondary antibody. **B**, Cells incubated with h14F7* (dilution series 5-0.625 μg/ml indicated in the colored legend) as primary antibody and goat anti-human Alexa Fluor 647 as secondary antibody. **C**, Cells incubated with PNA (concentration series

0.1-0.025 μg/ml indicated in the colored legend) and Streptavidin Alexa Fluor 647. **D**, Cells incubated with PanLectenz (dilution series 1-0.25 μg/ml indicated in the colored legend) mixed with Streptavidin Alexa Fluor 647. **E**, Cells incubated with anti-Neu5Gc GM3 as primary antibody and goat anti-chicken Alexa Fluor 488 as secondary antibody. **F**, Cells incubated with a mixture of secondary antibodies goat anti-human Alexa Fluor 647, Streptavidin Alexa Fluor 647 and goat anti-chicken Alexa Fluor 488. The experiment was performed one time with two replicates. The error bars represent the standard deviation of the measured median fluorescence signal for the replicates. This figure was created with Origin.

From the results showed in figure 16, 17 and 18, it appeared that the best combination for a strong signal was to use HEK KI Oslo cells treated with h14F7.

4.1.4 Comparison of EGFR expressed of HEK WT, KI Cph and KI Oslo

The results from section 4.1.1 and 4.1.3 indicated that humanized 14F7 bound stronger to HEK KI Oslo than to HEK KI Cph cells. We therefore wondered what the reason for this could be. It has already been established that Neu5Ac GM3 can inhibit growth factors (GF) in certain tumors leading to down-regulation of cell growth (Wang *et al.*, 2001). The interaction by Neu5Ac inhibits dimerization of growth factor receptors (GFRs), affecting the signaling pathways downstream of the GFRs (Bremer, Schlessinger and Hakomori, 1986; Chung *et al.*, 2009; Coskun *et al.*, 2011). It has been reported that removal of the sialic acids led to reduction of the inhibitory effect, resulting in active EGFR signaling and cell growth (Meuillet *et al.*, 1999; Coskun *et al.*, 2011). As the Neu5Ac was replaced by Neu5Gc in the HEK KI cells used for the experiments in this thesis, we therefore questioned if there were any differences in EGFR expression for HEK KI Oslo cells compared to HEK WT and HEK KI Cph. The fluorescent signal of Cetuximab (anti-EGFR) as primary antibody and goat anti-human Alexa Fluor 647 as secondary antibody was measured by flow cytometry. The red bars in Figure 19 illustrate the measure fluorescent signal from cells incubated with the primary and secondary antibody, while the blue bars indicate cells only incubated with the secondary antibody. The blue bars are very low compared to the red, illustrating that the secondary antibody did not bind to the cells without the primary antibody present. The median fluorescent signal was between $7.5*10^4$-$8.5*10^4$ for HEK WT, KI Cph and KI Oslo (Figure 19), indicating that there are no big differences in the amounts of EGFR on the cell surface of the different cells.

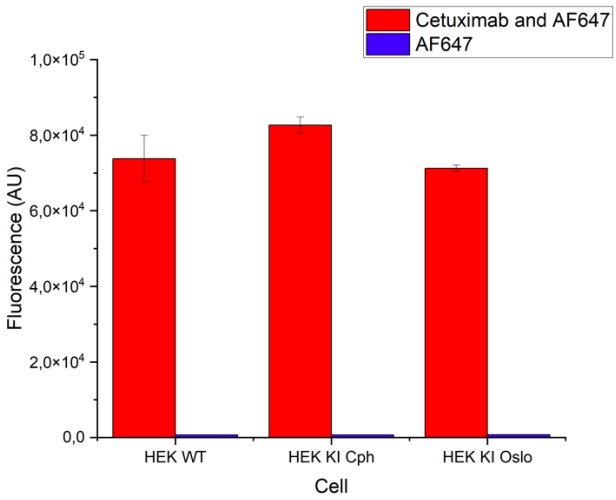

Figure 19. Median fluorescence signal of Cetuximab bound to HEK WT, HEK KI Cph and HEK KI Oslo. The red bars indicate the signal from cells incubated with Cetuximab as primary antibody and anti-human Alexa Fluor 647 (AF647) as secondary antibody. The blue bars indicate cells only incubated with secondary antibody. This figure shows that there were only small differences in the binding of Cetuximab to the different cells. The experiment was performed one time with three independent biological replicates. The error bars represent the standard deviation of the measured median fluorescence signal for the replicates. This figure was created with Origin.

4.1.5 Incubation of 14F7 to visualize possible cell death

14F7 has been reported to kill tumor cells (Roque-Navarro *et al.*, 2008; Fernández-Marrero *et al.*, 2011). We wanted to assess if we observed this when incubating cells overexpressing Neu5Gc GM3, simulating cancer cells, with h14F7. Incubation with h14F7 was also performed on HEK WT cells to compare with KI Cph. The cells were incubated with h14F7 to a final concentration of 60 μg/ml. After 24 hours of incubation at 37°C the cells were added PI to visualize membrane lesions and cell death. Figure 20 upper row illustrates the gating of live vs dead cells for one independent biological replicate of each sample, while the lower row illustrates the histogram of the three replicates by a black, red and blue curve. The cells in row A are untreated WT cells, B are treated WT cells, C are untreated KI Cph cells and D are treated KI Cph cells. The cells were gated into two groups, illustrated as group P7 and group P8 (Figure 20). The number marked in red defines the percent of cells gated into each group. FL-2 at the x-axis (Figure 20 all panels) indicates the use of a specific filter to detect PI. Cells located more to the right in the dot plot have more bound PI and indicate that the cells are dead. FSC-A at the y-axis (Figure 20 panel A-D) indicates the area of the FSC,

giving information about the cell size. The percent of cells in group P7 indicates the amount of live cells, while the percent of cells in group P8 indicate dead cells.

The percent of cells in group P7 and P8 are about identical for Figure 20 panel A and B, indicating no differences between the untreated WT (panel A) and 14F7-treated WT cells (panel B). This is also observed by similarity of the histograms in panel E and F. The percent of cells in group P7 in panel C, indicating live, untreated KI Cph cells, is 51.5%, while the percent of cells in group P7 in panel D, indicating the live, 14F7-treated KI Cph cells, is 40.8%. This demonstrates that more cells have died when KI Cph were treated with h14F7. This is also observed in the histograms in panel G and H where the peaks have shifted more to the right and the peak most to the right is higher in panel H than in panel G. All replicates for each condition showed similar population pattern in the dot plots. Dot plots for all replicates can be found in Appendix D.

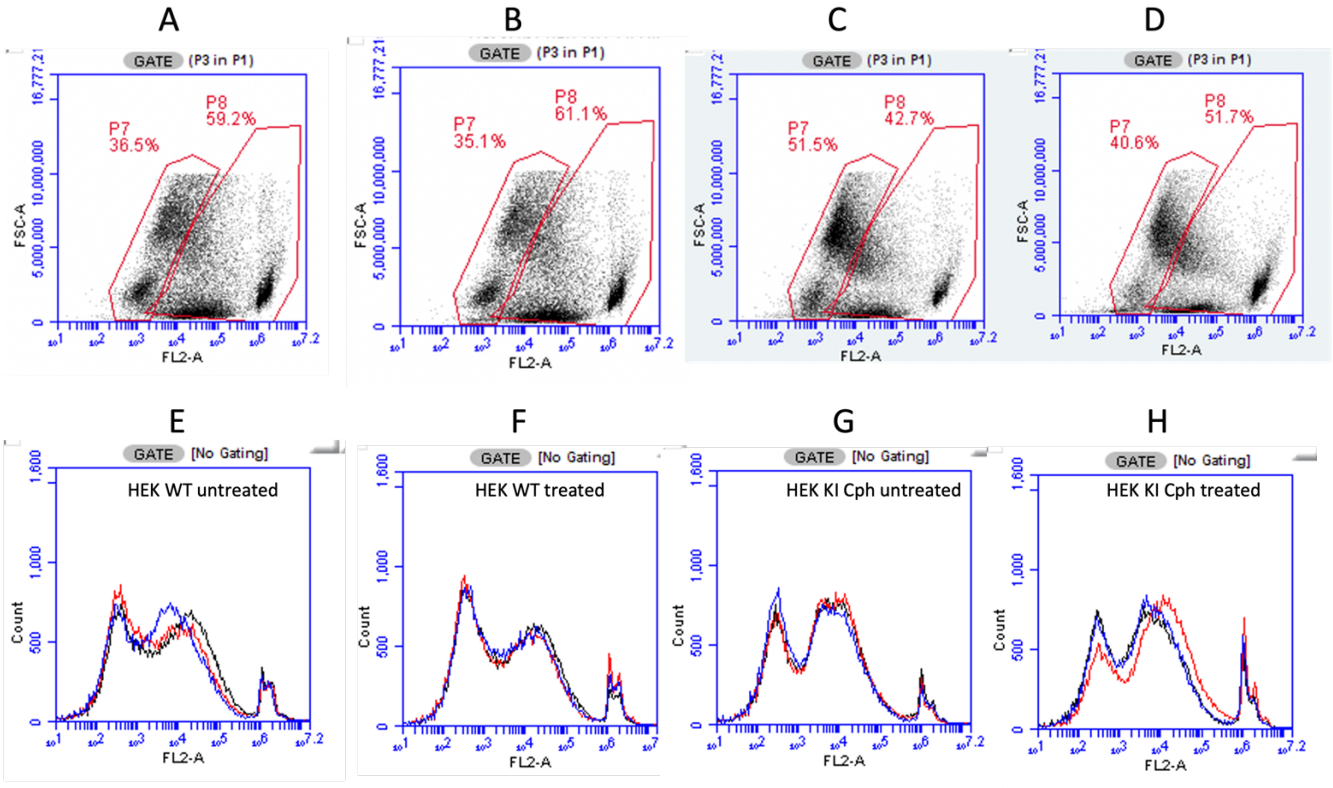

Figure 20. HEK WT, HEK KI Cph, P3X63 and L1210 incubated with 14F7. Panel A-D represent gateing of one independent biological replicate and panel E-H represent histograms of three independent replicates, illustrated as a black, red and blue curve. A, Gating of HEK WT untreated cells. **B**, gating of HEK WT treated with h14F7 for 24 hours. **C**, Gating of HEK KI Cph untreated cells. **D**, gating of HEk Ki Cph treated with h14F7 for 24 hours. **E**, HEK WT untreated cells. **F**, HEK WT treated with h14F7 for 24 hours. **G**, HEK KI Cph untreated cells. **H**, HEK KI Cph treated with h14F7 for 24 hours.

4.2 Investigation of the cellular journey of 14F7

Previously, our research group prepared a scFv-Nluc construct to use for bioluminescence microscopy (Pesci, 2020). Images of HEK KI Cph cells treated with the scFv-Nluc were acquired using an Andor Dragonfly spinning disk with 0.2 % laser power using a 405 nm laser by Khalisah L. B. Zulkefli in June 2020 (Figure 21). The images looked initially promising, but it turned out when attempting to reproduce the images that what was first assumed to be bioluminescence, actually was autofluorescence from the cells. The cells were challenging to handle during live imaging as the conditions used affected the health of the cells causing them to round up and blebb (Figure 21). Autofluorescence is natural emission of light form biological structures, such as mitochondria or lysosomes (Monici, 2005). After troubleshooting with Frode M. Skjeldal[15] on how to use bioluminescence for microscopy, we decided to change strategy to use fluorescence microscopy for live imaging instead.

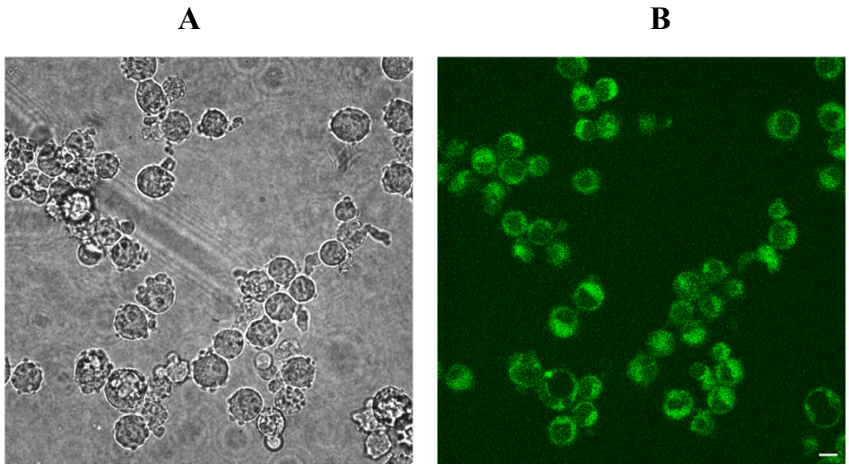

Figure 21. Autofluorescence from HEK KI Cph cells. A, Transmitted light. **B**, Autofluorescence from HEK KI Cph. Scale bar: 10 μM

4.2.1 Conjugation of 14F7 and comparison of the binding of Alexa Fluor 647 conjugated murine and humanized 14F7

To be able to use live imaging, the primary antibodies of interest had to be conjugated to a chromophore to give a fluorescent signal (section 4.2.2). For our purposes, Alexa Fluor 647 was chosen, kindly provided by Nextera. To determine if the conjugation of Alexa Fluor 647

[15] Senior Engineer, Department of Biosciences, University of Oslo, Norway

to h14F7* and m14F7 was successful, KI Cph and L1210 were incubated with respectively the conjugated humanized 14F7' and conjugated m14F7. Results from flow cytometry implied that only the conjugated m14F7 gave a detectable fluorescent signal. We therefore wanted to image the cells from the flow cytometry experiment to compare if the binding of the conjugated m14F7 looked similar as the binding using primary antibody and conjugated secondary antibody. We also wanted to see if there was any visible binding of the conjugated h14F7*, even though the fluorescent signal measured by flow cytometry was very low.

The cells left over from flow cytometry were mounted on microscope slides and imaged using a 405 nm and a 635 nm laser. Figure 22 shows the images of HEK KI Oslo cells in the top row and L1210 in the middle row stained with PI (blue). Column A marks the cells added nothing, B the cells added primary and secondary antibody, C the cells added only secondary and D the cells added conjugated primary antibody. The red signal in column B was caused by the fluorochrome-labeled secondary antibody (indirect staining), while the red signal in column D was caused by the fluorochrome conjugated to the primary antibody (direct staining).The images in column D correlates well with the signals measured by flow cytometry in which only the L1210 cells gave a visible signal for the murine conjugated antibody, as well as the HEK KI Oslo and L1210 cells treated with primary and secondary antibody (column B). It was observed by the magnified images in the lowest row (defined by orange boxes) a difference in the signal between the indirect and direct staining for L1210 (Figure 22). While the magnified image in column B shows a similar red ring around the cells as previously observed (Figure 14), the magnified image in column D had a more uneven binding with a visually weaker signal.

We attempted to use the AF647-conjugated m14F7 for live imaging to image internalization of the antibody. Unfortunately, this turned out to be difficult as the fluorescent signal was not detectable. We tried using uncoated and coated imaging dishes, but a signal was still not possible to detect.

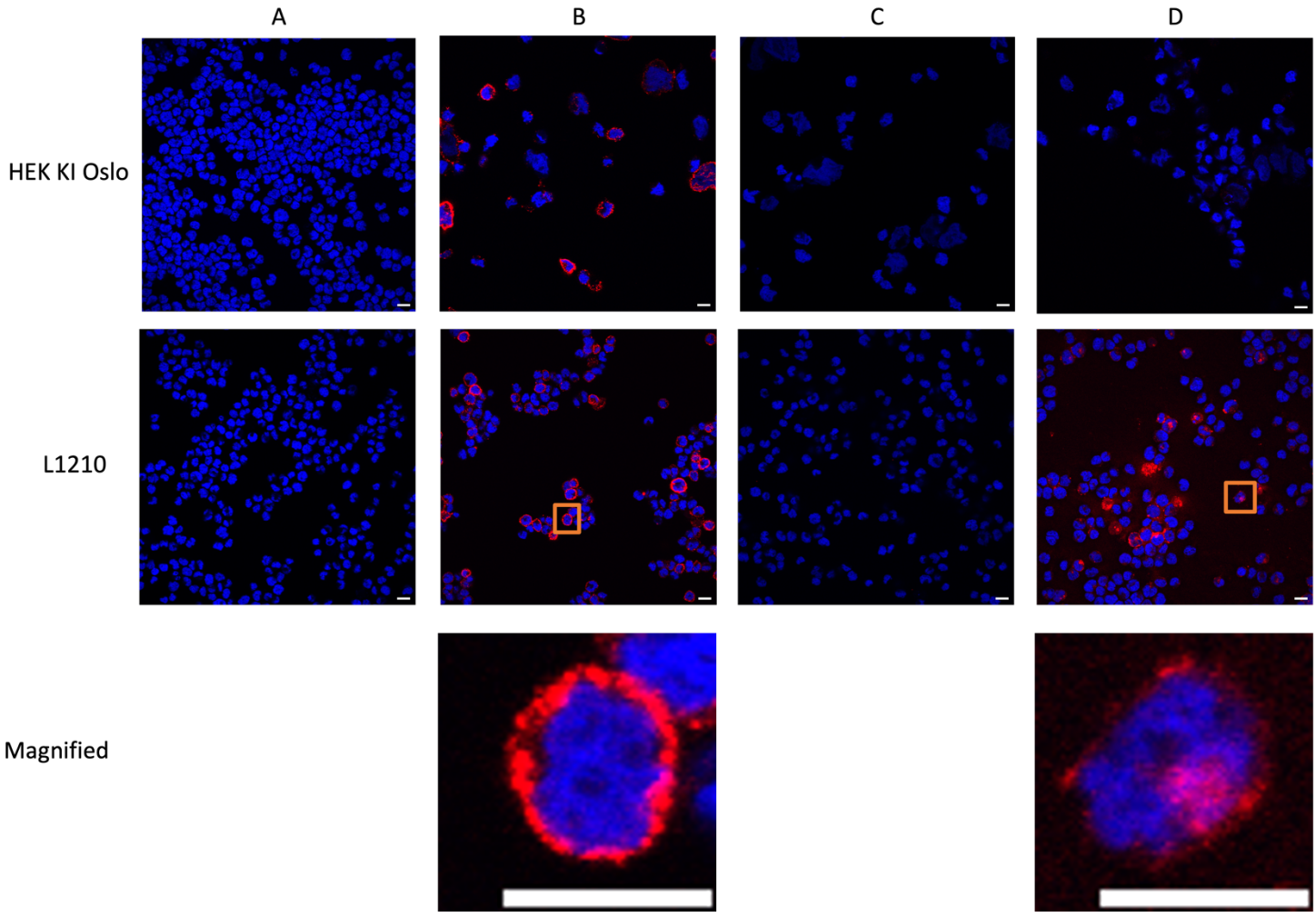

Figure 22. Microscope images of HEK KI Oslo and L1210 cells. Cells left over from the flow cytometry experiment (Figure 23) were fixed before staining with antibodies and dyes. **A**, Cells to which nothing was added. **B**, Cells to which primary and secondary antibody were added. H14F7* was used for the HEK KI Oslo as primary antibody and anti-human Alexa Fluor 647 as secondary antibody (red). M14F7 was used for the L1210 cells as primary antibody and goat anti-mouse Alexa Fluor 647 as secondary antibody (red). The orange box in the image of L1210 define the magnified image below. **C**, Cells to which only secondary antibody was added. Goat anti-human Alexa Fluor 647 was used for HEK KI Oslo, and goat anti-mouse Alexa Fluor 647 was used for L1210. **D**, Cells to which conjugated antibody was added. Humanized 14F7 Alexa Fluor 647 conjugate (red) was used for HEK KI Oslo, and m14F7 Alexa Fluor 647 conjugate (red) was used for L1210. The yellow box in the image of L1210 define the magnified image below. All samples were stained with PI (blue). This figure shows that there are signals from both cell lines in column B and only for the murine cell line in column D. The cells were imaged by Olympus FV1000 confocal laser scanning microscope with a PlanApo 60x/1.35 oil immersion objective. Scale bar: 10μm

4.2.2 Imaging the binding of 14F7 on the cell surface and its intracellular localization

When it turned out that live imaging was challenging to use, the strategy for imaging was changed to immunofluorescence on fixed samples. Based on the observations and results from the experiments described in section 4.1, we decided that the most interesting cells to use for confocal imaging were KI Oslo as they had the strongest binding measured by flow cytometry. Cells were seeded on four coated coverslips, all were fixed, and half of the coverslips were permeabilized with Triton-X (section 4.4.3). This would make it possible to investigate if 14F7 could bind to Neu5Gc on the cell surface as well as inside the cells for the permeabilized samples. If the antibody could bind to its target intracellularly, then we could follow up with investigating where in the cell the antibody would potentially go when and if it is internalized. Results from section 4.1 indicated that h14F7 had the strongest binding, but since we had limited amounts of this antibody and more of the h14F7*, we chose to use that instead for this and the following experiment. Figure 23 row A shows fixed cells and row B fixed and permeabilized cells. The cells were incubated with h14F7* as primary antibody (red) and Alexa Fluor 647 conjugated to goat anti-human secondary antibody, before they were stained with DAPI (blue). The images were acquired using a 405 nm and 647 nm laser. Only HEK KI Oslo were used for this and the following experiment. The GFP signal was similar for all samples, which is why GFP was excluded from Figure 23 and 24. The merged image in row A shows the signal from 14F7 located on the cell surface and row B inside the cell. Images of negative controls can be found in Appendix D.

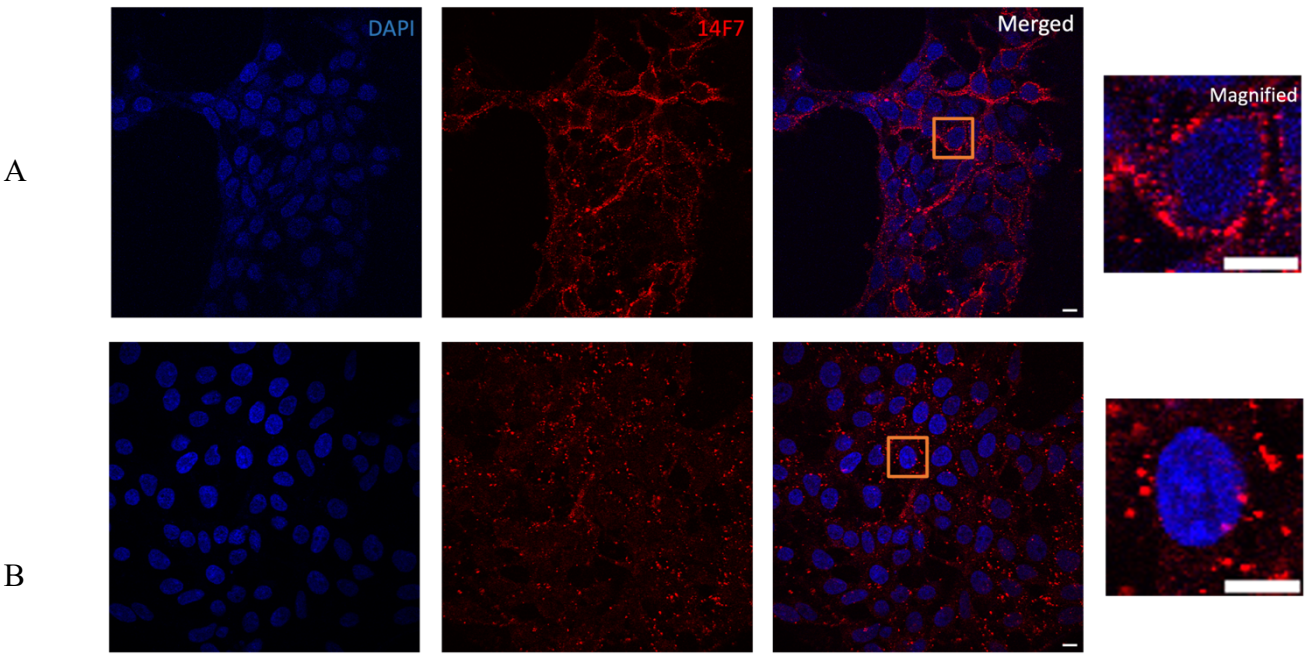

Figure 23. Images of h14F7* bound to HEK KI Oslo on the cell surface and inside the cell.

A, Cells fixed with 4% PFA and blocked with 5% FCS solved in PBS + 0.02% sodium azide. The cells were stained with h14F7* (red) as primary antibody, goat anti-human Alexa Fluor 647 as secondary antibody and DAPI (blue). The orange box defines the magnified image to the right. **B**, Cells fixed with 4% PFA and blocked with 5% FCS solved in PBS + 0.02% sodium azide, before they were permeabilized with Triton-X. The cells were stained with h14F7* (red) as primary antibody, goat anti-human Alexa Fluor 647 as secondary antibody and DAPI (blue). The orange box defines the magnified image to the right. 'This figure shows that there is a signal for 14F7 (red) on the cell surface for row A and inside the cell for row B. The cells were imaged by Olympus FV1000 confocal laser scanning microscope with a PlanApo 60x/1.35 oil immersion objective. Brightness and contrast were edited in a similar way for the signal of AF647 by Fiji. Scale bar: 10μm

4.2.3 Immunofluorescent staining

After we had demonstrated that 14F7 could bind to its intracellular target as well as on the cell surface, we wanted to investigate where in the cell it was localized to. The images illustrated in Figure 23 panel B showed a pattern similar to endosomal staining (Cinzia Progida, personal communication). We used antibodies as markers for EEA (early endosome antigen) and Lamp (lysosomal-associated membrane protein) to see if 14F7 colocalize with these markers. Cells were fixed with 4% PFA and permeabilized with 0.10% Saponin, before staining with antibodies and dyes. Cells in both panel A and B in Figure 24 were stained with h14F7* as primary antibody (red) and goat anti-human Alexa Fluor 647 as secondary antibody. Cells in panel A were then stained with mouse anti-EEA1 (green) and goat anti-mouse Alexa Fluor 555 as secondary antibody, before staining with DAPI (blue). The cells in panel B were stained with mouse anti-Lamp1 (green) and goat anti-mouse Alexa Fluor 555, before staining with DAPI (blue). The images were acquired using a 405 nm, 488 nm and 647 nm laser. Figure 26 shows that the signal from binding of 14F7 colocalizes with the late endosomal marker (panel B). Images of negative controls can be found in Appendix D. This result display that GM3, the target of 14F7, was internalized to the late endosome and that the antibody can be bound intracellularly. The questions raised are then if the antibody can be internalized with its target or if the antibody would separate at some point. And if it would stay bound during internalization, would the antibody be internalized to the late endosome, or would it go further?

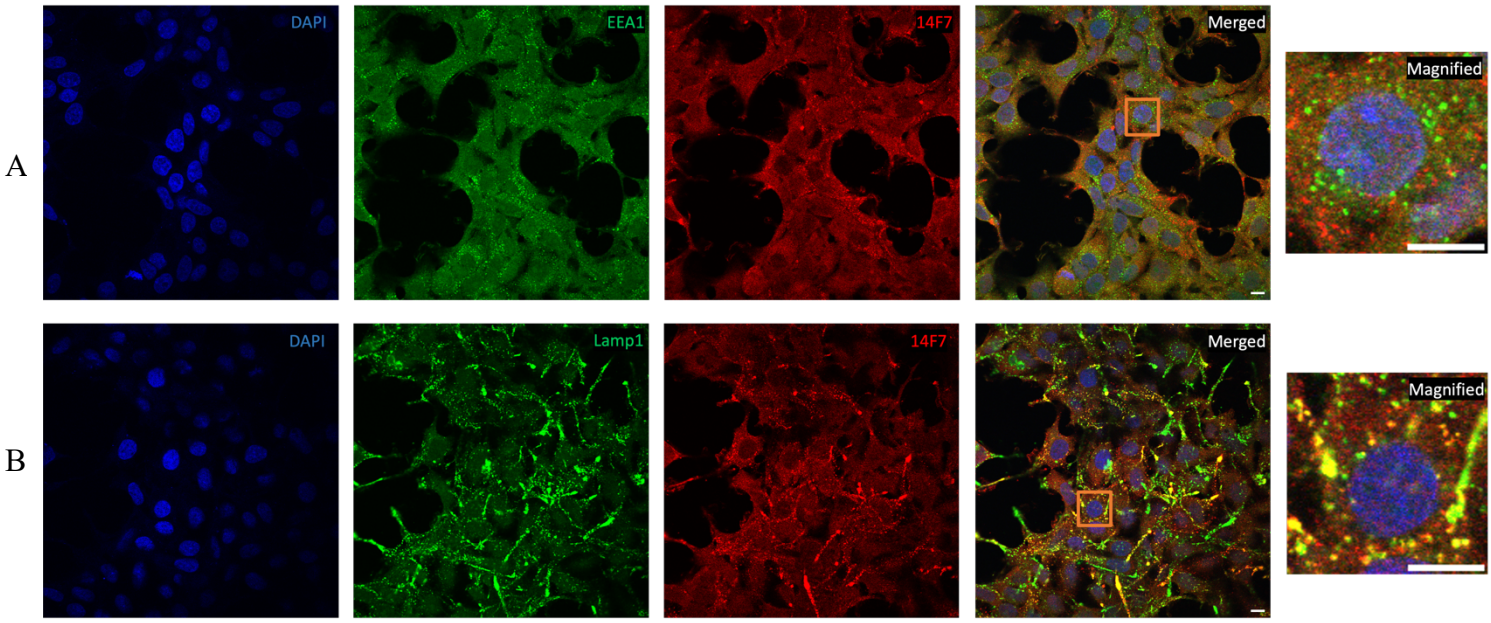

Figure 24. Localization of 14F7 within the endocytic pathway. Cells fixed with 4% PFA and blocked with 5% FCS solved in PBS + 0.02% sodium azide, before they were permeabilized with 0.10% Saponin. **A**, Cells were stained with h14F7* and mouse anit-EEA1 as primary antibodies, and goat anti-human Alexa Fluor 647 and goat anti-mouse Alexa Fluor 555 as secondary antibody, before staining with DAPI (blue). The orange box defines the magnified image to the right.
B, Cells were stained with h14F7* and mouse anit-Lamp1 as primary antibodies, and goat anti-human Alexa Fluor 647 and goat anti-mouse Alexa Fluor 555 as secondary antibodies, before staining with DAPI (blue). The orange box defines the magnified image to the right. This figure shows that the signal binding of 14F7 colocalizes with the late endosomal marker. The cells were imaged by Olympus FV1000 confocal laser scanning microscope with a PlanApo 60x/1.35 oil immersion objective. Brightness and contrast were edited in a similar way for the signal of EEA1, Lamp1 and 14F7 by Fiji. Scale bar: 10μm

4.3 Investigation of the effects of 14F7

We wanted to compare HEK WT, one of the KI constructs and one of the murine cell lines by quantitative proteomics. HEK KI Oslo gave the stonges binding by flow cytometry (Section 4.1) and these cells were also used for imaging. We therefore chose to use this KI construct for proteomic analysis.Since the amount of Neu5Gc expression was about the same on the two murine cell lines (Figure 13 panel B), we based our choice on the interesting observations of antibody-induced cell death reported by (Roque-Navarro *et al.*, 2008) using the cell line L1210. The cells were treated with h14F7. We chose this antibody format as we have previously used this for other experiments and consequently had more data on this antibody that could be of relevance.

4.3.1 Proteomic analysis of untreated and 14F7-treated cells

Samples of HEK WT, KI Oslo and L1210, treated with h14F7 and untreated, were submitted to LC-MS/MS analysis and protein identification and label-free quantification. 7684 proteins were identified for the human cells and 5305 for the murine cells. Following stringent criteria (a minimum of 2 out of 3 valid values in at least one group, standard imputation, t-test with $p<0.05$ and a fold-change at least 2.0), 31 proteins were found to be upregulated and 20 proteins downregulated when comparing the HEK WT treated cells to HEK WT untreated cells (Table 5). The protein tools Funrich and Panther were used to categorize the up- and downregulated proteins into biological process and protein class. The classification is illustrated by pie charts for HEK WT (Figure 27) and HEK KI Oslo (Figure 28). The proteins that were not classified into any biological process or protein class by the bioinformatic tools were categorized manually and are marked with *. The proteins that were not possible to categorize are marked as unknown and colored in black in Table 5 and 6, as well as in Figure 25 and 26. The tables also include the protein name, uniprot ID, ratio of regulation, number of peptides and p-value. 23 proteins were upregulated and 39 downregulated for HEK KI Oslo treated with h14F7 compared to HEK KI Oslo untreated cells (Table 7). 52 proteins were upregulated and 60 downregulated for L1210 cell treated with m14F7 compared to untreated L1210 (Table 8). Cell communication and/or signal transduction was upregulated as biological process in both HEK WT and KI Oslo. Scaffold/adaptor proteins and transporters were also upregulated in both WT and Ki Oslo, and cytoskeletal proteins were downregulated for both. The mass spectrometry proteomics data will be deposited to the ProteomeXchange Consortium via the PRIDE partner repository.

Table 5. Regulated proteins for HEK WT treated with h14F7 compared to HEK WT untreated cells. The columns biological process and protein class are color-coded according to the pie charts in Figure 27. Proteins marked with * have been categorized separately.

Protein	Uniprot ID	Ratio	Peptides	p-value	Biological process	Protein class
Upregulated						
Cytochrome c oxidase subunit 6A1, mitochondrial	P12074	27,242	3	<0.001	Metabolism	Metabolite interconversion enzyme
Rho guanine nucleotide exchange factor 28	Q8N1W1	20,012	3	<0.001	Cell communication and/or signal transduction	Protein-binding activity*
Vesicle-associated membrane protein 2	P63027	12,613	3	0.049	Transport	Membrane traffic protein
DENN domain-containing protein 5B	Q6ZUT9; Q6IQ26	11,438	4	0.001		Protein modifying enzyme*
Helicase with zinc finger domain 2	Q9BYK8	8,836	5	<0.001	Regulation of nucleobases, nucleoside and nucleic acid*	RNA metabolism protein
Ribosomal protein 63, mitochondrial	Q9BQC6	7,656	3	0.009	Metabolism	Protein-binding activity*
Zinc finger matrin-type protein 2	Q96NC0	7,372	1	0.003	Regulation of nucleobases, nucleoside and nucleic acid metabolism	RNA metabolism protein
Gem-associated protein 6	Q8WXD5	7,321	2	0.040	Regulation of nucleobases, nucleoside and nucleic acid metabolism	Protein modifying enzyme*
Heat shock 70 kDa protein 1-like	P34931	7,233	23	0.050	Metabolism	Chaperone
Protein shisa-2 homolog	Q6UWI4	6,902	3	0.034	Cell communication and/or signal transduction*	Scaffold/adaptor protein
Protein MGARP	Q8TDB4	6,032	3	0.001	Cell communication and/or signal transduction*	Protein-modifying enzyme*
MARCKS-related protein	P49006	5,615	4	0.048	Cell communication and/or signal transduction	Cytoskeletal protein*
Membrane cofactor protein	P15529	5,079	2	0.026	Cell communication and/or signal transduction	Defense protein
Transmembrane protein 101	Q96IK0	4,858	5	0.045		
Claspin	Q9HAW4	4,461	2	0.008	Cell communication and/or signal transduction	Protein-binding activity*
Serine/threonine-protein phosphatase 2B catalytic subunit beta isoform	P16298	3,790	10	0.049	Cell communication and/or signal transduction	Protein-binding activity
Embigin	Q6PCB8	3,608	4	0.017	Cell growth and/or maintenance	Scaffold/adaptor protein
RING finger protein 121	Q9H920	3,255	2	0.035		
Androgen-induced gene 1 protein	Q9NVV5	3,123	4	0.011	Metabolism*	

Nuclear envelope pore membrane protein POM 121	Q96HA1	2,981	13	0.011	Transport	Transporter
Sterol regulatory element-binding protein 2; Processed sterol regulatory element-binding protein 2	Q12772	2,660	6	0.004	Regulation of nucleobases, nucleoside and nucleic acid metabolism	Transcription regulator*
Transmembrane protein 168	Q9H0V1	2,651	6	0.025		
Protein unc-93 homolog B1	Q9H1C4	2,624	2	0.008	Immunity	Protein-binding activity*
Guanine nucleotide-binding protein G(I)/G(S)/G(O) subunit gamma-7	O60262	2,591	3	0.015	Cell communication and/or signal transduction	Protein-binding activity*
Homeobox protein Hox-C9	P31274	2,565	6	0.027	Regulation of nucleobases, nucleoside and nucleic acid metabolism	Transcriptional regulator*
Nuclear factor of activated T-cells 5	O94916	2,467	4	0.048	Regulation of nucleobases, nucleoside and nucleic acid metabolism	Transcriptional regulator
Histone-lysine N-methyltransferase SUV39H2	Q9H5I1	2,294	5	0.035	Metabolism	Chromatin-regulatory protein
Chondroitin sulfate synthase 2	Q8IZ52	2,278	5	0.025	Metabolism	Metabolite interconversion enzyme
Cytochrome c	P99999; CON__P62894	2,159	13	0.009	Metabolism	Protein-binding activity*
Ankyrin repeat domain-containing protein 46	Q86W74	2,115	3	0.014		Scaffold/adaptor protein
HIG1 domain family member 2A, mitochondrial	Q9BW72	2,010	5	0.001	Transport*	Scaffold/adaptor protein
Downregulated						
CDKN2AIP N-terminal-like protein	Q96HQ2	5,143	3	0.010		
p53 and DNA damage-regulated protein 1	Q9NUG6	5,028	2	0.035	Regulation of nucleobases, nucleoside and nucleic acid metabolism	Protein-binding activity*
Ubiquitin-associated protein 1	Q9NZ09	3,407	3	0.012	Transport*	Protein-binding activity*
Cyclin-dependent kinase 2-interacting protein	Q9BW66	3,227	5	0.032	Cell growth and/or maintenance*	
Tumor necrosis factor receptor type 1-associated DEATH domain protein	Q15628	2,874	2	0.004	Cell communication and/or signal transduction	Protein-binding activity*
RING finger protein 219	Q5W0B1	2,866	4	0.016	Metabolism	Protein-binding actiyity*
Homeobox protein Hox-A6; Homeobox protein Hox-C6;Homeobox protein Hox-C5;Homeobox protein Hox-A7;Homeobox protein Hox-	P31267; P09630; Q00444; P31268; P09067; P20719	2,574	2	0.015	Regulation of nucleobases, nucleoside and nucleic acid metabolism	Transcriptional regulator*

B5;Homeobox protein Hox-A5						
Phostensin	Q6NYC8	2,461	2	0.049		Protein-binding activity*
MAP7 domain-containing protein 3	Q8IWC1	2,446	13	0.009		Cytoskeletal protein
PR domain zinc finger protein 2	Q13029	2,416	5	0.008	Regulation of nucleobases, nucleoside and nucleic acid metabolism	Transcriptional regulator
Alpha-mannosidase 2C1	Q9NTJ4	2,379	3	0.021	Metabolism	Protein-binding activity*
DNA replication complex GINS protein SLD5; DNA replication complex GINS protein SLD5. N-terminally processed	Q9BRT9	2,305	9	0.007	Regulation of nucleobases, nucleoside and nucleic acid*	
Signal peptide peptidase-like 2B	Q8TCT7	2,233	3	0.030	Proteolysis and peptidolysis	Protein modifying enzyme
BET1-like protein	Q9NYM9	2,175	2	0.018	Transport	Membrane traffic protein
TRAF-type zinc finger domain-containing protein 1	O14545	2,171	4	0.039	Immunity*	
Kinetochore protein Nuf2	Q9BZD4	2,137	10	0.018	Chromosome segregation	Cytoskeletal protein
Haloacid dehalogenase-like hydrolase domain-containing protein 2	Q9H0R4	2,136	6	0.006	Metabolism	Membrane traffic protein
Prefoldin subunit 2	Q9UHV9	2,132	7	0.032	Metabolism	Chaperone
Small kinetochore-associated protein	Q9Y448	2,115	3	0.047	Chromosome segregation*	
V-type proton ATPase subunit E 1	P36543; Q96A05	2,082	6	0.045	Transport	

The HEK WT cells treated with h14F7 had cell communication and/or signal transduction upregulated, while transport, chromatin segregation and proteolysis and peptidolysis downregulated compared to the untreated HEK WT cells. The protein classes that were upregulated were scaffold/adaptor protein, transporter, protein modifying enzyme, metabolite interconversion enzyme, chromatin-regulatory protein and defense protein, while the downregulated protein classes were protein-binding activity, membrane traffic protein and cytoskeletal protein.

Four proteins were upregulated more than 10-fold, while the highest ratio for the downregulated proteins were by 5-fold. The highest upregulated protein, with more than 10-fold, was Cytochrome c oxidase subunit 6A1 (mitochondrial). This protein is a component of cytochrome c oxidase. Cytochrome c oxidase, also known as complex IV, is a transmembrane enzyme found in the cell membrane involved in the respiratory electron transport chain. The second highest upregulated protein was Pho guanine nucleotide exchange factor 28 that regulatet downstream pathways of integrins and growth factor

receptors. The third highest upregulated protein was Vesicle-associated membrane protein 2 that is involved in targeting and fusion of transport vesicles to their target membrane. The fourth highest upregulated protein was DENN domain-containing protein 5B. This protein is involved in conversion of GDP-bound Rab proteins to the active GTP form. The two 5-fold downregulated proteins were CDKN2AIP N-terminal-like protein, which was not categorized by the proteomic tools nor was possible to categorize manually due to inadequate information about the protein in the Uniprot database, and p53 and DNA damage-regulated protein 1 involved in chaperone-mediated protein folding.

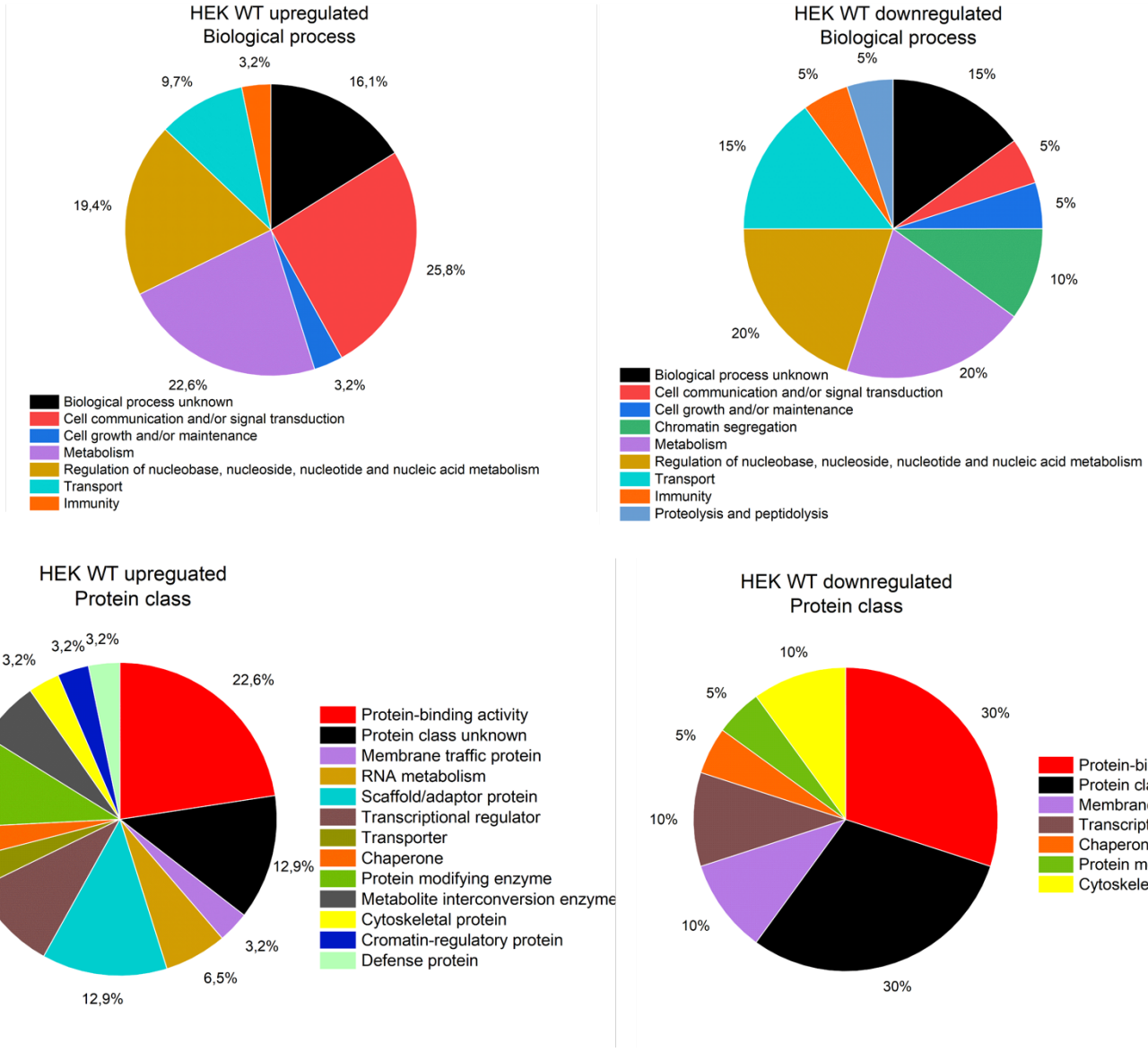

Figure 25. Regulation of proteins in HEK WT treated with h14F7 compared to untreated HEK WT cells. A, Biological processes for upregulated proteins. **B**, Biological processes for downregulated proteins. **C**, Protein classes of the upregulated proteins. **D**, Protein classes of the downregulated proteins. This figure was created using BioRender.

Table 6. Regulated proteins for HEK KI Oslo treated with h14F7 compared to HEK KI Oslo untreated cells. The columns biological process and protein class are color-coded according to the pie charts in Figure 28. Proteins marked with * have been categorized sepearately.

Protein	Uniprot ID	Ratio	Peptides	p-value	Biological process	Protein class
Upregulated						
N-acetylglucosamine-1-phosphotransferase subunit gamma	Q9UJJ9	122,278	3	<0.001	Metabolism	Protein-binding activity enzyme
MLN64 N-terminal domain homolog	O95772	21,230	2	<0.001	Transport	
RWD domain-containing protein 1	Q9H446	12,099	3	<0.001	Cell communication and/or signal transduction*	
Poliovirus receptor	P15151	9,550	5	<0.001	Cell communication and/or signal transduction	Cell adhesion molecule
Guanine nucleotide-binding protein subunit alpha-12	Q03113	9,463	2	0.036	Cell communication and/or signal transduction	Protein-binding activity
Centromere protein K	Q9BS16	5,500	4	0.021	Chromatin-segregation*	
Protein sidekick-1	Q7Z5N4	4,756	7	0.005	Cell growth and/or maintenance	Structural protein
Growth hormone-inducible transmembrane protein	Q9H3K2	4,150	10	0.032	Cell growth and/or maintenance*	Transporter
Protein lin-54 homolog	Q6MZP7	3,648	3	0.019	Cell growth and/or maintenance*	Transcriptonal regulator*
Anaphase-promoting complex subunit 16	Q96DE5	3,239	2	0.049	Cell growth and/or maintenance*	
Vesicle-associated membrane protein 8	Q9BV40	2,886	4	0.042	Transport	Membrane traffic protein
Adenosine 3-phospho 5-phosphosulfate transporter 2	Q9H1N7	2,881	2	0.008	Transport	Transporter
Peroxisome assembly protein 26	Q7Z412	2,819	6	0.037	Cell growth and/or maintenance	Chaperone
Integrin beta-5	P18084	2,764	9	0.041	Cell communication and/or signal transduction	Cell adhesion protein
Mitotic spindle assembly checkpoint protein MAD2A	Q13257	2,709	5	0.016	Cell communication and/or signal transduction	Protein-binding activity*
Transcription factor Sp1	P08047	2,358	4	0.002	Regulation of nucleobases, nucleoside and nucleic acid metabolism	Transcription regulator

Cold-inducible RNA-binding protein	Q14011	2,348	8	0.001	Cell communication and/or signal transduction	RNA metabolism protein
rRNA methyltransferase 1, mitochondrial	Q6IN84	2,345	3	0.033		RNA metabolism protein
Hypermethylated in cancer 2 protein	Q96JB3	2,126	4	0.048	Regulation of nucleobases, nucleoside and nucleic acid metabolism	Transcriptional regulator
Liprin-alpha-3	O75145	2,123	4	0.034	Cell communication and/or signal transduction	Scaffold/adaptor protein
Exosome complex component CSL4	Q9Y3B2	2,047	7	0.041	Regulation of nucleobases, nucleoside and nucleic acid metabolism	RNA metabolism protein
Gamma-soluble NSF attachment protein	Q99747	2,025	11	0.041	Transport	Membrane traffic protein
Probable phospholipid-transporting ATPase IIA	O75110	2,015	12	0.028	Regulation of enzyme activity	Transporter
Downregulated						
Transketolase-like protein 1	P51854	108,046	2	<0.001	Metabolism	Metabolite interconversion enzyme
Surfeit locus protein 1	Q15526	6,739	4	0.004	Metabolism	Chaperone
Induced myeloid leukemia cell differentiation protein Mcl-1	Q07820	6,517	5	0.010	Cell communication and/or signal transduction	
ELAV-like protein 2; ELAV-like protein 4	Q12926; P26378	6,205	6	0.002	Regulation of nucleobases, nucleoside and nucleic acid metabolism	
Envoplakin	Q92817	5,700	2	0.012	Cell growth and/or maintenance	Cytoskeletal protein
Ubiquitin-conjugating enzyme E2 A	P49459	5,167	3	0.043	Regulation of cell cycle and/or DNA repair	Protein modifying enzyme
MARCKS-related protein	P49006	4,955	4	0.035	Cell communication and/or signal transduction	Protein-binding-activity*
Dynein light chain Tctex-type 1	P63172	4,881	5	0.013	Cell growth and/or maintenance*	Cytoskeletal protein
Charged multivesicular body protein 3	Q9Y3E7	4,821	3	<0.001	Cell communication and/or signal transduction*	Membrane traffic protein

Mitochondrial import inner membrane translocase subunit Tim13	Q9Y5L4	4,720	7	0.015	Transport	
Protein IMPACT	Q9P2X3	4,596	5	0.009	Cell communication and/or signal transduction*	Translational regulator*
Dr1-associated corepressor	Q14919	4,504	4	0.026	Regulation of nucleobases, nucleoside and nucleic acid metabolism	Transcriptional regulator
Vacuolar-sorting protein SNF8	Q96H20	4,378	4	0.025	Regulation of nucleobases, nucleoside and nucleic acid metabolism	
Migration and invasion enhancer 1	Q9BRT3	4,345	5	0.001	Cell communication and/or signal transduction*	
Chondroitin sulfate N-acetylgalactosaminyltransferase 2	Q8N6G5	4,284	4	0.025	Metabolism	Metabolite interconversion enzyme
Ribonuclease P protein subunit p25-like protein	Q8N5L8	4,163	3	0.040		RNA metabolism protein
RNA polymerase-associated protein LEO1	Q8WVC0	4,156	3	0.032	Cell growth and/or maintenance*	RNA metabolism protein*
RNA polymerase II subunit A C-terminal domain phosphatase SSU72	Q9NP77	3,879	8	0.030		Protein-modifying enzyme
Protocadherin-9	Q9HC56	3,766	4	0.006	Cell communication and/or signal transduction	Transcriptional regulator
RNA-binding protein 40	Q96LT9	3,275	2	0.018	Regulation of nucleobases, nucleoside and nucleic acid metabolism	
Poly [ADP-ribose] polymerase 9	Q8IXQ6	3,199	7	0.018		
Homeobox protein Hox-B9; Homeobox protein Hox-D9	P17482; P28356	3,126	4	0.012	Regulation of nucleobases, nucleoside and nucleic acid metabolism	
DNA replication complex GINS protein PSF2	Q9Y248	2,762	5	0.041		DNA metabolism protein
Coiled-coil domain-containing protein 85C	A6NKD9	2,757	2	0.005		
Nucleoside diphosphate kinase 6	O75414	2,639	5	0.015	Metabolism	Metabolite interconversion enzyme
Diphthine synthase	Q9H2P9	2,568	6	0.036		Metabolite interconversion enzyme

Protein SHQ1 homolog	Q6PI26	2,503	3	0.029	Regulation of nucleobases, nucleoside and nucleic acid metabolism*	
Geminin	O75496	2,502	3	0.026	Regulation of nucleobases, nucleoside and nucleic acid metabolism	Transcriptional regulator*
Ubiquitin-associated domain-containing protein 1	Q9BSL1	2,460	4	0.004	Cell growth and/or maintenance	
AP-3 complex subunit mu-2	P53677	2,418	3	0.044	Transport	Membrane traffic protein
Protein FAM8A1	Q9UBU6	2,402	3	0.042		
CBP80/20-dependent translation initiation factor	O43310	2,332	3	0.018	Metabolism	RNA metabolism protein
Neugrin	Q9NPE2	2,238	2	0.004	Cell growth and/or maintenance	
Tetratricopeptide repeat protein 33	Q6PID6	2,210	3	0.005		
ER membrane protein complex subunit 7	Q9NPA0	2,175	7	0.026	Transport*	
Muskelin	Q9UL63	2,154	9	0.009	Cell growth and/or maintenance	
Sin3 histone deacetylase corepressor complex component SDS3	Q9H7L9	2,110	4	0.018	Regulation of nucleobases, nucleoside and nucleic acid metabolism	Transcriptional regulator*
Synaptojanin-2-binding protein	P57105	2,073	9	0.039	Transport	
Ras-related protein Rab-22A	Q9UL26	2,064	9	0.012	Cell communication and/or signal transduction	Protein-binding activity enzyme

HEK KI Oslo cells treated with h14F7 had cell communication and/or signal transduction, cell growth and/or maintenance, chromatin segregation, transport and regulation of enzyme activity upregulated, while metabolism, regulation of nucleobase, nucleoside, nucleotide and nucleic acid metabolism and regulation of cell cycle and/or DNA repair were downregulated compared to untreated KI Oslo cells. The protein classes that were upregulated were protein-binding activity protein, cell adhesion, structural protein, RNA metabolism, scaffold/adaptor protein and transporter, while the downregulated protein classes were DNA metabolism, protein modifying enzymes, metabolite interconversion enzyme and cytoskeletal protein.

The upregulated protein with the highest ratio of 122-fold was N-acetylglucosamine-1-phosphotransferase subunit gamma. The subunit is part of the N-acetylglucosamine-1-phosphotransferase complex, which bind and present glycans high in mannose to acceptors. The following four upregulated proteins were MLN64 N-terminal domain homolog by 21-fold RWD domain-containing protein 1 by 12-fold, Poliovirus receptor by 10-fold and Guanine nucleotide-binding protein subunit alpha-12 by 9-fold. MLN64 N-terminal domain homolog creates contact sites between the endoplasmic reticulum and late endosome, RWD domain-containing protein 1 protect developmentally regulated GTP binding protein 2 (DRG2) from proteolytic degradation, Poliovirus receptor mediate adhesion and trigger effector functions in NK cells, and Guanine nucleotide-binding protein subunit alpha-12 is involved in various transmembrane signaling system such as invasion and metastasis of tumor cells. The highest downregulated protein by 200-fold was Transketolase-like protein 1. The protein catalyzes transfer of a two-carbon ketol-group from a ketose donor to an aldose acceptor. Surfeit locus protein is responsible for regulation of cytochrome c oxidase assembly and is downregulated by 7-fold. Further was Induced myeloid leukemia dell differentiation protein Mcl-1 downregulated by 7-fold, which is involved in regulation between cell survival or apoptosis.

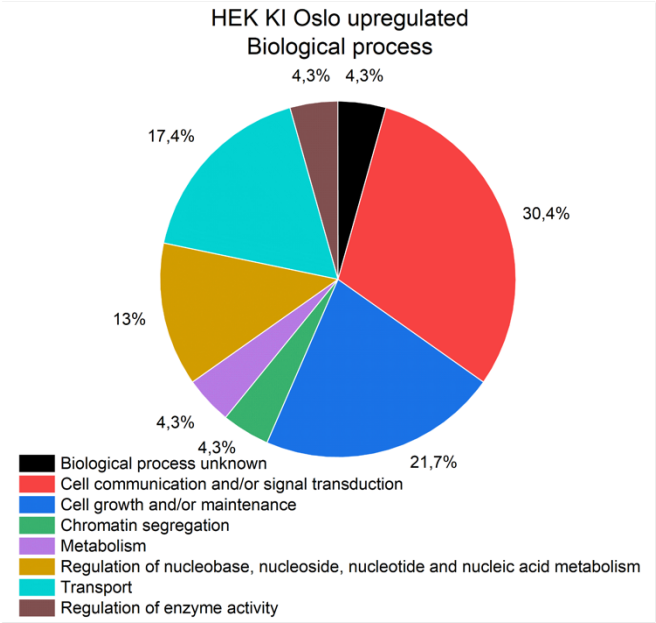

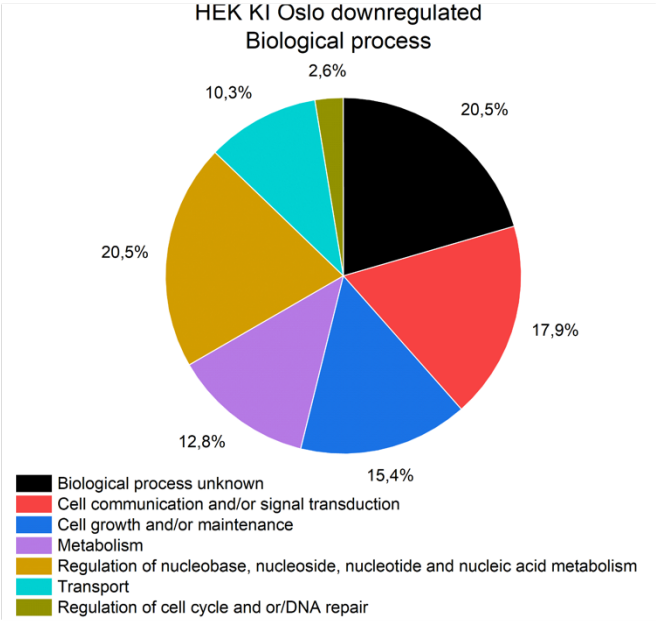

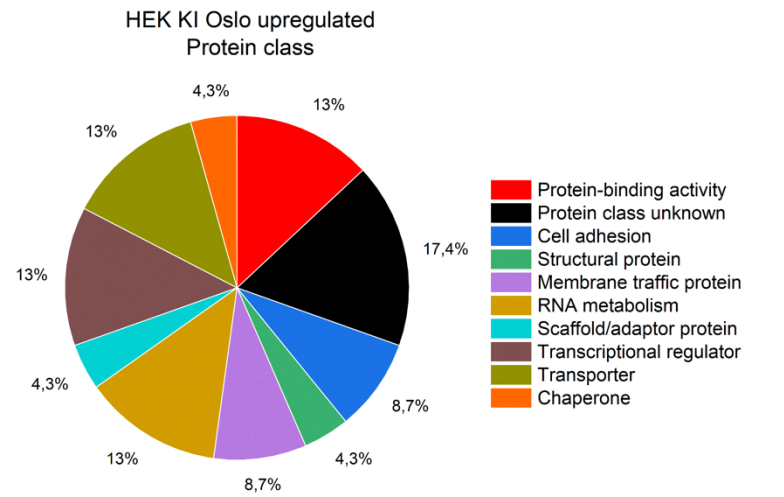

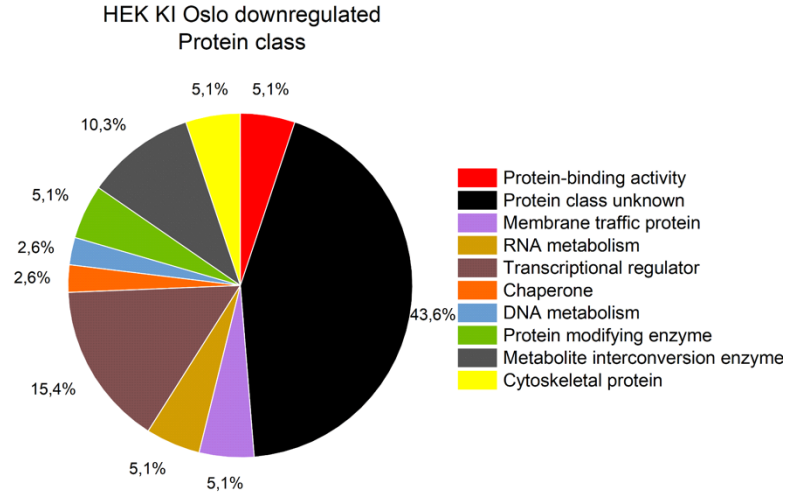

Figure 26. Regulation of proteins in HEK KI Oslo cells treated with h14F7 compared to untreated HEK KI Oslo cells. **A**, Biological processes for upregulated proteins. **B**, Biological processes for downregulated proteins. **C**, Protein classes of the upregulated proteins. **D**, Protein classes of the downregulated proteins. Thos figure was created using BioRender.i

Table 7. Regulated proteins for L1210 treated with m14F7 compared to L1210 untreated cells.

Protein	Uniprot ID	Ratio	Peptides	p-value
Upregulated				
Ig gamma-1 chain C region secreted form; Ig gamma-1 chain C region, membrane-bound form	P01868; P01869	204,393	9	<0.001
Ig kappa chain C region	P01837	40,366	6	<0.001
Ig gamma-2A chain C region, A allele; Ig gamma-2A chain C region, membrane-bound form	P01863; P01865; P84751; P01864	28,949	8	0.013
Centromere-associated protein E	Q6RT24	12,604	4	<0.001
Ig kappa chain V-III region PC 3741/TEPC 111; Ig kappa chain V-III region 50S10.1; Ig kappa chain V-III region PC 2485/PC 4039; Ig kappa chain V-III region PC 7769; Ig kappa chain V-III region PC 6308; Ig kappa chain V-III region MOPC 70; Ig kappa chain V-III region PC 2880/PC 1229; Ig kappa chain V-III region TEPC 124; Ig kappa chain V-III region PC 7132	P01660; P03977; P01673; P01669; P01667; P01656; P01654; P01659; P01655	12,181	2	<0.001
Cysteine-rich protein 1	P63254	9,945	3	0.041
Ig gamma-3 chain C region	P03987	8,934	6	0.005
ATPase inhibitor, mitochondrial	O35143	6,808	2	0.004
E3 ubiquitin-protein ligase Itchy; NEDD4-like E3 ubiquitin-protein ligase WWP1	Q8C863; Q8BZZ3; Q9DBH0	6,225	4	0.021
Ig lambda-1 chain C region	P01843	5,873	2	0.003
Ig kappa chain V-V region K2	P01635	5,868	2	0.006
Ig heavy chain V region AC38 205.12; Ig heavy chain V region J558; Ig heavy chain V region MOPC 104E	P06330; P01757; P01756	4,724	4	0.006
Serine/threonine-protein phosphatase 4 catalytic subunit	P97470	4,524	7	0.030
DnaJ homolog subfamily C member 21	E9Q8D0	4,520	3	0.011
Transcription and mRNA export factor ENY2	Q9JIX0	4,232	2	0.044
Ig heavy chain V region 5-84	P18525	4,164	2	0.001
Phosphorylated adapter RNA export protein	Q9JJT9	4,147	2	0.028
39S ribosomal protein L55, mitochondrial	Q9CZ83	4,132	2	0.014
Ig kappa chain V-III region ABPC 22/PC 9245; Ig kappa chain V-III region PC 4050; Ig kappa chain V-III region MOPC 63	P01662; P01663; P01661	4,009	2	0.029
Ig kappa chain V-V region L6; Ig kappa chain V-V region T1	P01638; P01637	3,993	2	<0.001
Transmembrane protein 168	Q91VX9	3,763	3	0.006
Protein LLP homolog	Q9D945	3,646	3	0.011
Muscleblind-like protein 2	Q8C181	3,512	6	0.018
39S ribosomal protein L54, mitochondrial	Q9CPW3	3,402	3	0.027
Ribosome biogenesis protein BRX1 homolog	Q9DCA5	3,179	8	0.046
Ragulator complex protein LAMTOR3	O88653	3,151	3	0.035
Copper transport protein ATOX1	O08997	3,118	3	0.032
NIF3-like protein 1	Q9EQ80	3,032	4	0.038
Box C/D snoRNA protein 1	Q3UFB2	3,018	2	0.024
Rapamycin-insensitive companion of mTOR	Q6QI06	2,953	3	0.022
Dynein light chain 2, cytoplasmic	Q9D0M5	2,904	4	0.028
60S ribosomal protein L10a	P53026	2,866	10	0.009
Ig kappa chain V-V region HP 93G7; Ig kappa chain V-V region HP R16.7; Ig kappa chain V-V region HP 124E1; Ig kappa chain V-V region HP 123E6	P01645; P01644; P01647; P01646; P01643	2,831	3	0.022

E3 ubiquitin-protein ligase KCMF1	Q80UY2	2,682	5	0.032
Actin-related protein 2/3 complex subunit 5-like protein	Q9D898	2,626	3	0.015
Complex III assembly factor LYRM7	Q9DA03	2,582	2	0.031
Alpha-1,2-mannosyltransferase ALG9	Q8VDI9	2,539	4	0.034
Polypeptide N-acetylgalactosaminyltransferase 2; Polypeptide N-acetylgalactosaminyltransferase 2 soluble form	Q6PB93	2,522	5	0.035
Tripeptidyl-peptidase 1	O89023	2,519	3	0.001
39S ribosomal protein L3, mitochondrial	Q99N95	2,470	3	0.030
5-nucleotidase domain-containing protein 1	Q8C5P5	2,466	2	0.014
NADH dehydrogenase [ubiquinone] 1 subunit C2	Q9CQ54	2,435	4	0.036
Zinc finger CCHC domain-containing protein 8	Q9CYA6	2,403	7	0.009
Coiled-coil domain-containing protein 25	Q78PG9	2,378	3	0.016
60S ribosomal protein L35	Q6ZWV7	2,366	5	0.008
Ig heavy chain V region 914	P18527	2,226	2	0.005
Marginal zone B- and B1-cell-specific protein	Q9D8I1	2,136	8	0.038
DET1- and DDB1-associated protein 1	Q9D9Z5	2,135	2	0.027
Inhibitor of nuclear factor kappa-B kinase subunit beta	O88351	2,103	9	0.039
39S ribosomal protein L48, mitochondrial	Q8JZS9	2,087	3	0.029
40S ribosomal protein S7	P62082	2,070	15	0.023
CCR4-NOT transcription complex subunit 7	Q60809	2,069	3	0.049
Downregulated				
Zinc finger protein 706	Q9D115	42,042	2	<0.001
Transmembrane and coiled-coil domain-containing protein 1	Q921L3	29,796	2	0.002
NADH dehydrogenase [ubiquinone] 1 beta subcomplex subunit 3	Q9CQZ6	11,831	3	0.034
Protein HIRA	Q61666	10,824	2	0.014
Small integral membrane protein 4	Q8C1Q6	8,513	2	0.050
Glycogen synthase kinase-3 alpha	Q2NL51	7,603	4	<0.001
Histone H3.1	P68433	5,590	8	0.026
Creatine kinase B-type	Q04447	5,582	2	0.029
Clathrin light chain A	O08585	5,326	2	0.010
Apoptosis-enhancing nuclease	Q9CZI9	5,293	4	0.008
Major facilitator superfamily domain-containing protein 1	Q9DC37	5,231	2	0.001
Zinc finger protein 750	Q8BH05	4,966	2	0.013
Atypical kinase ADCK3, mitochondrial	Q60936	4,628	2	0.044
ER membrane protein complex subunit 6	Q9CQW0	4,387	3	0.022
Rab proteins geranylgeranyltransferase component A 1	Q9QXG2	4,302	6	0.001
Cyclin-Y	Q8BGU5	4,254	3	0.016
NEDD4-binding protein 1	Q6A037	3,858	2	<0.001
Cell division cycle-associated 7-like protein	Q922M5	3,687	4	0.029
Transmembrane protein 147	Q9CQG6	3,663	2	0.012
Protein FAM134A	Q6NS82	3,590	5	0.035
Zinc finger protein 41	Q02526	3,399	3	0.016
B-cell lymphoma/leukemia 10	Q9Z0H7	3,287	4	0.041
Mis18-binding protein 1	Q80WQ8	3,170	3	0.040
L-lactate dehydrogenase B chain	P16125	3,135	7	0.040

Transportin-2	Q99LG2	3,124	6	0.038
TBC1 domain family member 24	Q3UUG6	3,088	2	0.014
Sorting nexin-8	Q8CFD4	2,904	2	0.028
N-alpha-acetyltransferase 16, NatA auxiliary subunit	Q9DBB4	2,838	6	0.031
Four and a half LIM domains protein 3	Q9R059	2,828	6	0.020
Glycerophosphodiester phosphodiesterase domain-containing protein 1	Q9CRY7	2,794	4	0.016
Type 1 phosphatidylinositol 4,5-bisphosphate 4-phosphatase	Q3TWL2	2,779	5	0.018
Neudesin	Q9CQ45	2,728	2	0.028
Ubiquitin-conjugating enzyme E2 R2	Q6ZWZ2; Q8CFI2	2,725	4	0.007
CMP-sialic acid transporter	Q61420	2,724	2	0.001
CD48 antigen	P18181	2,680	4	0.006
Endoplasmic reticulum-Golgi intermediate compartment protein 3	Q9CQE7	2,646	5	0.026
SAGA-associated factor 29 homolog	Q9DA08	2,543	2	0.013
Protein FAM195A	Q9CQB2	2,509	2	0.014
Large neutral amino acids transporter small subunit 1	Q9Z127	2,433	6	0.012
Serine/threonine-protein phosphatase 4 regulatory subunit 2	Q0VGB7	2,360	7	0.007
L-fucose ligase	Q7TMC8	2,356	2	0.006
Transmembrane channel-like protein 8	Q7TN58	2,309	2	0.033
Protein diaphanous homolog 3	Q9Z207	2,299	5	0.034
Protein yippee-like 5	P62700	2,291	3	0.005
Lysosomal Pro-X carboxypeptidase	Q7TMR0	2,254	3	0.032
N-alpha-acetyltransferase 25, NatB auxiliary subunit	Q8BWZ3	2,248	8	0.025
dCTP pyrophosphatase 1	Q9QY93	2,239	6	0.025
GMP reductase 2	Q99L27	2,224	5	0.049
Density-regulated protein	Q9CQJ6	2,200	6	0.039
Transmembrane protein 70, mitochondrial	Q921N7	2,174	2	0.005
BAG family molecular chaperone regulator 4	Q8CI61	2,172	2	0.045
Ras-related protein Rab-35	Q6PHN9	2,122	5	0.011
Eukaryotic translation initiation factor 1A	Q60872	2,101	6	0.008
DDB1- and CUL4-associated factor 8	Q8N7N5	2,068	8	0.029
Translocation protein SEC62	Q8BU14	2,067	5	0.015
Partner of Y14 and mago	Q8CHP5	2,016	9	0.028
Protein SDA1 homolog	Q80UZ2	2,016	6	0.022
Autophagy protein 5	Q99J83	2,001	4	0.036
Nucleolar complex protein 2 homolog	Q9WV70	1,997	9	0.027
Dehydrogenase/reductase SDR family member 1	Q99L04	1,996	5	0.002

The upregulated and downregulated proteins for L1210 cells differ the most from the dataset of regulated proteins for HEK WT and HEK KI Oslo. There were more proteins found to be up- and downregulated for L1210. The highest up-regulated proteins are related to immunoglobulins. Ig gamma-1 chain C region secreted form; Ig gamma-1 chain C region, membrane-bound form was the upregulated protein with highest ratio by 204-fold. Four proteins were downregulated by 10-fold. The first was Zinc finger protein 706 involved in repression of transcription for embryonic stem cells exiting self-renewal. The second protein was Transmembrane and coiled-coil domains protein 1, which there was very inadequate information on through the Uniprot database. The third protein was NADH dehydrogenase 1 beta subcomplex subunit 3, an accessory subunit of Complex I in the respiratory chain. The fourth protein downregulated protein was protein HIRA, required during the cell cycle for repression of histone gene transcription.

5. Discussion

5.1 Considerations

5.1.1 Choice of median vs mean fluorescence signal for flow cytometry results

The median fluorescent signal measured by flow cytometry was chosen to use for the figures in the results for this thesis instead of the mean signal because the histograms were not uniform. They were instead skewing, either to the left or the right, as illustrated in Figure 27. This led to the fact that the mean value was positioned more to the side of the skewing. The median value gave a more homogeneous representation of the population of cells measured and was therefore chosen as the value used for all the flow cytometry results in this thesis.

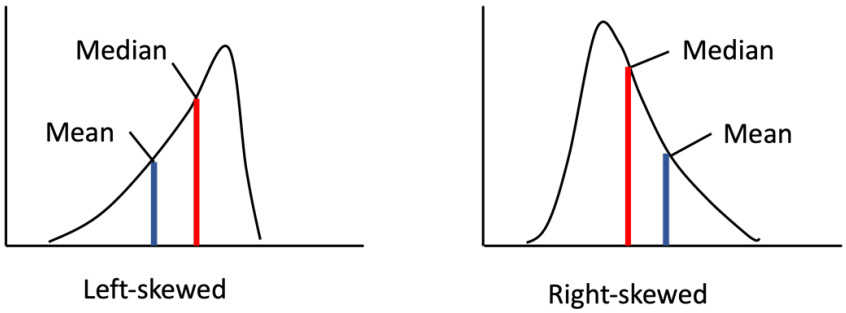

Figure 27. Sketch of left-skewed and right-skewed histograms. The median is indicated in red and the mean in blue for both the left- and right-skewed histograms. This figure was created with Microsoft PowerPoint.

5.1.2 Controls for flow cytometry experiments

One of our initial challenges for the flow cytometry experiments (Section 4.1.1 and 4.1.2) was the fact that we did not have appropriate controls available. A positive control, that is known to bind to the desired target, and a negative control, known to not bind to the target, should be used for these analyses to confirm that the antibody does not bind unspecifically. This was the strength of the second round of flow cytometry experiments, performed at Copenhagen Center for Glycomics. An anti-Neu5Gc antibody, known to bind Neu5Gc, was used as a positive control (Biolegend, Cat: 146903). Neuraminidase (Sigma-Aldrich) was used as a negative control. Neuraminidase can cleave off terminal α-glycosidically linked sialic acid residues by hydrolysis (Miyagi *et al.*, 2018). By cleaving off the sialic acids, we

wanted to demonstrate that 14F7 recognizes and binds to sialic acids. However, we observed that the binding of 14F7 was about identical for the neuraminidase-treated cells as for the untreated (Figure 16 panel A and B, Figure 17 panel A and Figure 18 panel A and B). To test whether the neuraminidase was active, we used PNA and PanLectenz as additional controls. PNA binds to terminal galactose units and would only be expected to bind after sialic acids of GM3 are removed by neuraminidase. Binding of PNA was observed from the flow cytometry data (Figure 16 panel C, Figure 17 panel B and Figure 18 panel C). PanLectenz was used as a second control that only binds to sialylated glycans. There was a surprisingly difference in binding between WT and KO compared to KI (Figure 16 panel D and Figure 17 panel C). WT and KO, expressing Neu5Ac, had a stronger binding of PanLectenz than KI cells expressing Neu5Gc. These observations were made for both HEK and CHO cells, suggesting a stronger binding of PanLectenz to Neu5Ac. The experiment was repeated with HEK WT, KI Cph and KI Oslo, where no binding of PanLectenz was measured, even for the WT cells. The Panlectenz was most likely forgotten during sample preparation or prepared incorrectly for that specific experiment (Figure 18 panel D).

We made the conclusion based on the two controls that neuraminidase was active, but specific for Neu5Ac. There were unfortunately no publications to be found stating a specificity for Neu5Ac by neuraminidase purchased from Sigma-Aldrich, but resistance of hydrolysis of α2-8-linked Neu5Gc for mammalian and bacterial sialidases have been hypothesized (Davies *et al.*, 2012). The experiments were not further repeated due to limited time, but would be interesting to repeat with neuraminidase from another supplier. A suggested supplier could be New England BioLabs as they state in their product information for Neuraminidase A (Cat. P0722S) that it can act on both Neu5Gc and Neu5Ac.

5.2 Which cells gave the strongest signal?

Independent of the antibody used, HEK KI Oslo always gave the highest signal compared to HEK WT and KI Cph. The results in Figure 13 panel A illustrated that different 14F7 formats used as primary antibodies with different conjugated secondary antibodies, showed a stronger binding for HEK KI Oslo. Surprisingly, HEK KI Oslo had a much higher binding of h14F7* as primary antibody and anti-human Alexa Fluor 647 as secondary antibody, compared to this antibody combination used for KI Cph. We imaged the cells by confocal microscopy to see if this difference in fluorescent signal also was visibly detectable. The signal, illustrated as a red ring around the cells (Figure 14), showed a difference in

fluorescent signal. HEK KI Cph had fewer cells with a visible signal for 14F7 than HEK KI Oslo. The same observation for binding by flow cytometry was made from the experiments performed in Copenhagen (Figure 18 panel A and B). HEK KI Oslo had a higher median fluorescence signal with h14F7 and h14F7* bound, compared to HEK KI Cph. These observations together made us wonder what the reason could be for the difference in binding between these two KI cell constructs.

5.2.1 Possible explanations for the difference in antibody binding

The cells were knocked-in with the same gene, but by different methods (Section 3.1.1). This has probably led to different positioning of the knocked-in *CMAH*-gene in the cells' genome, resulting in differences in e.g., protein expression. As mentioned in section 4.1.4, it has been established that Neu5Ac inhibits dimerization of growth factor receptors (GFRs) and its downstream signaling pathways. A possibility could be that the two KI constructs expressed EGFRs in different amounts, that further influenced the binding of 14F7 to Neu5Gc. The amounts of expressed EGFRs on the cell surface of HEK WT, KI Cph and KI Oslo were compared by incubating the cells with Cetuximab, a chimeric anti-EGFR mAb. Figure 19 shows the median fluorescence signals, demonstrating that there are no big differences in EGFR expression between the three cells. Consequently, there must be some other explanation for the difference in 14F7 binding. With the observations from the flow cytometry experiments, binding of Cetuximab to EGFRs and visualization of 14F7 bound to KI Cph and KI Oslo by confocal microscopy, we hypothesize that this difference could be because the HEK KI Oslo cells express a higher amount of Neu5Gc GM3. Based on the observations in Figure 14, it also looked like the cells within the same sample express Neu5Gc to varying degrees. It is worth mentioning that flow cytometry is a more sensitive analytical method to use for detection of fluorescence than what can be imaged by a confocal microscope. Therefore, there could be fluorescent signal from all the cells in the sample (Figure 14), but too low for the microscope to detect with the settings used for these acquired images.

A higher amount of Neu5Gc on the cell surface might not be the only explanation for the higher binding to KI Oslo. The amount of gangliosides have been demonstrated to influence the binding of 14F7 (Bjerregaard-Andersen *et al.*, 2020). Liposomes containing different combinations of Neu5Gc and Neu5Ac were measured by electrochemiluminescence immunoassay (EIA). The binding of 14F7 to liposomes containing a mixture of 2% Neu5Gc and 8% Neu5Ac GM3 had a significantly higher binding than liposomes containing only 2% Neu5Gc. A higher concentration of gangliosides may lead to different packing, i.e.

through carbohydrate stacking (Stewart and Boggs, 1993). The *N*-glycolyl group could then be exposed.

An «all-or-nothing» effect have been suggested for the binding of 14F7, meaning a binding was only observed above a concentration threshold of the Neu5Gc GM3 (Bjerregaard-Andersen *et al.*, 2020). Assuming that KI Oslo express more Neu5Gc, this could explain the higher signal for the positive control of anti-Neu5Gc in Figure 18 panel E than for WT and KI Cph. The “all-or-nothing” effect has been observed for other antibodies previously (Nores *et al.*, 1987). Either the reason for higher binding for HEK KI Oslo is due to a higher amount of Neu5Gc expressed, a higher amount of gangliosides or impact of other proteins, it would be interesting to sequence the two KI constructs to compare where in the genome the *CMAH* gene was put. The placement of the gene could give a response in protein expression or regulation that can explanation for the differences in binding observed.

5.3 Hypoxic conditions in malignant tumors

Murine cell lines that express Neu5Gc and model organisms are useful tools for understanding antibody binding and their mechanisms. Yet, for the purpose of potentially using 14F7 for immunotherapy in humans, one must also study the binding to human cells, and further down the line in humans through clinical trials. The two KI constructs were prepared to simulate cancer cells for the use of studying the binding specificity of 14F7 to human cells. However, to knock in a specific gene in a cell line does not mimic a natural event that can explain how Neu5Gc is expressed on cancerous cells. Hypoxia is a common feature in malignant tumors and can lead to alterations in gene expression (Manoochehri Khoshinani, Afshar and Najafi, 2016; Batie and Rocha, 2020; Rakotomalala *et al.*, 2021). This could possibly be an explanation for the expression of Neu5Gc in human cancer cells.

Figure 15 panel A shows that HEK WT cells placed under hypoxia does not divide following the same growth curve as HEK WT in normoxia. This can be explained by the fact that the HEK cells are not a cancerous cell line and are accordingly not adapted to grow or survive under the condition of low oxygen levels (>5% O_2). The median fluorescent signal from flow cytometry with m14F7 as primary antibody and anti-mouse FITC as secondary antibody for HEK WT cells grown under hypoxia for 24 hours (Figure 15 panel C) was approximately $4*10^4$ compared to $2*10^4$ for HEK WT grown under normoxia. The 2-fold difference in measured signal could indicate that Neu5Gc was expressed on the cells subjected to hypoxic conditions. However, these experiments were performed on different days and the

measured fluorescent signal can therefore not be directly compared as there might be differences affecting the samples or the flow cytometer between the days the experiments were performed. The signal measured for cells only treated with the FITC-conjugated secondary antibody had almost as high measured signal as the cells treated with both the primary and secondary antibody, weakening the accuracy of our results for this ecperiment. For direct comparison, HEK WT cells grown under hypoxic and normoxic conditions should be prepared in parallel and the fluorescent signal measured the same day. The choice of conjugated secondary antibody should also be considered, as the goat anti-mouse FITC seemed to have an interaction with the cells. This experiment was only performed once with three independent biological replicates and should therefore be repeated to demonstrate reproducibility before a conclusion about Neu5Gc expression on HEK WT cells under hypoxic conditions can be made.

5.4 What is the target?

It has previously been showed that 14F7 binds specificly to Neu5Gc with high affinity (Carr *et al.*, 2000; Krengel *et al.*, 2004; Rojas *et al.*, 2004; Bjerregaard-Andersen *et al.*, 2018), but the results illustrated in Figure 13 did not comply with that. Different combinations of 14F7 formats as primary antibodies and conjugated secondary antibodies showed a binding, although weaker than to KI cells, to HEK WT cells. The proteomic data (Table 5 and figure 27) also strengthen the observations that 14F7 do interact in some way with HEK WT cells. Does 14F7 only recognize Neu5Gc GM3, or also other surface molecules like glycoproteins? A KI-KO cell could be made for the purpose of investigating 14F7's true target. The cell would be knocked-in with *CMAH* to only express Neu5Gc and not Neu5Ac, and then the B4Gal5/6 gene would be knocked out. A binding of 14F7 to the cells would indicate the antibody recognize something else on the cell surface, but in the case the antibody does not bind, we would show that it is glycolipid specific.

5.5 Which antibody format gave the best binding?

The binding analysis illustrated in Figure 13 panel A and Figure 16-18 indicated two things. First, the humanized antibody gave a stronger binding than the m14F7. Second, the h14F7 gave a stronger binding than h14F7*. The three formats have some differences in their amino acid sequence, but have been reported to have the same specificity (Krengel *et al.*,

2004; Bjerregaard-Andersen *et al.*, 2018, 2020). The two humanized formats vary by their variable light chain, where h14F7* have a variable light chain (Rojas *et al.*, 2004). Although the results from section 4.1 points to h14F7 as the best humanized format, further investigations should be carried out to determine which light chain is the preferable and why. One could start by performing an equivalent liposome experiment as described by Bjerregaard-Andersen *et al.* (2018). Liposomes a range of different percentage of Neu5Gc can be used to investigate if the two humanized antibodies have dissimilar binding for the different lipid compositions.

5.6 What can we tell about 14F7's cellular journey?

Information about antibody binding and specificity is important, but knowing where an antibody goes in the cell, if internalized, is vital information for making the best possible format to be used in the clinic. Preliminary binding studies indicated that the antibody is internalized (Pesci, 2020). Taken together with the observation made by immunofluorescent staining, the internalized receptor is localized to the late endosome (Figure 24). The cholera toxin, which binds to GM1 gangliosides, can be internalized by various modes of endocytosis (Wernick *et al.*, 2010). It can traffic retrograde from the plasma membrane to the *trans*-Golgi Network and reach the endoplasmic reticulum (ER). The trafficking of the Cholera toxin is assumed to be dependent on GM1 to associate with lipid rafts. Since the GM1 ganglioside with the Cholera toxin is internalized and traffics all the way to the ER, maybe GM3 follows the same path, but it would depend on how strong 14F7 binds to GM3. The Cholera toxin binds to GM1 through its five B subunits (T. *et al.*, 2001), giving a 5-fold binding compared the 14F7. The difference in binding could implicate how far 14F7 can traffic, and whether if hops off earlier in the retrograde pathway.

To our knowledge, the internalization of 14F7 and its intracellular journey have not been demonstrated yet. Thus, these comparison of the Cholera toxins uptake and trafficking is only a speculation. Experiments to demonstrate internalization and uptake kinetics using appropriate controls would be the next step for the imaging experiments. However, we experienced difficulties using HEK cells for live imaging because the conditions used during live imaging caused the cells to round up and blebbed. Optimization of live imaging of HEK cells must be performed before internalization of 14F7 can be studied.

5.7 What effects do 14F7-treatment have on different cells?

Comparing the tables for the up- and downregulated proteins for HEK WT (Table 5), KI Oslo (Table 6) and L1210 (Table 7), there are no same proteins found. This could be partially explained with having only three replicates and not very good statistics. The dataset for L1210 was the most different from the two other datasets. The dataset contains several up- and downregulated protein with higher ratio and with different biological processes involved. Many of the up-regulated protein for L1210 are involved in regulation of immunoglobulins, which is not to be found in the two other datasets. Funrich and Panther, the two bioinformatic tools used (both free versions online or to download), did not recognize or categorize the murine proteins as well as the human proteins, i.e., only 7 of the 60 downregulated proteins in the dataset for L1210 were recognized. Pie charts for the regulated L1210 proteins were therefore not created. With access to other bioinformatic tools, there might have had better recognition of the murine proteins. It would be interesting to investigate why regulation of immunoglobulins were so highly upregulated for the murine cells, but since the dataset was so different from the two others, it was decided to rather focus our attention on the datasets for the HEK WT and KI Oslo.

31 proteins were upregulated and 20 downregulated with at least a 2-fold for HEK WT cells treated with h14F7 compared to untreated. Correspondingly were 23 proteins found upregulated and 39 downregulated for KI Oslo treated cells compared to untreated. The ratio of the most upregulated protein in the dataset for KI Oslo was 122-fold (Table 6), while the most upregulated for WT had a 27-fold difference (Table 5). Similarly, the most downregulated protein for KI Oslo of 108-fold (Table 6) were higher than the most downregulated protein for WT with its 5-fold (Table 5). These observations may indicate that the KI Oslo cells had a stronger response to the antibody treatment. This would be reasonable as 14F7 binds to Neu5Gc which are only present on the KI cells, and therefore give a stronger response. However, the WT cells do have an effect by the antibody treatment as well. We do not at the current time know how or why these effects are detected.

Cell communication and/or signal transduction was upregulated for both WT and KI Oslo treated cells, but other than that there are not any other biological processes regulated similarly. While chromatin segregation and transport are upregulated in KI treated cells, these processes are downregulated for WT treated cells. The other biological processes were either up-or downregulated for only WT or KI treated cells. For protein classification, scaffold/adaptor protein and transporters were upregulated for both WT and KI treated cells,

while downregulation of cytoskeletal protein was similar. Protein modifying enzymes and metabolite interconversion enzymes were upregulated for WT treated cells, and downregulated for KI Oslo, together with downregulation of protein-binding activity for WT that were upregulated for KI. The differences in up-and downregulation make it harder to get a clear interpretation of what effects the treatment of 14F7 have on these cells. Still, the results suggest that the treatment led to changes in proteins involved in cell communication and signaling pathways, as well as cytoskeletal proteins. These findings correspond with changes reported from a similar experiment previously performed by our group. HeLa cells were kept either in normoxic or hypoxic environment, before the cells were submitted to quantitative proteomic analysis to investigate the differences in protein expression (Bousquet *et al.*, 2015). The reported regulation also suggested that treatment of 14F7 led to upregulation of cellular processes and transport, while structural molecule activity, such as cytoskeletal proteins, were downregulated (Bousquet *et al.*, 2015). Additionally, proteomic analysis of HeLa cells grown in normoxia treated with h14F7 also exhibited upregulation of cellular processes and downregulation of cytoskeletal proteins (Bousquet, 2014).

The proteins found to be regulated by HeLa cells subjected to hypoxic conditions were compared to the regulated proteins for WT and KI treated cells. 15 shared proteins were found, but with different ratio and effect, illustrated in Table 8. If suggested that HeLa cells under hypoxia respond similar as 14F7-treated KI Oslo cells, as they both express Neu5Gc, the 7 first proteins in Table 8 would describe proteomic changes analogously. Glucose phosphate isomerase, pyruvate kinase PMK and thymine kinase were upregulated in HeLa and downregulated in HEK WT. ERO1-like protein alpha, isocitrate dehydrogenase 2 and Prolyl 4-hydroxylase subunit alpha-1 and Vimentin were upregulated in HeLa and also upregulated in KI Oslo. These 7 proteins described the same effect for these two experiments. The remaining 8 proteins in Table 8 show opposite regulation. This could be a result of differences in cell lines reacting in a distinctive way, but it could also imply that the reported protein regulations do not give a reliable representation, especially since only three replicates were used.

Table 8. Proteins regulated in HeLa cells grown under hypoxic conditions also regulated in HEK WT or KI Oslo treated with h14F7.

Protein	Biological process	Uniprot ID	Regulation in HeLa cells	Ratio	p-value	Regulation in HEK WT or KI Oslo cells	Ratio	p-value
Glucose phosphate isomerase	glycolysis/ gluconeogenesis, pentose phosphate pathway	P06744	Upregulated	2,46	<0,001	Downregulated in WT	1,53	0,037
Pyruvat kinase PKM	glycolysis/ glukoneo-genesis, pyruvate metabolism	P14618	Upregulated	1,79	0,012	Downregulated in WT	1,17	0,047
Thymidine kinase, cytosolic	translation	P04183	Upregulated	1,67	0,033	Downregulated in WT	1,23	0,024
ERO1-like protein alpha	generation of precursor metabolites and energy	Q96HE7	Upregulated	3,13	<0,001	Upregulated in KI Oslo	1,20	0,021
Isocitrate dehydrogenase 2 (NADP), mitocondrial	citric acid cycle (TCA cycle)	P48735	Upregulated	1,67	0,034	Upregulated in KI Oslo	1,23	0,011
Prolyl 4-hydroxylase subunit alpha-1	amino acid metabolism, oxido-reductase activity	P13674	Upregulated	5,3	<0,001	Upregulated in KI Oslo	1,43	0,008
Vimentin	cell motion	P08670	Upregulated	1,54	0,093	Upregulated in KI Oslo	1,28	0,025
Cytochrome c oxidase assembly factor 6 homolog	cytochrome-c oxidase activity	Q5JTJ3	Downregulated	0,6	0,095	Upregulated in KI Oslo	1,42	0,036
Electron transfer flavoprotein subunit alpha, mitochondrial	generation of precursor metabolites and energy	P13804	Downregulated	0,59	0,077	Upregulated in KI Oslo	1,19	0,047
Ferritin, light polypeptide	ion binding, ion transport	P02792	Downregulated	0,55	0,035	Upregulated in KI Oslo	1,51	0,004
Hydroxysteroid dehydrogenase-like protein 2	oxidation reduction	Q6YN16	Downregulated	0,59	0,08	Upregulated in KI Oslo	1,27	0,032
Mitochondrial ribosomal protein L9	translation	Q9BYD2	Downregulated	0,5	0,009	Upregulated in KI Oslo	1,26	0,031
Mitochondrial ribosomal protein S7	translation	Q9Y2R9	Downregulated	0,41	<0,001	Upregulated in KI Oslo	1,40	0,011
Prostagladin E synthase 2	Oxido-reductase activity, fatty acid metabolic process	Q9H7Z7	Downregulated	0,54	0,029	Upregulated in KI Oslo	1,57	0,015
SRA stem-loop-interacting RNA-binding protein, mitochondrial	regulation of transcription	Q9GZT3	Downregulated	0,55	0,031	Upregulated in KI Oslo	1,52	0,026

The reported treatment of L1210 with m14F7 by Roque-Navarro *et al.* (2008) suggested antibody-induced tumor cell death by loss of membrane integrity (Roque-Navarro *et al.*, 2008). The cell death was also accompanied by cellular swelling and cytoskeleton activation. We observed an increased amount of dead cells upon treatment with h14F7 and a decrease in cell size (Figure 20 panel C and D) compared to untreated KI Cph. However, the gating of this experiment was very challenging as there were several populations of cells that were not easily determined if were alive or dead (Figure 20 panel A-D). There also seemed to be a lot of cell debris in the samples, but could potentially also have been cells very small in size. Nevertheless, everything points to something happening to the cytoskeletal proteins and cell death to some extent with cells are treated with the antibody 14F7.

6. Conclusions and future perspectives

Experiments were designed to investigate which of the two HEK KI constructs that gave the strongest binding. Independent of the antibody used, HEK KI Oslo always gave the highest signal. It was also demonstrated that out of the three formats of 14F7 investigated, the humanized antibody produced in Cuba (h14F7) gave the strongest binding to HEK KI cells. Confocal microscopy was used to demonstrate binding of 14F7 to its target on the cell surface as well as internalized receptors in the late endosome. The proteomic results showed that something happened to the cytoskeletal proteins upon antibody treatment, but not as dramatic as described in the publication from Roque-Navarro *et al.* (2008) where membrane lesions were reported. Furthermore, observations were made of increased cell death and change of morphology for cells treated with h14F7.

The two KI constructs showed a difference in antibody binding. They were made by different protocols that assumingly resulted in different placement of the *CMAH*-gene in the genome of the HEK cells. It would be of interest to sequence the genome to see where the gene was placed, as it resulted in difference of binding. Additionally, we want to investigation of why the differences in F_V for the two humanized 14F7 formats gave different binding affinity when it previously have been demonstrated that the scFv of these construct gave similar binding affinity (Rojas *et al.*, 2004; Bjerregaard-Andersen *et al.*, 2018). The experiments performed in Copenhagen should be followed up with the use of neuraminidase from a different supplier to investigate if 14F7 only recognizes sialic acids. Moreover, it would be interesting to make a B4Gal5/6-KO of the *CMAH*-KI cells to examine if 14F7 is glycolipid specific.

The further steps in understanding then cellular journey of 14F7 would be to investigate the uptake kinetics, as well as the intracellular pathway and the final destination for 14F7 in the cell. There are certainly more information from the quantitative proteomics that should be interpreted, that might reveal ofther important aspects of the antibody treatment to the cells. Together, this would provide vital information for further development toward cancer treatment using this antibody in the clinic.

7. References

Aatbio (2019) *Fundamentals of flow cytometry*, *AssayWise Letters*. Available at: https://www.aatbio.com/resources/assaywise/2019-8-1/fundamentals-of-flow-cytometry.

Abbas, A. K., Lichtman, A. H. and Pillai, S. (2018) *Cellular and molecular immunology*. 9th edn.

Abcam (no date) *Introduction to flow cytometry*. Available at: https://www.abcam.com/protocols/introduction-to-flow-cytometry (Accessed: 5 March 2022).

Adan, A. *et al.* (2017) 'Flow cytometry: basic principles and applications', *Critical Reviews in Biotechnology*, 37(2), pp. 163–176. doi: 10.3109/07388551.2015.1128876.

Alisson-Silva, F., Kawanishi, K. and Varki, A. (2016) 'Human risk of diseases associated with red meat intake: Analysis of current theories and proposed role for metabolic incorporation of a non-human sialic acid.', *Molecular aspects of medicine*, 51, pp. 16–30. doi: 10.1016/j.mam.2016.07.002.

Allen, C., Her, S. and Jaffray, D. A. (2017) 'Radiotherapy for cancer: Present and future', *Advanced Drug Delivery Reviews*, 109, pp. 1–2. doi: https://doi.org/10.1016/j.addr.2017.01.004.

Aslam, B. *et al.* (2017) 'Proteomics: Technologies and their applications', *Journal of Chromatographic Science*, 55(2), pp. 182–196. doi: 10.1093/chromsci/bmw167.

Bajwa, R. *et al.* (2019) 'Adverse effects of immune checkpoint inhibitors (programmed death-1 inhibitors and cytotoxic T-lymphocyte-associated protein-4 inhibitors): Results of a retrospective study', *Journal of Clinical Medicine Research; Vol. 11, No. 4, Apr 2019*. Available at: https://doi.org/10.14740/jocmr3750.

Banda, K. *et al.* (2012) 'Metabolism of vertebrate amino sugars with N-glycolyl groups: Mechanisms underlying gastrointestinal incorporation of the non-human sialic acid xeno-autoantigen N-glycolylneuraminic acid', *Journal of Biological Chemistry*, 287(34), pp. 28852–28864. doi: 10.1074/jbc.M112.364182.

Batie, M. and Rocha, S. (2020) 'Gene transcription and chromatin regulation in hypoxia.', *Biochemical Society transactions*, 48(3), pp. 1121–1128. doi: 10.1042/BST20191106.

Berger, C. *et al.* (2011) 'Nimotuzumab and cetuximab block ligand-independent EGF receptor signaling efficiently at different concentrations.', *Journal of immunotherapy (Hagerstown, Md. : 1997)*, 34(7), pp. 550–555. doi: 10.1097/CJI.0b013e31822a5ca6.

Bjerregaard-Andersen, K. *et al.* (2018) 'Crystal structure of an L chain optimised 14F7 anti-ganglioside Fv suggests a unique tumour-specificity through an unusual H-chain CDR3 architecture', *Scientific reports*, 8(1), p. 10836. doi: 10.1038/s41598-018-28918-5.

Bjerregaard-Andersen, K. *et al.* (2020) 'Insight into glycosphingolipid crypticity: Crystal structure of the anti-tumor antibody 14F7 and recognition of NeuGc GM3 ganglioside', *bioRxiv*, p. 2020.09.18.294777. doi: 10.1101/2020.09.18.294777.

Bjerregaard-Andersen, K. *et al.* (2021) 'Key role of a structural water molecule for the specificity of 14F7—An antitumor antibody targeting the NeuGc GM3 ganglioside', *Glycobiology*, 31(11), pp. 1500–1509. doi: 10.1093/glycob/cwab076.

Blanco, R. *et al.* (2011) 'Immunorecognition of the 14F7 mab raised against N-Glycolyl GM3 ganglioside in some normal and malignant tissues from genitourinary system', *ISRN Pathology*. Edited by T. Yazawa and A.-J. Kruse, 2011, p. 953803. doi: 10.5402/2011/953803.

Blanco, R. *et al.* (2015) 'Prognostic significance of N-glycolyl GM3 ganglioside expression in non-small cell lung carcinoma patients: New evidences', *Pathology Research International*. Edited by M. Volante, 2015, p. 132326. doi: 10.1155/2015/132326.

Bonilla, F. A. and Oettgen, H. C. (2010) 'Adaptive immunity', *Journal of Allergy and Clinical Immunology*, 125(2), pp. S33–S40. doi: 10.1016/j.jaci.2009.09.017.

Bousquet, P. (2014) *N-glycolyl GM3 as potential target for cancer immunotherapy*. University of Oslo.

Bousquet, P. A. *et al.* (2015) 'Hypoxia strongly affects mitochondrial ribosomal proteins and translocases, as shown by quantitative proteomics of HeLa cells', *International journal of proteomics*. 2015/09/02, 2015, p. 678527. doi: 10.1155/2015/678527.

Bousquet, P. A. *et al.* (2018) 'Hypothesis: Hypoxia induces de novo synthesis of NeuGc gangliosides in humans through CMAH domain substitute', *Biochemical and Biophysical Research Communications*, 495(1), pp. 1562–1566. doi: https://doi.org/10.1016/j.bbrc.2017.11.183.

Boute, N. *et al.* (2016) 'NanoLuc luciferase - a multifunctional tool for high throughput antibody screening.', *Frontiers in pharmacology*, 7, p. 27. doi: 10.3389/fphar.2016.00027.

Bremer, E. G., Schlessinger, J. and Hakomori, S. (1986) 'Ganglioside-mediated modulation of cell growth. Specific effects of GM3 on tyrosine phosphorylation of the epidermal growth factor receptor.', *The Journal of biological chemistry*, 261(5), pp. 2434–2440.

Carr, A. *et al.* (2000) 'A mouse IgG1 monoclonal antibody specific for N-glycolyl GM3 ganglioside recognized breast and melanoma tumors.', *Hybridoma*, 19(3), pp. 241–247. doi: 10.1089/02724570050109639.

Carr, A. *et al.* (2002) 'In vivo and in vitro anti-tumor effect of 14F7 monoclonal antibody.', *Hybridoma and hybridomics*, 21(6), pp. 463–468. doi: 10.1089/153685902321043990.

Chung, T.-W. *et al.* (2009) 'Ganglioside GM3 inhibits VEGF/VEGFR-2-mediated angiogenesis: direct interaction of GM3 with VEGFR-2.', *Glycobiology*, 19(3), pp. 229–239. doi: 10.1093/glycob/cwn114.

Cole, R. (2014) 'Live-cell imaging', *Cell adhesion & migration*. 2014/10/31, 8(5), pp. 452–459. doi: 10.4161/cam.28348.

Conchello, J.-A. and Lichtman, J. W. (2005) 'Optical sectioning microscopy', *Nature Methods*, 2(12), pp. 920–931. doi: 10.1038/nmeth815.

Coskun, Ü. *et al.* (2011) 'Regulation of human EGF receptor by lipids.', *Proceedings of the National Academy of Sciences of the United States of America*, 108(22), pp. 9044–9048. doi: 10.1073/pnas.1105666108.

Dahmani, M. *et al.* (2021) 'Contribution of classical complement activation and IgM to the control of Rickettsia infection', *Molecular microbiology*. 2021/11/13, 116(6), pp. 1476–1488. doi: 10.1111/mmi.14839.

Davies, L. R. L. *et al.* (2012) 'Metabolism of vertebrate amino sugars with N-glycolyl groups: resistance of α2-8-linked N-glycolylneuraminic acid to enzymatic cleavage.', *The Journal of biological chemistry*, 287(34), pp. 28917–28931. doi: 10.1074/jbc.M112.365056.

Dhar, C., Sasmal, A. and Varki, A. (2019) 'From "Ssrum sickness" to "xenosialitis": Past, present, and future significance of the non-human sialic acid Neu5Gc.', *Frontiers in immunology*, 10, p. 807. doi: 10.3389/fimmu.2019.00807.

Diebolder, C. A. *et al.* (2014) 'Complement is activated by IgG hexamers assembled at the cell surface', *Science (New York, N.Y.)*, 343(6176), pp. 1260–1263. doi: 10.1126/science.1248943.

Dillman, R. O. *et al.* (1994) 'Human anti-mouse antibody response in cancer patients following single low-dose injections of radiolabeled murine monoclonal antibodies', *Cancer Biotherapy*, 9(1), pp. 17–28. doi: 10.1089/cbr.1994.9.17.

Dorvignit, D. *et al.* (2015) 'Antitumor and cytotoxic properties of a humanized antibody specific for the GM3(Neu5Gc) ganglioside', *Immunobiology*, 220(12), pp. 1343–1350. doi: https://doi.org/10.1016/j.imbio.2015.07.008.

Elliott, A. D. (2020) 'Confocal m icroscopy: Principles and modern practices.', *Current protocols in cytometry*, 92(1), p. e68. doi: 10.1002/cpcy.68.

England, C. G., Ehlerding, E. B. and Cai, W. (2016) 'NanoLuc: A small luciferase is brightening up the field of bioluminescence', *Bioconjugate Chemistry*, 27(5), pp. 1175–1187. doi: 10.1021/acs.bioconjchem.6b00112.

Ettinger, A. and Wittmann, T. (2014) 'Chapter 5 - Fluorescence live cell imaging', in Waters, J. C. and Wittman, T. B. T.-M. in C. B. (eds) *Quantitative Imaging in Cell Biology*. Academic Press, pp. 77–94. doi: https://doi.org/10.1016/B978-0-12-420138-5.00005-7.

Fernández-Marrero, Y. *et al.* (2011) 'A cytotoxic humanized anti-ganglioside antibody produced in a murine cell line defective of N-glycolylated-glycoconjugates', *Immunobiology*, 216(12), pp. 1239–1247. doi: https://doi.org/10.1016/j.imbio.2011.07.004.

Finn, O. J. (2017) 'Human tumor antigens yesterday, today, and tomorrow', *Cancer Immunology Research*, 5(5), pp. 347–354. doi: 10.1158/2326-6066.CIR-17-0112.

Fonseka, P. *et al.* (2021) 'FunRich enables enrichment analysis of OMICs datasets.', *Journal of molecular biology*, 433(11), p. 166747. doi: 10.1016/j.jmb.2020.166747.

Fornasier, G., Francescon, S. and Baldo, P. (2018) 'An update of efficacy and safety of cetuximab in metastatic colorectal cancer: A narrative review', *Advances in Therapy*, 35(10), pp. 1497–1509. doi: 10.1007/s12325-018-0791-0.

Graham, F. L. *et al.* (1977) 'Characteristics of a human cell line transformed by DNA from human adenovirus type 5', *J Gen Virol*, 36(1), pp. 59–72. doi: 10.1099/0022-1317-36-1-59.

Graves, P. R. and Haystead, T. A. J. (2002) 'Molecular biologist's guide to proteomics', *Microbiology and molecular biology reviews : MMBR*, 66(1), pp. 39–63. doi: 10.1128/MMBR.66.1.39-63.2002.

Gullick, W. J. (1991) 'Prevalence of aberrant expression of the epidermal growth factor receptor in human cancers.', *British medical bulletin*, 47(1), pp. 87–98. doi: 10.1093/oxfordjournals.bmb.a072464.

Hakomori, S. (2002) ‘The glycosynapse’, *Proceedings of the National Academy of Sciences*, 99(1), pp. 225–232. doi: 10.1073/pnas.012540899.

Hakomori, S. and Handa, K. (2015) ‘GM3 and cancer’, *Glycoconjugate Journal*, 32(1), pp. 1–8. doi: 10.1007/s10719-014-9572-4.

Hall, M. P. *et al.* (2012) ‘Engineered luciferase reporter from a deep sea shrimp utilizing a novel imidazopyrazinone substrate’, *ACS Chemical Biology*, 7(11), pp. 1848–1857. doi: 10.1021/cb3002478.

Hayashi, N. *et al.* (2013) ‘Detection of N-glycolyated gangliosides in non-small-cell lung cancer using GMR8 monoclonal antibody.’, *Cancer science*, 104(1), pp. 43–47. doi: 10.1111/cas.12027.

Hoos, A. *et al.* (2010) ‘Improved endpoints for cancer immunotherapy trials’, *JNCI: Journal of the National Cancer Institute*, 102(18), pp. 1388–1397. doi: 10.1093/jnci/djq310.

Howard, D. R. and Batsakis, J. G. (1982) ‘Peanut agglutinin: a new marker for tissue histiocytes.’, *American journal of clinical pathology*, 77(4), pp. 401–408. doi: 10.1093/ajcp/77.4.401.

Icha, J. *et al.* (2017) ‘Phototoxicity in live fluorescence microscopy, and how to avoid it.’, *BioEssays : news and reviews in molecular, cellular and developmental biology*, 39(8). doi: 10.1002/bies.201700003.

Janeway, C. A. and Medzhitov, R. (2002) ‘Innate immune recognition’, *Annual Review of Immunology*, 20(1), pp. 197–216. doi: 10.1146/annurev.immunol.20.083001.084359.

Johannesen, H. (2020) *Unmasking the assassin*. University of Oslo.

Kelleher, N. (2004) ‘Peer reviewed: Top-down proteomics’, *Analytical Chemistry*, 76(11), pp. 196 A-203 A. doi: 10.1021/ac0415657.

Kempeni, J. (1999) ‘Preliminary results of early clinical trials with the fully human anti-TNFα monoclonal antibody D2E7’, *Annals of the Rheumatic Diseases*, 58(suppl 1), p. I70 LP-I72. doi: 10.1136/ard.58.2008.i70.

Kennett, R. H. (1981) ‘Hybridomas: A new dimension in biological analyses’, *In Vitro*, 17(12), pp. 1036–1050. doi: 10.1007/BF02618601.

Köhler, G. and Milstein, C. (1975) ‘Continuous cultures of fused cells secreting antibody of predefined specificity.’, *Nature*, 256(5517), pp. 495–497. doi: 10.1038/256495a0.

Krengel, U. *et al.* (2004) ‘Structure and molecular interactions of a unique antitumor antibody specific for N-glycolyl GM3.’, *The Journal of biological chemistry*, 279(7), pp. 5597–5603. doi: 10.1074/jbc.M311693200.

Krengel, U. and Bousquet, P. A. (2014) ‘Molecular recognition of gangliosides and their potential for cancer immunotherapies’, *Frontiers in Immunology*. Available at: https://www.frontiersin.org/article/10.3389/fimmu.2014.00325.

Lehmann, F., Tiralongo, E. and Tiralongo, J. (2006) ‘Sialic acid-specific lectins: occurrence, specificity and function.’, *Cellular and molecular life sciences : CMLS*, 63(12), pp. 1331–1354. doi: 10.1007/s00018-005-5589-y.

Ma, H. and O’Kennedy, R. (2015) ‘The structure of natural and recombinant antibodies BT -

peptide antibodies: Methods and protocols', in Houen, G. (ed.). New York, NY: Springer New York, pp. 7–11. doi: 10.1007/978-1-4939-2999-3_2.

Maloney, D. G., Smith, B. and Rose, A. (2002) 'Rituximab: Mechanism of action and resistance.', *Seminars in oncology*, 29(1S2), pp. 2–9. doi: 10.1053/sonc.2002.30156.

Malykh, Y. N., Schauer, R. and Shaw, L. (2001) 'N-Glycolylneuraminic acid in human tumours.', *Biochimie*, 83(7), pp. 623–634. doi: 10.1016/s0300-9084(01)01303-7.

Manoochehri Khoshinani, H., Afshar, S. and Najafi, R. (2016) 'Hypoxia: A double-edged sword in cancer therapy.', *Cancer investigation*, 34(10), pp. 536–545. doi: 10.1080/07357907.2016.1245317.

Meuillet, E. J. *et al.* (1999) 'Sialidase gene transfection enhances epidermal growth factor receptor activity in an epidermoid carcinoma cell line, A431.', *Cancer research*, 59(1), pp. 234–240.

Mi, H. *et al.* (2019) 'PANTHER version 14: more genomes, a new PANTHER GO-slim and improvements in enrichment analysis tools.', *Nucleic acids research*, 47(D1), pp. D419–D426. doi: 10.1093/nar/gky1038.

Miyagi, T. *et al.* (2018) 'Biological and pathological roles of ganglioside sialidases.', *Progress in molecular biology and translational science*, 156, pp. 121–150. doi: 10.1016/bs.pmbts.2017.12.005.

Modjtahedi, H. *et al.* (1998) 'EGFR blockade by tyrosine kinase inhibitor or monoclonal antibody inhibits growth, directs terminal differentiation and induces apoptosis in the human squamous cell carcinoma HN5.', *Int J Oncol*, 13(2), pp. 335–377. doi: 10.3892/ijo.13.2.335.

Monici, M. B. T.-B. A. R. (2005) 'Cell and tissue autofluorescence research and diagnostic applications', in. Elsevier, pp. 227–256. doi: https://doi.org/10.1016/S1387-2656(05)11007-2.

Morrison, S. L. *et al.* (1984) 'Chimeric human antibody mplecules: Mouse antigen-binding domains with human constant region domains', *Proceedings of the National Academy of Sciences of the United States of America*, 81(21), pp. 6851–6855. Available at: http://www.jstor.org.ezproxy.uio.no/stable/24845.

Muz, B. *et al.* (2015) 'The role of hypoxia in cancer progression, angiogenesis, metastasis, and resistance to therapy', *Hypoxia (Auckland, N.Z.)*, 3, pp. 83–92. doi: 10.2147/HP.S93413.

National cancer institute (no date) *Cancer Moonshot*. Available at: https://www.cancer.gov/research/key-initiatives/moonshot-cancer-initiative (Accessed: 11 May 2022).

Nobel Prize Organisation (2022a) *Nobel prize in medicine or physiology 1984*. Available at: https://www.nobelprize.org/prizes/medicine/1984/summary/ (Accessed: 8 May 2022).

Nobel Prize Organisation (2022b) *Nobel prize in physiology or medicine 2018*. Available at: https://www.nobelprize.org/prizes/medicine/2018/summary/ (Accessed: 11 May 2022).

Nores, G. A. *et al.* (1987) 'Density-dependent recognition of cell surface GM3 by a certain anti-melanoma antibody, and GM3 lactone as a possible immunogen: requirements for tumor-associated antigen and immunogen.', *Journal of immunology (Baltimore, Md. : 1950)*, 139(9), pp. 3171–3176.

Normanno, N. *et al.* (2006) 'Epidermal growth factor receptor (EGFR) signaling in cancer',

Gene, 366(1), pp. 2–16. doi: https://doi.org/10.1016/j.gene.2005.10.018.

Okerblom, J. J. *et al.* (2017) 'Loss of CMAH during human evolution primed the monocyte-macrophage lineage toward a more inflammatory and phagocytic state', *Journal of immunology (Baltimore, Md. : 1950)*. 2017/02/01, 198(6), pp. 2366–2373. doi: 10.4049/jimmunol.1601471.

Oliva, J. P. *et al.* (2006) 'Clinical evidences of GM3 (NeuGc) ganglioside expression in human breast cancer using the 14F7 monoclonal antibody labelled with (99m)Tc.', *Breast cancer research and treatment*, 96(2), pp. 115–121. doi: 10.1007/s10549-005-9064-0.

Omuro, A. and DeAngelis, L. M. (2013) 'Glioblastoma and other malignant gliomas: a clinical review.', *JAMA*, 310(17), pp. 1842–1850. doi: 10.1001/jama.2013.280319.

OriginLab Corporation (2022) 'Origin(Pro)'. Northampton, MA, USA.

Pam, T. *et al.* (2003) 'Human uptake and incorporation of an immunogenic nonhuman dietary sialic acid', *Proceedings of the National Academy of Sciences*, 100(21), pp. 12045–12050. doi: 10.1073/pnas.2131556100.

Pan, S. *et al.* (2009) 'Mass spectrometry based targeted protein quantification: Methods and applications', *Journal of Proteome Research*, 8(2), pp. 787–797. doi: 10.1021/pr800538n.

Pawluczkowycz, A. W. *et al.* (2009) 'Binding of submaximal C1q promotes complement-dependent cytotoxicity (CDC) of B cells opsonized with anti-CD20 mAbs ofatumumab (OFA) or rituximab (RTX): considerably higher levels of CDC are induced by OFA than by RTX.', *Journal of immunology (Baltimore, Md. : 1950)*, 183(1), pp. 749–758. doi: 10.4049/jimmunol.0900632.

Pérez-Herrero, E. and Fernández-Medarde, A. (2015) 'Advanced targeted therapies in cancer: Drug nanocarriers, the future of chemotherapy.', *European journal of pharmaceutics and biopharmaceutics : official journal of Arbeitsgemeinschaft fur Pharmazeutische Verfahrenstechnik e.V*, 93, pp. 52–79. doi: 10.1016/j.ejpb.2015.03.018.

Pesci, G. (2020) *Follow the light*.

Posner, J. *et al.* (2019) 'Monoclonal antibodies: Past, present and future BT - concepts and principles of pharmacology: 100 years of the handbook of experimental pharmacology', in Barrett, J. E., Page, C. P., and Michel, M. C. (eds). Cham: Springer International Publishing, pp. 81–141. doi: 10.1007/164_2019_323.

Queen, C. *et al.* (1989) 'A humanized antibody that binds to the interleukin 2 receptor', *Proceedings of the National Academy of Sciences of the United States of America*, 86(24), pp. 10029–10033. Available at: http://www.jstor.org.ezproxy.uio.no/stable/34791.

Rakotomalala, A. *et al.* (2021) 'Hypoxia in solid tumors: How low oxygenation impacts the "Six Rs" of sadiotherapy.', *Frontiers in endocrinology*, 12, p. 742215. doi: 10.3389/fendo.2021.742215.

Rojas, G. *et al.* (2004) 'Light-chain shuffling results in successful phage display selection of functional prokaryotic-expressed antibody fragments to N-glycolyl GM3 ganglioside.', *Journal of immunological methods*, 293(1–2), pp. 71–83. doi: 10.1016/j.jim.2004.07.002.

Roque-Navarro, L. *et al.* (2008) 'Anti-ganglioside antibody-induced tumor cell death by loss of membrane integrity', *Molecular Cancer Therapeutics*, 7(7), pp. 2033–2041. doi: 10.1158/1535-7163.MCT-08-0222.

Salomon, D. S. *et al.* (1995) 'Epidermal growth factor-related peptides and their receptors in human malignancies', *Critical Reviews in Oncology/Hematology*, 19(3), pp. 183–232. doi: https://doi.org/10.1016/1040-8428(94)00144-I.

Schirrmacher, V. (2019) 'From chemotherapy to biological therapy: A review of novel concepts to reduce the side effects of systemic cancer treatment (Review).', *International journal of oncology*, 54(2), pp. 407–419. doi: 10.3892/ijo.2018.4661.

Sharpless, N. E. and Singer, D. S. (2021) 'Progress and potential: The cancer moonshot', *Cancer Cell*, 39(7), pp. 889–894. doi: 10.1016/j.ccell.2021.04.015.

Steentoft, C., Bennett, E. P. and Clausen, H. (2013) 'Glycoengineering of human cell lines using zinc finger nuclease gene targeting: SimpleCells with homogeneous GalNAc O-glycosylation allow isolation of the O-glycoproteome by one-step lectin affinity chromatography.', *Methods in molecular biology (Clifton, N.J.)*, 1022, pp. 387–402. doi: 10.1007/978-1-62703-465-4_29.

Stewart, R. J. and Boggs, J. M. (1993) 'A carbohydrate-carbohydrate interaction between galactosylceramide-containing liposomes and cerebroside sulfate-containing liposomes: dependence on the glycolipid ceramide composition.', *Biochemistry*, 32(40), pp. 10666–10674. doi: 10.1021/bi00091a017.

Su, S. *et al.* (2018) 'Immune Checkpoint Inhibition Overcomes ADCP-Induced Immunosuppression by Macrophages.', *Cell*, 175(2), pp. 442-457.e23. doi: 10.1016/j.cell.2018.09.007.

Swain, S. L., McKinstry, K. K. and Strutt, T. M. (2012) 'Expanding roles for CD4+ T cells in immunity to viruses', *Nature Reviews Immunology*, 12(2), pp. 136–148. doi: 10.1038/nri3152.

T., A. A. *et al.* (2001) 'A mutant cholera toxin B subunit that binds GM1- ganglioside but lacks immunomodulatory or toxic activity', *Proceedings of the National Academy of Sciences*, 98(15), pp. 8536–8541. doi: 10.1073/pnas.161273098.

Varki, A. (2001) 'N-glycolylneuraminic acid deficiency in humans.', *Biochimie*, 83(7), pp. 615–622. doi: 10.1016/s0300-9084(01)01309-8.

Wang, Q. *et al.* (2018) 'Antibody glycoengineering strategies in mammalian cells.', *Biotechnology and bioengineering*, 115(6), pp. 1378–1393. doi: 10.1002/bit.26567.

Wang, X. *et al.* (2001) 'Ganglioside modulates ligand binding to the epidermal growth factor receptor.', *The Journal of investigative dermatology*, 116(1), pp. 69–76. doi: 10.1046/j.1523-1747.2001.00222.x.

Wehr, T. (2006) 'Top-down versus bottom-up approches in proteomics', *LCGC N. Am*, 24(9), pp. 1004–1010.

Weinberg, R. A. (2018) *The biology of cancer*. 2nd edn.

Wernick, N. L. B. *et al.* (2010) 'Cholera toxin: an intracellular journey into the cytosol by way of the endoplasmic reticulum', *Toxins*. 2010/03/05, 2(3), pp. 310–325. doi: 10.3390/toxins2030310.

WHO (no date) *Cancer*. Available at: https://www.who.int/news-room/fact-sheets/detail/cancer (Accessed: 15 April 2022).

Widakowich, C. *et al.* (2007) 'Review: Side effects of approved molecular targeted therapies

in solid cancers', *The Oncologist*, 12(12), pp. 1443–1455. doi: 10.1634/theoncologist.12-12-1443.

Wyld, L., Audisio, R. A. and Poston, G. J. (2015) 'The evolution of cancer surgery and future perspectives.', *Nature reviews. Clinical oncology*, 12(2), pp. 115–124. doi: 10.1038/nrclinonc.2014.191.

Yang, Z. *et al.* (2015) 'Engineered CHO cells for production of diverse, homogeneous glycoproteins', *Nature Biotechnology*, 33(8), pp. 842–844. doi: 10.1038/nbt.3280.

Yin, J. *et al.* (2006) 'Hypoxic culture induces expression of sialin, a sialic acid transporter, and cancer-associated gangliosides containing non–human sialic acid on human cancer cells', *Cancer Research*, 66(6), pp. 2937–2945. doi: 10.1158/0008-5472.CAN-05-2615.

Zahavi, D. and Weiner, L. (2020) 'Monoclonal antibodies in cancer therapy', *Antibodies (Basel, Switzerland)*, 9(3), p. 34. doi: 10.3390/antib9030034.

8. Appendix

8.1 Appendix A: Antibodies, dyes, reagents, kits, disposables, instruments, and software

Table S1. Primary antibodies used for flow cytometry and confocal microscopy.

Antibody	Concentration of stock	Concentration used	Supplier
Anti-Neu5Gc	1 mg/ml	1:1000	Biolegend Ref: 146903 LOT: B195725
Cetuximab	5 mg/ml	60 μg/ml	Kindly provided by Espen Stang, Rikshospitalet, Oslo, Norway
h14F7	5 mg/ml	See Section 3	Kindly provided by Center for Molecular Immunology, Havana, Cuba
h14F7*	1 mg/ml	See Section 3	Kindly provided by Anders Tveita at Rikshospitalet, Oslo, Norway
Mouse EEA1	0.25 mg/ml	1:200	BD Biosciences Ref: 610456 LOT: 45223
Mouse Lamp1	Supernatant	1:1000	Developmental Studies Hybridoma Bank, code H4A3
m14F7	1 mg/ml	See Section 3	Creative biolabs Developed by (Carr *et al.*, 2000)

Table S2. Secondary conjugated antibodies used for flow cytometry and confocal microscopy.

Antibody	Type	Absorbs at wavelength (nm)	Concentration of stock	Supplier
Anti-chicken Alexa Fluor 488	Goat polyclonal IgG	488	2 mg/ml	Life Tec LOT: 1759025
Anti-human Alexa Fluor 647	Goat polyclonal IgG	640	2 mg/ml	Invitrogen REF: A21445 LOT: 2B90672
Anti-human FITC	Goat polyclonal IgG	488		Southern Biotech Ref: sb 2040-02
Anti-mouse Alexa Fluor 555	Goat IgG	555	2 mg/ml	Invitrogen Ref: A21424 LOT: 1003213
Anti-mouse Alexa Fluor 647	Goat polyclonal IgG	640		Invitrogen Ref: A32728
Anti-mouse FITC	Goat polyclonal IgG	488	2 mg/ml	Abcam Ref: ab6785 Lot: GR3274516-6
Streptavidin Alexa Fluor 647 conjugate	Binds to biotin	640	2 mg/ml	Invitrogen LOT: 2179341

Table S3. Fluorescent dyes used for flow cytometry and confocal microscopy.

Name	Description	Concentration of stock	Concentration used	Supplier
PI	DNA-binding stain	1 mg/ml	1:71	Thermo Scientific
DAPI	DNA-binding stain	1 mg/ml	1:5000	Invitrogen

Table S4. Reagents and suppliers.

Reagent	Supplier
BalanCD CHO growth A	Fujifilm
Bovine Serum Albumin	Sigma-Aldrich
Dimethyl sulfoxide (DMSO)	Sigma-Aldrich
DMEM with 4.5 g/L D-Glucose, L-Glutamine, Pyruvate	Gibco
EDTA	Sigma-Aldrich
Ex-cell CD CHO Serum	SAFC
Fetal Bovine Serum Superior (FBS)	Biochrom
Fetal Calf Serum (FCS)	Sigma-Aldrich
Fibronectin	Sigma-Aldrich
IMMOIL-F30CC	Olympus
Mowiol	Sigma-Aldrich
M14F7	Creative Biolabs
Neuraminidase from *Clostridium perfringens*	Sigma-Aldrich
Non-Essential Amino Acids (NEAA)	Thermo Scientific
PanLectenz	Lectenz Bio
Paraformaldehyde (PFA)	Merck
Peanut Agglutinin (PNA)	Vector Laboratories
Penicillin Streptomycin (Pen-Strep)	Lonza
Ribonuclease A from bovine pancreas (RNase)	Sigma Ref: 9001-99-4 LOT: 020M13801
RPMI 1640 with L-Glutamine	Lonza
Phospate-buffered Saline (PBS)	Sigma-Aldrich
Saponin (from quillaja bark)	Sigma-Aldrich
Sodium azide	Sigma-Aldrich
Sodium Bicarbonate	Sigma-Aldrich
Sodium Pyruvate	Thermo Scientific
Triton-X	Sigma-Aldrich
Trypan Blue	Gibco
Trypsin EDTA	Lonza

Table S5. Kits and suppliers.

Kit	Supplier
Alexa Fluor 647 Antibody Labeling Kit	Thermo Scientific, Cat. A20186

Table S6. Disposables and suppliers.

Disposables	Supplier
1.5 ml Eppendorf tube	Eppendorf
15 ml Falcon tube	Thermo Scientific
50 ml Falcon tube	Thermo Scientific
Coverslip	Hecht Assistant
Microscope slide	Thermo scientific
Nitrile gloves, powder free	VWR
Nunc cell culture 6 well plate	Thermo Scientific
Nunc cell culture 24 well plate	Thermo Scientific
Nunc 96 well plate	Thermo Scientific
Serological pipet (volume 1-50 ml)	Sarstedt
T25 Cell flask	Nunc and VWR

Table S7. Instruments and suppliers.

Instrument	Supplier
371 Steri-Cycle CO_2 incubator	Thermo Scientific
BD Accuri C6 Flow Cytometer	Accuri
Iprasense	Iprasense
MEGA STAR 600R centrifuge	VWR
Spectral Cell Analyzer SA3800	Sony
SUB Aqua 12 (waterbath)	VWR

Table S8. Software and suppliers.

Software	Supplier
BioRender	BioRender
Cflow Plus	Accuri
Fiji	ImageJ
FlowJo X	BD Biosciences
Funrich	(Fonseka *et al.*, 2021)
Microsoft Excel	Microsoft Office
Norma XS	Iprasense
Origin	(OriginLab Corporation, 2022)
Panther	(Mi *et al.*, 2019)

8.2 Appendix B: Solutions and buffers

Cell cultures

Table S9. Composition of medium for CHO cells (500 ml).

Reagent	Volume (ml)
BalanCD CHO growth A	250
Ex-cell CD CHO Serum	250

Table S10. Composition of medium for HEK cells (560 ml).

Reagent	Volume (ml)
DMEM	500
FBS	56
Pen-Strep	5

Table S11. Composition of medium for L1210 cells (570 ml).

Reagent	Volume (ml)
RPMI	500
FBS	56
NEAA	5
Sodium pyruvate	5
Pen-Strep	5

Table S12. Composition of medium for P3X63 Ag.8 cells (570 ml).

Reagent	Volume (ml)
RPMI	500
FBS	56
NEAA	5
Sodium pyruvate	5
Pen-Strep	5

Conjugation of 14F7

Table S13. Composition of 1 M sodium bicarbonate (1 L).

Reagent	Volume (ml)	Amount (g)
$NaHCO_3$	-	84
Milli-Q H_2O	1000	-

pH 8.5, stored at 4°C

Flow cytometry

Table S14. Composition of PFA (25 ml).

Reagent	Volume (ml)	Amount (g)
PFA	-	1
PBS	25	-

Heated in a water bath at 56 °C for one hour (or until fully dissolved). PFA was always made fresh 1-3 days before use and handled under a fume hood.
Same composition and preparation as when used for fixation of cells for imaging.

Table S15. Composition of wash buffer (50 ml).

Reagent	Volume (ml)
PBS	49
FBS	1
EDTA (0.5 M, pH 8)	0.2

Table S16. Composition of FACS buffer for experiment A, B and D (50 ml).

Reagent	Volume (ml)
PBS	36.8
RNase (0.4 mg/ml)	12.5
PI (1 mg/ml)	0.7

Table S17. Composition of FACS buffer for experiment C (50 ml).

Reagent	Volume (ml)
PBS	50
BSA	0.5

Imaging

Table S18. Composition of 0.1% Triton X-100 (50 ml).

Reagent	Volume (ml)
Triton X-100 (10%)	0.5
PBS	50

Table S19. Composition of 5% FCS + 0.02% sodium azide (50 ml).

Reagent	Volume (ml)
FCS	2.5
Sodium azide	0.01
PBS	50

Table 20. Composition of 0.25% Saponin (50) ml.

Reagent	Volume (ml)
Saponin (10%)	1.25
PBS	48.75

8.3 Appendix C: Raw data from flow cytometry

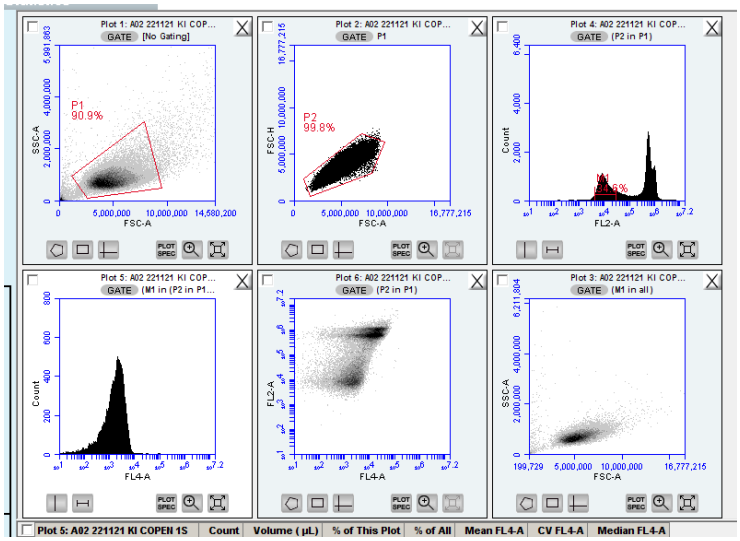

Figure S1. Illustration of gating for flow cytometry analysis of HEK WT, KI Cph and KI Oslo (Section 4.1.1)

Table S21. Raw data from flow cytometry of HEK WT, KI Cph and KI Oslo (Section 4.1.1)

Cell	Mean replicate 1	Median replicate 1	Mean replicate 2	Median replicate 2	Mean replicate 3	Median replicate 3
HEK WT m14F7 anti-mouse AF647	51992.04	26599.5	59424.32	27182	40914.15	15663
HEK WT anti-mouse AF647	720.,5	4009	7132.97	3639	6971.07	3547
HEK KI Cph m14F7 anti-mouse AF647	51556,89	27074	70484,91	33642	48015,73	24683
HEK KI Cph anti-mouse AF647	6237,44	3389	7299,11	4090	5927,99	2847
HEK KI Oslo m14F7 anti-mouse AF647	106489,21	51020	82995,58	37688	113756,36	51806
HEK KI Oslo anti-mouse AF647	6436,99	3216	5963,94	2830,5	6462,2	3126
HEK WT m14F7 anti-mouse FITC	19185,8	18663	21474,97	20502	-	-
HEK WT anti-mouse FITC	17777,12	17498	18555,36	18233	-	-

HEK KI Cph m14F7 anti-mouse FITC	50823,66	22905	36686,73	20313,5	**-**	**-**
HEK KI Cph anti-mouse FITC	18176,56	17825	17640,81	17230	**-**	**-**
HEK KI Oslo m14F7 anti-mouse FITC	-	-	-	-	**-**	**-**
HEK KI Oslo anti-mouse FITC	-	-	-	-	**-**	**-**
HEK WT h14F7* anti-human AF647	3898	3040	3673,62	2594	4267	2765
HEK WT anti-human AF647	1388,05	997	1252,59	843	1234,18	875
HEK KI Cph h14F7* anti-human AF647	48494,08	5348	40280,47	3882	36075,88	3852
HEK KI Cph anti-human AF647	1239	800	1217,85	797	1183,84	794
HEK KI Oslo h14F7* anti-human AF647	201808,58	131553	174179,28	120155	162420,68	107995
HEK KI Oslo anti-human AF647	1703,56	857	1720,58	854,5	1639,03	827,5
HEK WT h14F7 anti-human FITC	10520,75	9770	9886,38	9245	9974,48	9359
HEK WT anti-human FITC	7734,03	7174	8183,53	7625	7852,66	7301
HEK KI Cph h14F7 anti-human FITC	15812,39	8801	13883	8332	13087,26	7767
HEK KI Cph FITC	5380,29	5099	5590,68	5329	6038,32	5667
HEK KI Oslo h14F7* anti-human FITC	**-**	**-**	**-**	**-**	**-**	**-**
HEK KI Oslo anti-human FITC	**-**	**-**	**-**	**-**	**-**	**-**

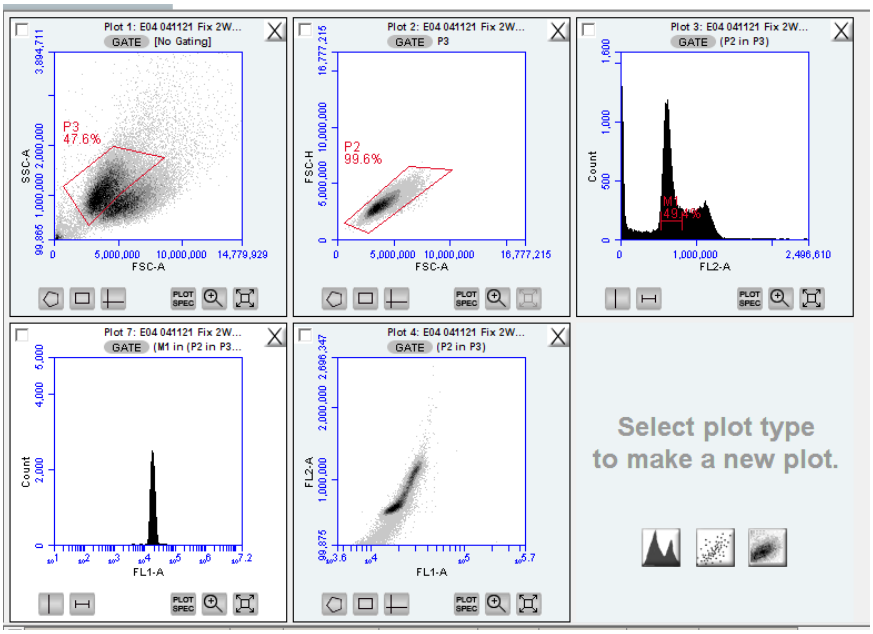

Figure S2. Illustration of gating for flow cytometry analysis of L1210 and P3X63 (Section 4.1.1).

Table S22. Raw data from flow cytometry of L1210 and P3X63 (Section 4.1.1).

Cell	Mean replicate 1	Median replicate 1	Mean replicate 2	Median replicate 2	Mean replicate 3	Median replicate 3
L1210 m14F7 anti-mouse FITC	488105,83	477795	511334,53	499614	430939,91	413947
L1210 anti-mouse FITC	13418,79	12669	12614,55	12264	11678,3	11475
P3X63 m14F7 anti-mouse FITC	636847,51	620760,5	525422,16	504166	443917,4	435944
P3X63 anti-mouse FITC	16187,23	15795,5	16534,33	16070,5	15874,29	15431

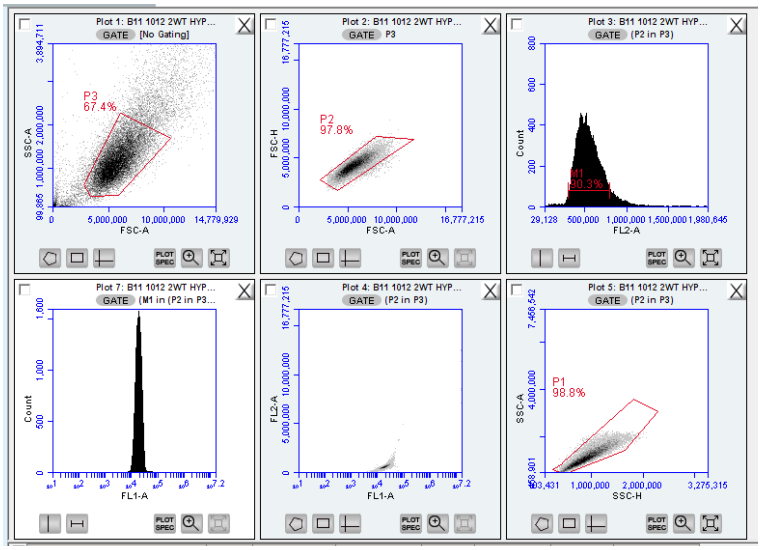

Figure S3. Illustration of gating for flow cytomatry analysis of HEK WT under hypoxia.

Table S23. Raw data from flow cytometry of HEK WT under hypoxia (Section 4.1.2)

Cell	Mean replicate 1	Median replicate 1	Mean replicate 2	Median replicate 2	Mean replicate 3	Median replicate 3
HEK WT 24 hours m14F7 anti-mouse FITC	44477.37	40787.5	45442.65	41177	38280.13	35564.5
HEK WT 24 hours anti-mouse FITC	21020.4	20518.5	19154.6	18663.5	18136.37	17593
HEK WT 72 hours m14F7 anti-mouse FITC	39043.26	36790	41989	38697	41038.84	38106
HEK WT 72 hours anti-mouse FITC	21038.23	20584	19831.87	19379	19250.87	18839

Table S24. Raw data from flow cytometry of HEK cells (Section 4.3).

		No neuraminidase						Neuraminidase					
Antibody	Concentratio	HEK WT (2 replicates)		HEK KI (2 replicates)		HEK KO (2 replicates)		HEK WT (2 replicates)		HEK KI (2 replicates)		HEK KO (2 replicates)	
	5	211	231	4562	5681	313	264	310	249	4964	3933	311	291
	2,50	204	237	2884	2340	277	267	191	297	2624	2469	286	46,1
	1,25	198	246	1003	1983	168	297	318	288	1020	357	259	454
h14F7	0,625	218	243	541	589	281	292	303	263	607	731	38,8	392
	5	220	248	848	681	247	296	134	282	1208	1249	373	338
	2,5	224	244	483	389	242	204	346	220	683	303	66,2	319
	1,25	201	198	357	329	259	254	132	114	323	347	351	289
h14F7*	0,625	199	218	324	131	195	183	316	245	303	140	280	322

		No neuraminidase						Neuraminidase					
Antibody	Concentratio	HEK WT (2 replicates)		HEK KI (2 replicates)		HEK KO (2 replicates)		HEK WT (2 replicates)		HEK KI (2 replicates)		HEK KO (2 replicates)	
	5	228	244	5996	4947	253	202	316	289	7291	5065	311	335
	2,50	226	234	2973	2923	278	286	309	270	2347	2894	293	301
	1,25	222	218	1550	1571	250	186	306	295	1266	1582	259	247
h14F7	0,625	224	200	697	597	272	237	244	221	660	733	150	245
	5	200	188	2478	2826	242	241	253	256	5151	3726	280	276
	2,5	190	245	1970	967	271	216	294	224	769	904	238	229
	1,25	243	220	571	453	220	208	330	211	529	397	220	185
h14F7*	0,625	210	191	297	272	178	160	259	201	319	349	223	212

		No neuraminidase						Neuraminidase					
		HEK WT (2 replicates)		HEK KI (2 replicates)		HEK KO (2 replicates)		HEK WT (2 replicates)		HEK KI (2 replicates)		HEK KO (2 replicates)	
PNA	0,1	1762	1664	2217	1604	1188	1114	23186	23265	15573	14027	12133	11115
	0,05	932	1010	1114	947	719	761	14508	11971	6770	7242	6656	6523
	0,025	550	583	723	513	459	545	6612	6286	3003	3095	3095	2563
Neu5Gc	1/1000	822	809	581	619	571	567	795	865	654	654	545	599
Panlectenz	1	15057	15159	1010	901	9078	6545	685	892	415	307	330	389
	0,5	17407	14314	1031	1114	9549	5239	761	748	343	303	417	253
	0,25	19326	20744	1141	842	9233	7073	853	845	385	417	429	419
only 2nd	-	258	248	372	297	508	413	335	579	298	413	396	250

		No neuraminidase						Neuraminidase					
Ab/reagent	Concentratio	HEK WT (2 replicates)		HEK KI (2 replicates)		HEK KO (2 replicates)		HEK WT (2 replicates)		HEK KI (2 replicates)		HEK KO (2 replicates)	
PNA		753	792	806	947	716	699	18126	16886	11040	9679	9910	6036
		400	447	456	541	595	615	8013	7618	4609	4751	4703	4848
		390	416	550	436	566	508	3841	3880	2150	2136	2324	2285
Neu5Gc		831	803	1727	1609	753	695	928	960	1045	1196	632	611
PanLectenz		69862	63780	11613	5681	60839	65968	1636	1204	327	372	377	419
		70572	67317	13933	8837	60634	52981	1406	1873	368	509	388	143
		53882	66191	13290	12465	69158	64429	2051	2194	332	467	357	454
only 2nd		448	257	344	263	370	904	417	216	325	218	386	216

Table S25. Raw data from flow cytometry of CHO cells (Section 4.3).

		No neuraminidase						Neuraminidase					
Ab/reagent	Concentratio	CHO WT		CHO KI A2		CHO KO		CHO WT		CHO KI A2		CHO KO	
	5 ug/ml	234	233	130828	118237	2202	1823	252	252	126916	118237	1499	1237
	2.5 ug/ml	216	233	129948	84671	1237	1188	257	222	105426	115089	776	652
	1.25 ug7ml	206	199	59419	58425	833	803	228	227	65525	64429	488	486
h14F7	0.675 ug/ml	329	163	35108	33376	665	667	247	245	39110	48206	481	511
	5 ug/ml	173	204	218	253	935	935	22043	22117	24638	24144	25226	23422
PNA	2.5 ug/ml	311	185	197	231	951	973	11574	8429	11419	10079	13839	10710
Neu5Gc	1/1000	871	549	2545	2554	790	753	615	573	1860	1631	667	609
PanLectenz	0.5 ug/ml	1382	951	259	253	1811	1698	218	206	231	262	607	564
2nd	-	221	256	258	314	1524	1614	339	325	402	589	1041	817

		No neuraminidase				Neuraminidase			
Ab/reagent	Concentratio	CHO WT		CHO KI A2		CHO WT		CHO KI A2	
	5 ug/ml	256	301	73570	57126	432	330	85053	76609
	2.5 ug/ml	237	300	33982	35625	382	447	46818	34560
	1.25 ug7ml	239	284	19876	21192	388	400	27292	19217
h14F7	0.675 ug/ml	237	247	10436	10193	378	358	13395	13902
	5 ug/ml	261	255	332	314	18580	20215	15538	16126
PNA	2.5 ug/ml	232	314	280	276	9822	7782	6421	8410
Neu5Gc	1/1000	784	778	3364	3101	834	926	2182	2263
PanLectenz	0.5 ug/ml	4416	4837	486	490	652	459	307	688
2nd	-	483	337	675	452	1115	1086	594	425

Table S26. Raw data from flow cytometry of HEK WT and the two HEK KI constructs (Section 4.3).

		No neuraminidase						Neuraminidase					
Antibody	Conc	HEK WT		HEK KI Copen		HEK KI Oslo		HEK WT		HEK KI Copen		HEK KI Oslo	
h14F7	5	11850	13290	16492	22043	94960	77040	14607	13746	8927	9485	107945	93372
	2,5	4294	5719	5151	5604	31623	37813	6180	6634	4441	4411	46608	55543
	1,25	3448	4751	2993	2633	12936	13839	2705	2633	2705	2624	23265	24888
	0,625	2404	1860	2254	1620	7516	8177	1756	2044	1598	1561	11692	10638
h14F7*	5	3054	3003	3148	5257	34638	43567	4294	5895	2903	6201	46294	46451
	2,5	1786	1687	1509	2100	8316	12298	1892	2678	1212	1848	23821	25226
	1,25	695	1144	549	1000	7193	4095	1129	2093	751	643	8601	7774
	0,625	566	603	457	448	1990	1088	492	889	516	357	2760	2779

		No neuraminidase						Neuraminidase					
Ab/Reagent	Conc	HEK WT		HEK KI Copen		HEK KI Oslo		HEK WT		HEK KI Copen		HEK KI Oslo	
PNA	0,1	3003	2732	2760	2520	1879	1571	19721	19721	16604	17584	14805	13112
	0,05	1420	1550	1401	1164	960	983	8344	8095	7002	6978	5856	6160
	0,025	787	787	736	639	599	607	3790	3425	3519	2973	3127	2554
Neu5Gc	1/1000	2340	2254	2436	2428	10819	12133	1494	1430	736	1382	3764	4352
Panlectenz	1	562	663	523	589	426	436	536	566	518	435	438	445
	0,5	432	484	269	268	370	278	516	425	375	271	426	436
	0,25	353	370	275	257	357	314	371	360	238	313	350	309
only 2nd	-	543	748	238	370	702	427	654	681	364	400	549	589

Table S27. Raw data from flow cytometry of comparison of conjugated antibody (Section 4.2.1)

Cell	Mean replicate 1	Median replicate 1	Mean replicate 2	Median replicate 2	Mean replicate 3	Median replicate 3
HEK KI Oslo Nothing added	1338,96	755.00	1304.91	719.00	1329.37	722.00
HEK KI Oslo h14F7* anti-human AF647	116804.81	51901.50	117032.94	54653.00	127146.77	56864.00
HEK KI Oslo anti-human AF647	1524.75	807.00	1345.72	738.00	1500.64	799.00
¸HEK KI Oslo Conjugated h14F7*	5011.37	2744.00	4930.92	2739.50	3975.37	2297.00
L1210 Nothing added	3967.25	1162	3779.37	987	3876.44	1158
L1210 m14F7 anti-mouse AF647	100013.49	46492	121725.07	55093	118697.95	56065
L1210 anti-mouse AF647	4691.84	1934.5	4269.61	1754	4415.06	2002
L1210 Conjugated m14F7	133585.26	78969	155944.16	92206	124200.84	71985

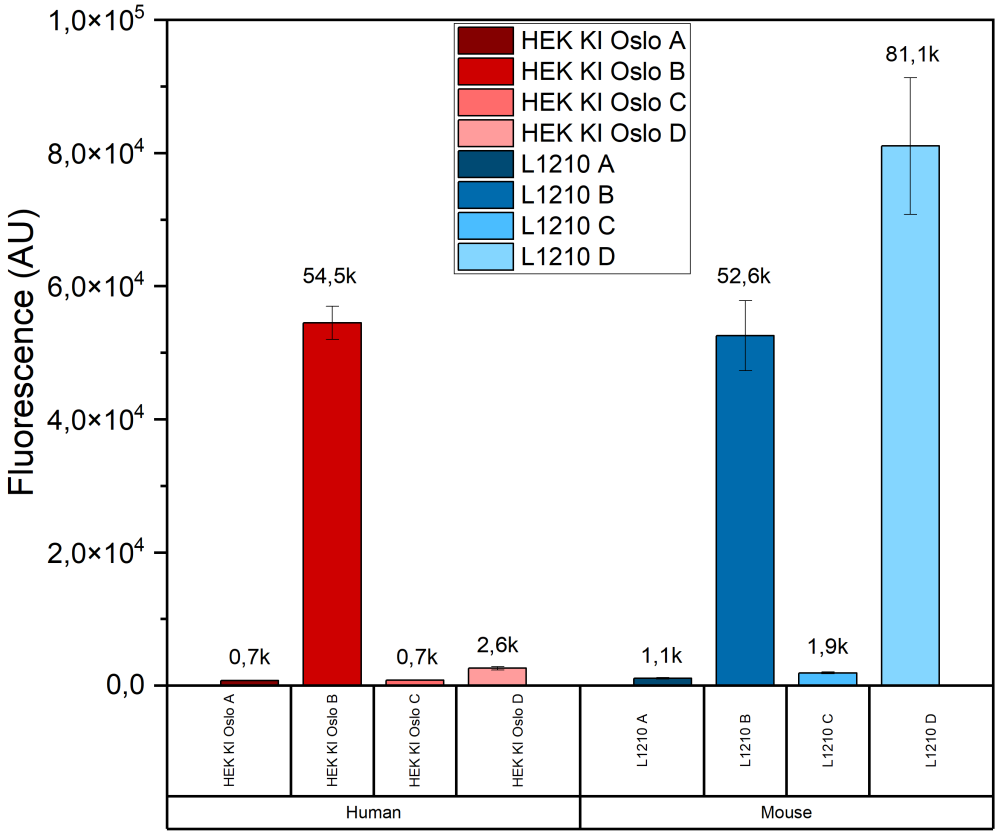

Figure S4. Comparison of cells incubated with conjugated primary antibody versus incubated with primary and secondary antibody The HEK KI Oslo and L1210 cells were divided into four samples each. The cells to which nothing was added were marked A, primary and secondary antibody added marked B , only secondary antibody was added were marked S and where AF647 conjugated antibody was added were marked C. H14F7* was used as primary antibody, goat anti-human Alexa Fluor 647 as secondary antibody, and h14F7* Alexa Fluor 647 conjugate as conjugated antibody for the HEK KI Oslo cells. M14F7 was used as primary antibody, goat anti-mouse Alexa Fluor 647 as secondary antibody, and m14F7 Alexa Fluor 647 conjugate as the conjugated antibody for the L1210 cells. This figure illustrates that the conjugation of the murine antibody was successful. The experiment was performed once with three independent replicates for each cell type. The error bar indicates the standard deviation for the measured median fluorescent signal for the three replicates. This figure was created using Origin.

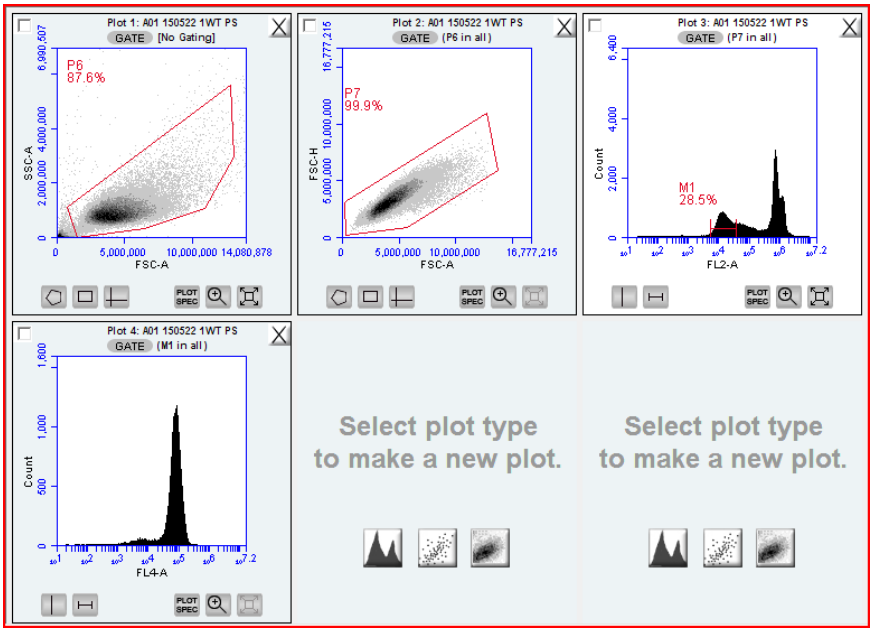

Figure S5. Illustration of gating for flowcytometry analysis of Cetuximab (Section 4.4).

Table S28. Raw data from flow cytometry of Cetuximab (Section 4.4).

		Mean rep 1	Median rep 1	Mean rep 2	Median rep 2	Mean rep 3	Median rep 3
WT	Cetuximab	81168,15	79050	80294,81	77122	67082,91	65183
	secondary	1437,27	707	1404,44	701	1454,99	694
KI CPh	Cetuximab	77425,38	80399,5	84250,23	85538	80021,69	82031
	secondary	1527,73	680	1435,38	743	1389,92	679
KI Oslo	Cetuximab	75091,48	70206	76550,55	71172	78614,67	72301
	secondary	2081,49	705	2090,79	775	2871,79	743

Raw data from results described in section 4.1.5.

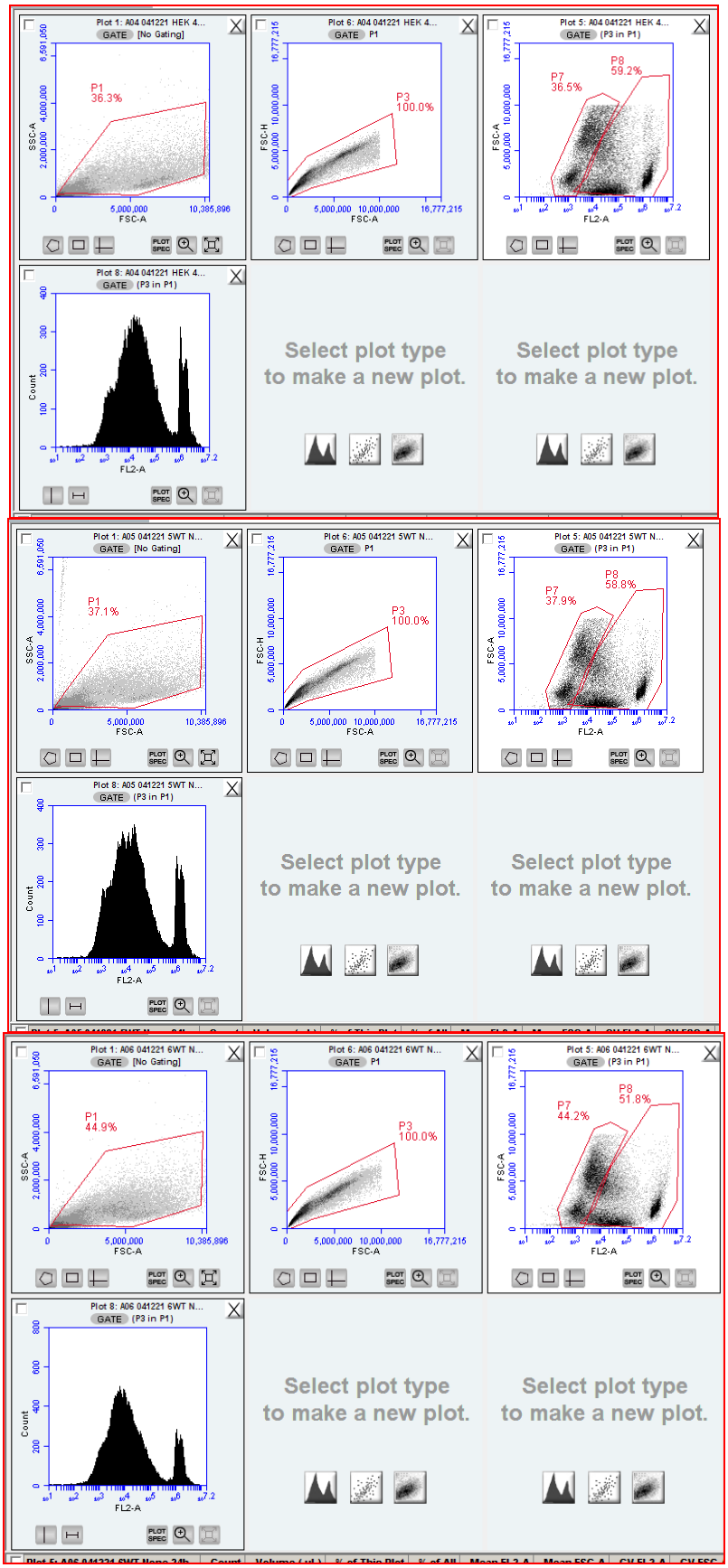

Figure S6. HEK WT untreated and incubated for 24 hours. A, B and C represent three independent biological replicates.

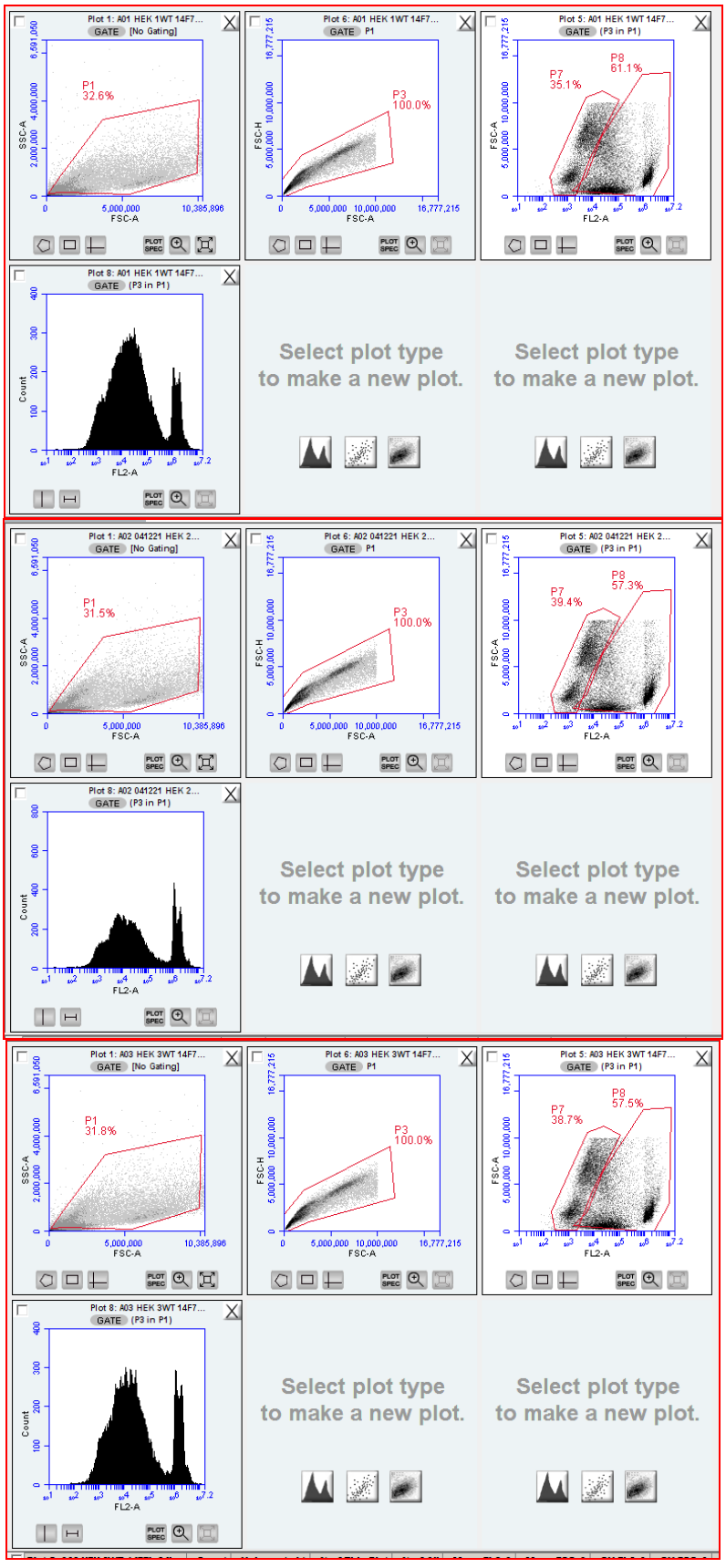

Figure S7. HEK WT treated with h14F7 and incubated for 24 hours. A, B and C represent three independent biological replicates.

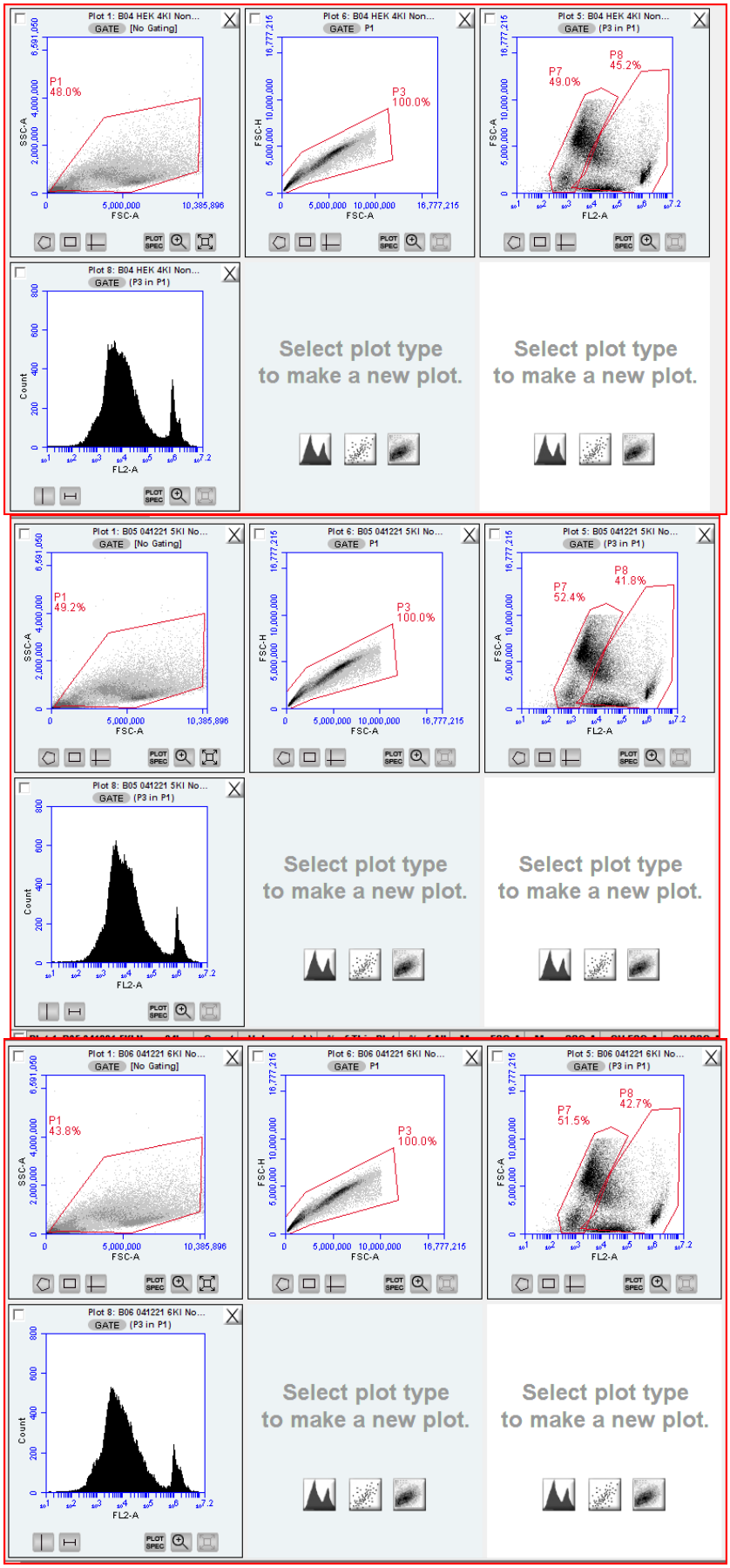

Figure S8. HEK KI Cph untreated and incubated for 24 hours. A, B and C represent three independent biological replicates.

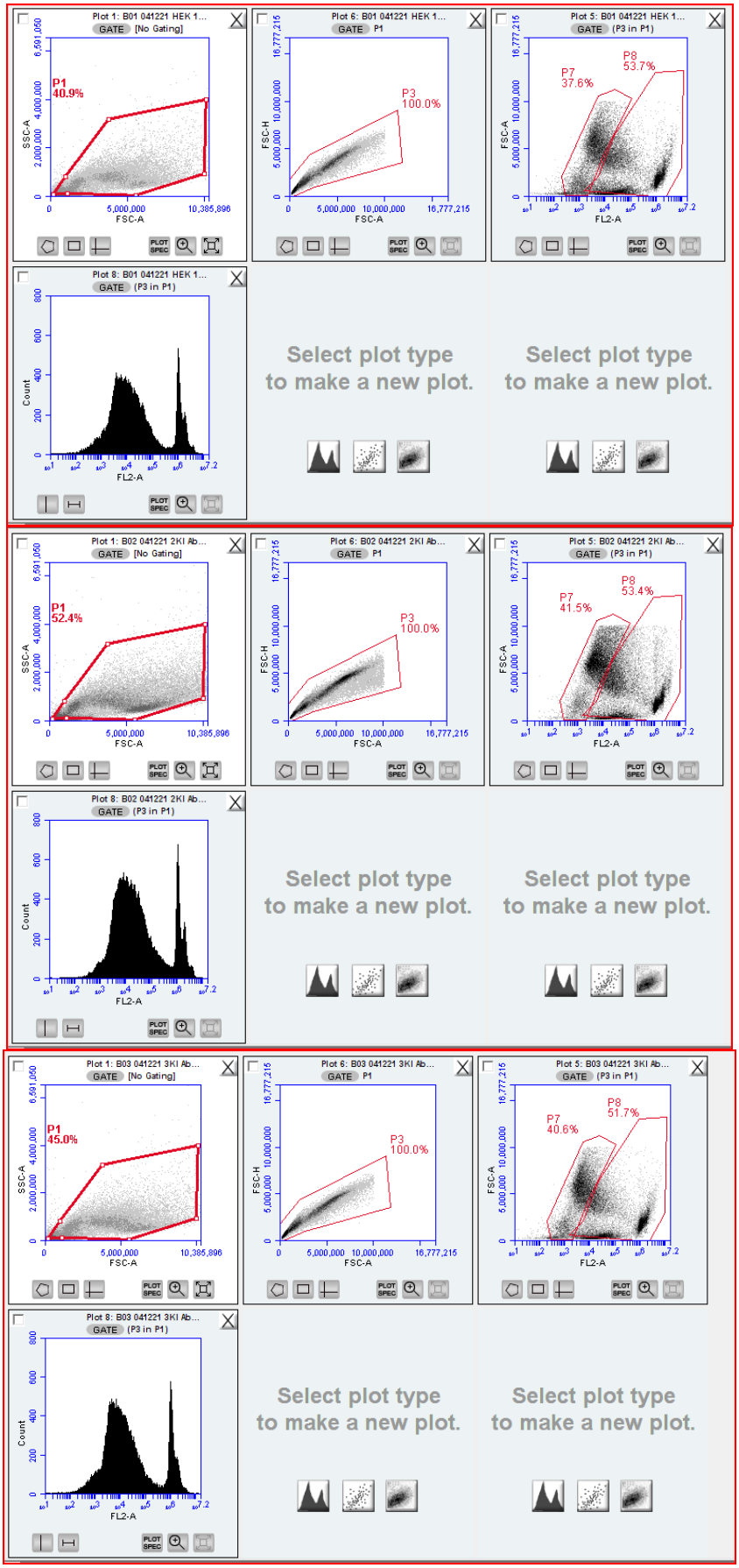

Figure S9. HEK KI Cph treated with h14F7 and incubated for 24 hours. A, B and C represent three independent biological replicates

8.4 Appendix D: Controls for confocal microscopy experiments

Negative controls for results described in section 4.1.1.

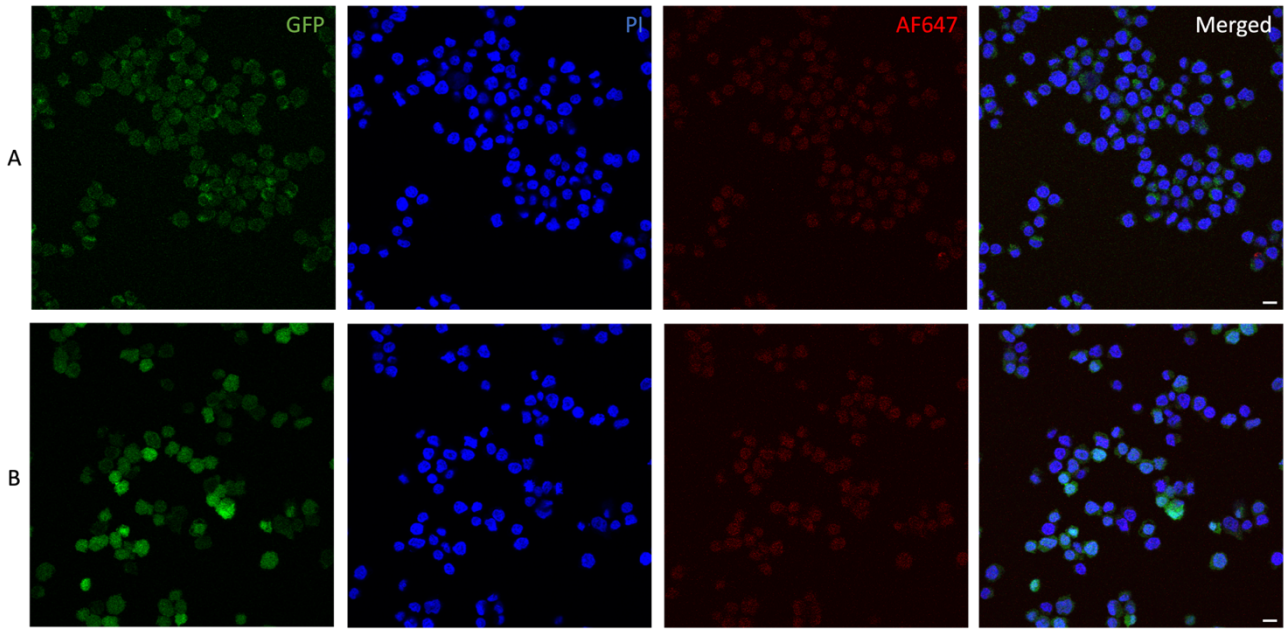

Figure S10. Negative controls for HEK KI Cph and Ki Oslo stained with h14F7*. A, HEK KI Cph stained with goat anti-human Alexa Fluor 647 (AF647, red) and DAPI (blue). **B**, HEK KI Oslo stained with goat anti-human Alexa Fluor 647 (AF647, red) and DAPI (blue). GFP protein is expressed in the HEK KI Oslo cells they therefore emit green fluorescent signal. The merged images are in the rightmost column. The cells were imaged by Olympus FV1000 confocal laser scanning microscope with a PlanApo 60x/1.35 oil immersion objective. Scale bar: 10μm

Negative controls for results described in section 4.2.2.

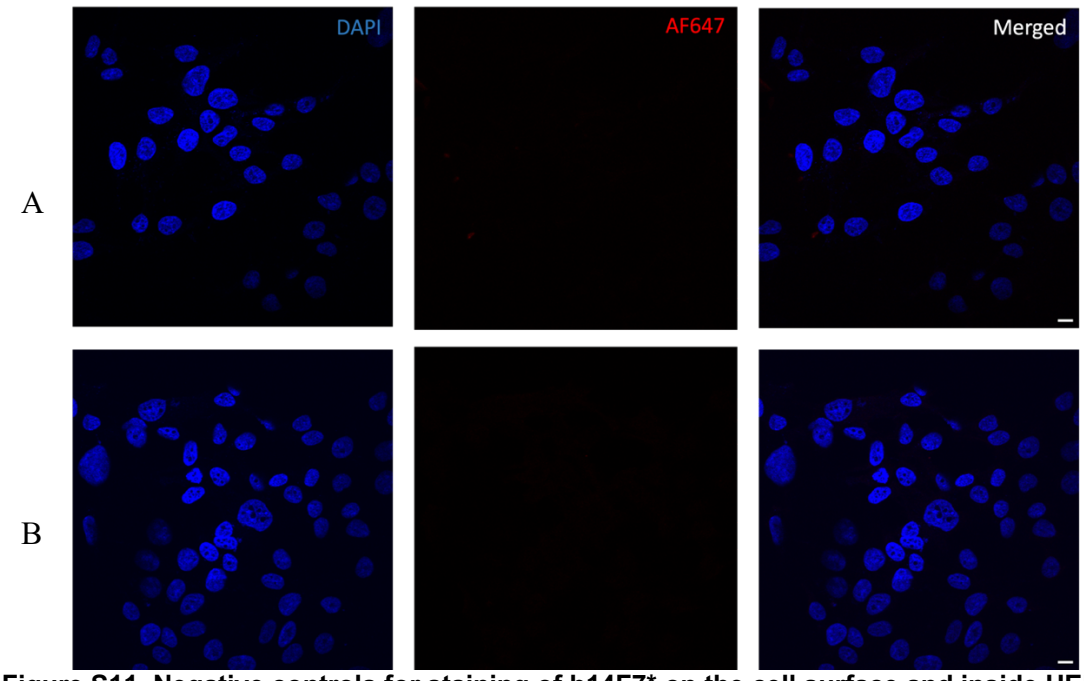

Figure S11. Negative controls for staining of h14F7* on the cell surface and inside HEK KI Oslo cells. A, HEK KI Oslo fixed with 4% PFA and stained with goat anti-human Alexa Fluor 647 (AF657,

red) and DAPI (blue). **B,** HEK KI Oslo fixed with 4% PFA and permeabilized with Triton-X, stained with goat anti-human Alexa Fluor 647 (AF647, red) and DAPI (blue). The merged images are in the rightmost column. The cells were imaged by Olympus FV1000 confocal laser scanning microscope with a PlanApo 60x/1.35 oil immersion objective. Scale bar: 10μm

Negative controls for results described in section 4.2.3.

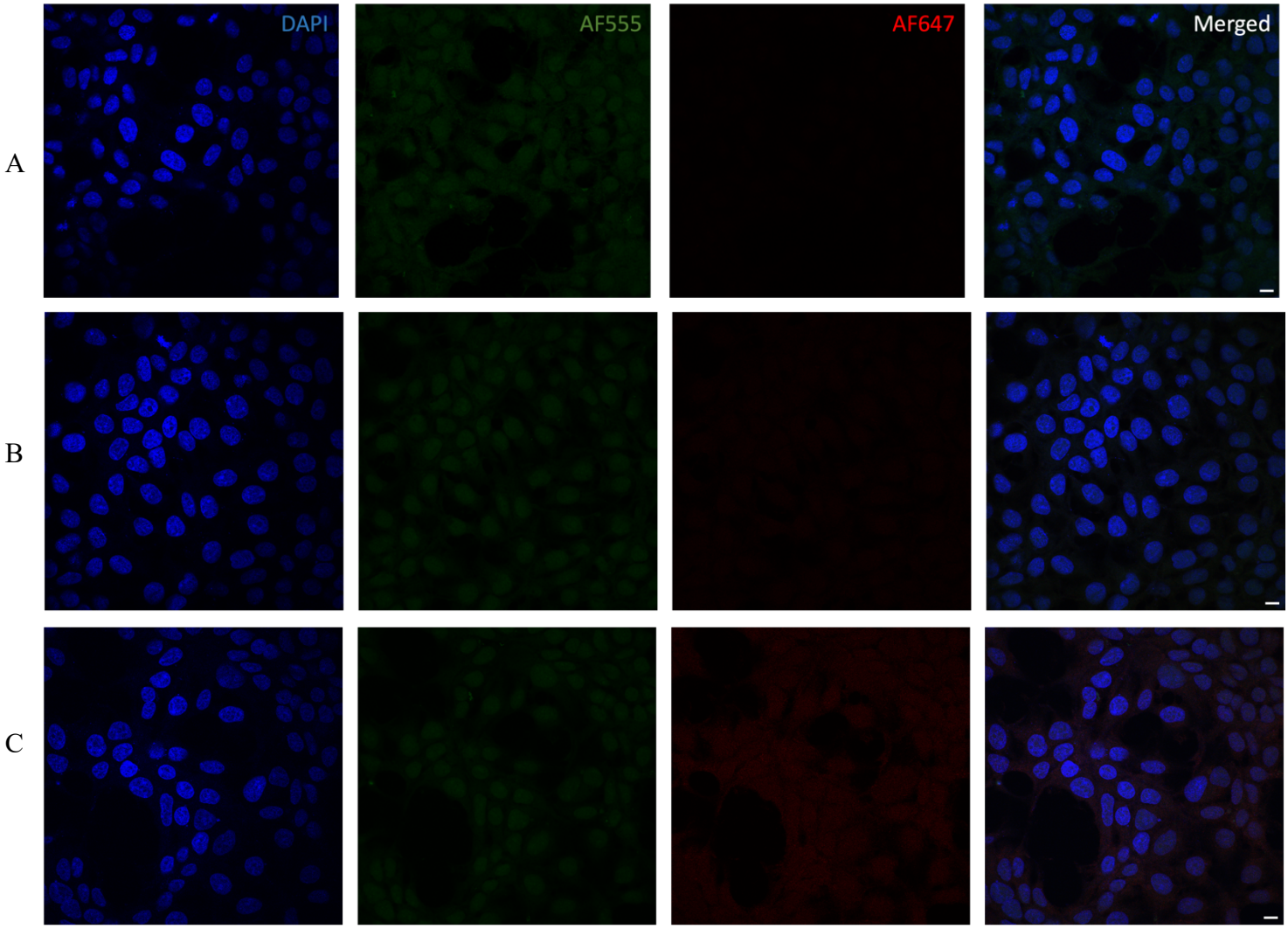

Figure S12. Negative controls for staining of h14F7* with early and late endosomal markers. A, HEK KI Oslo stained with h14F7* (red) as primary antibody and goat anti-mouse Alexa Fluor 555 as secondary antibody. **B**, HEK KI Oslo immunostained with an antibody directed against the early endosomal marker EEA1 (green) as primary antibody and goat anti-human Alexa Fluor 647 as secondary antibody. **C**, HEK KI Oslo immunostained with an antibody directed against the late endosomal marker Lamp1 (green) as primary antibody and goat anti-human Alexa Fluor 647 as secondary antibody. All cells were stained with DAPI (blue). The merged images are in the rightmost column. This figure shows that there was no cross-binding between the human and mouse antibodies. The cells were imaged by Olympus FV1000 confocal laser scanning microscope with a PlanApo 60x/1.35 oil immersion objective. Scale bar: 10μm

8.7 Appendix F: Amino acid sequences

A

VH-CDR1 VH-CDR2

QVQLQQSGNELAKPGASMKMSCRASGYSFTSYWIHWLKQRPDQGLEWIGYIDPATAYTESNQKFKK

VH-CDR3

AILTADRSSNTAFMYLNSLTSEDSAVYYCARESPRLRRGIYYYAMDYWGQGTSVIVSS

B

VL-CDR1 VL-CDR2

DLVLTQSPATLSVTPGDSVSFSCRASQSISNNLHWYQQRTHESPRLLIKYASQSISGIPSRFSGSGSG

VL-CDR3

TDFTLSISSVETEDFGMYFCQQSNRWPLTFGAGTKLELK

Figure S13. Amino acid sequence of m14F7 F_V with murine V_H (A) and murine (V_K). CDRs are highlighted in yellow. The corrected sequence (Ser 108 and Ile 110) based on MS analysis is marked in magenta (Anonsen, J. H., Bousquet, P., & Krengel, U., personal communication).

A

VH-CDR1 VH-CDR2

QVQLVQSGAEVVKPGASMKMSCKASGYSFTSYWIHWLKQRPDQGLEWVGYIDPAT

AYTESNQKFKDKAILTADRSSNTAFMYLNSLTSEDSAVYYCARESPRLRRGIYYY

VH-CDR1

AMDYWGQGTTVTVSS

B

VL-CDR1 VL-CDR2

DLVLTQSPATLSVTPGDSVSFSCRASQSISNNLHWYQQKPGQSPRLLIKYASQSISGPSRFSGSGSG

VL-CDR3

TDFTLSISSVETEDFGMYFCQQSNRWPLTFGAGTKLELK

Figure S14. Amino acid sequence of h14F7 with humanized V_H chain (A) and humanized V_K chain (B). CDRs are highlighted in yellow. The corrected sequence (Ser 108 and Ile 110) based on MS analysis is marked in magenta (Anonsen, J. H., Bousquet, P., & Krengel, U., personal communication). Sequence from (Fernández-Marrero *et al.*, 2011).

A

VH-CDR1
QVQLQQSGAELAKPGASMKMSCRASGYSFTSYWIHWLKQRPDQGLEWIG
VH-CDR2
YIDPATAYTESNQKFKDKAILTADRSSNTAFMYLNSLTSEDSAVYYCAR
VH-CDR3
ESPRLRRGIYYYAMDYWGQGTTVTVSSKLSGSASAPKLEE

B

VL-CDR1
GEFSEARVDIQMTQTPSSLSASLGDRVTISCRASQDISNYLNWYQQKPDGTVKLLI
VL-CDR2 VL-CDR3
YYTSRLHSGVPSRFSGSGSGTDYSLTISNLEQEDIATYFCQQGNTLPPTFGAGTKLELK

Figure S15. Amino acid sequence of 14F7* F_V with murine heavy chain (A) and humanized alternative light chain (B). CDRs are highlighted in yellow.

MAQVQLQQSGAELAKPGASMKMSCRASGYSFTSYWIHWLKQRPDQGLEWIGY

IDPATAYTESNQKFKDKAILTADRSSNTAFMYLNSLTSEDSAVYYCARESPRLRR

GIYYYAMDYWGQGTTVTVSSKLSGSASAPKLEEGEFSEARVDIQMTQTPSSLSAS

LGDRVTISCRASQDISNYLNWYQQKPDGTVKLLIYYTSRLHSGVPSRFSGSGSGT

DYSLTISNLEQEDIATYFCQQGNTLPPTFGAGTKLELK

Figure S16. Amino acid sequence of scFv C1. The scFv sequence is marked in bold. The biophysical features are listed below the figure, calculated by ProtParam (ExPASy).

Molecular weight: 28292.56 Da.
Theoretical pI: 6.73.
Ext. coefficient (ε): 52830 $M^{-1}cm^{-1}$; assuming that all cysteine residues are reduced.

MAQVQLQQSGAELAKPGASMKMSCRASGYSFTSYWIHWLKQRPDQGLEWIGY

IDPATAYTESNQKFKDKAILTADRSSNTAFMYLNSLTSEDSAVYYCARESPRLRR

GIYYYAMDYWGQGTTVTVSSKLSGSASAPKLEEGEFSEARVDIQMTQTPSSLSAS

LGDRVTISCRASQDISNYLNWYQQKPDGTVKLLIYYTSRLHSGVPSRFSGSGSGT

DYSLTISNLEQEDIATYFCQQGNTLPPTFGAGTKLELKAAAGGGGSMVFTLEDFV

GDWRQTAGYNLDQVLEQGGVSSLFQNLGVSVTPIQRIVLSGENGLKIDIHVIIPYEGLS

GDQMGQIEKIFKVVYPVDDHHFKVILHYGTLVIDGVTPNMIDYFGRPYEGIAVFDGK

KITVTGTLWNGNKIIDERLINPDGSLLFRVTINGVTGWRLSERILAGGGGSHHHHHH

Figure S17. Amino acid sequence of scFv C1-Nluc. The scFv sequence is marked in bold and Nluc sequence highlighted in cyan. The biophysical features are listed below the figure, calculated by ProtParam (ExPASy).

Molecular weight: 49020.11 Da
Theoretical pI: 6.07
Ext. coefficient (ε): 78270 $M^{-1}cm^{-1}$; assuming that all cysteine residues are reduced.